Los Alamos
NATIONAL LABORATORY
EST.1943

LA-UR-16-28380
Approved for public release; distribution is unlimited.

Title: EMP/GMD Phase 0 Report, A Review of EMP Hazard Environments and Impacts

Author(s): Rivera, Michael Kelly
Backhaus, Scott N.
Woodroffe, Jesse Richard
Henderson, Michael Gerard
Bos, Randall J.
Nelson, Eric Michael
Kelic, Andjelka

Intended for: Report

Issued: 2016-11-07 (rev.1)

Disclaimer:
Los Alamos National Laboratory, an affirmative action/equal opportunity employer, is operated by the Los Alamos National Security, LLC for the National Nuclear Security Administration of the U.S. Department of Energy under contract DE-AC52-06NA25396. By approving this article, the publisher recognizes that the U.S. Government retains nonexclusive, royalty-free license to publish or reproduce the published form of this contribution, or to allow others to do so, for U.S. Government purposes. Los Alamos National Laboratory requests that the publisher identify this article as work performed under the auspices of the U.S. Department of Energy. Los Alamos National Laboratory strongly supports academic freedom and a researcher's right to publish; as an institution, however, the Laboratory does not endorse the viewpoint of a publication or guarantee its technical correctness.

EMP/GMD Phase 0 Report
A Review of EMP Hazard Environments and Impacts

Michael K. Rivera, PhD

Scott N. Backhaus, PhD

Jesse Woodroffe, PhD

Michael Henderson, PhD

Randy Bos, PhD

Eric Nelson, PhD

Los Alamos National Laboratory

Andjelka Kelic, PhD

Sandia National Laboratory

October 24, 2016

Los Alamos National Laboratory, an affirmative action/equal opportunity employer, is operated by Los Alamos National Security, LLC, for the National Nuclear Security Administration of the U.S. Department of Energy under contract DE-AC52-06NA25396.

This report was prepared as an account of work sponsored by an agency of the U.S. Government. Neither Los Alamos National Security, LLC, the U.S. Government nor any agency thereof, nor any of their employees make any warranty, express or implied, or assume any legal liability or responsibility for the accuracy, completeness, or usefulness of any information, apparatus, product, or process disclosed, or represent that its use would not infringe privately owned rights. Reference herein to any specific commercial product, process, or service by trade name, trademark, manufacturer, or otherwise does not necessarily constitute or imply its endorsement, recommendation, or favoring by Los Alamos National Security, LLC, the U.S. Government, or any agency thereof. The views and opinions of authors expressed herein do not necessarily state or reflect those of Los Alamos National Security, LLC, the U.S. Government, or any agency thereof.

Table of Contents

Table of Figures

1 Summary of Approach and Path Forward

The purpose of this study is to determine methods to analyze the hazard environments, impacts, and consequences of different sources of electromagnetic pulse (EMP), including nuclear electromagnetic pulse (NEMP) and geomagnetic disturbance (GMD) on the U.S. electric power infrastructures and to use those methods to determine EMP and GMD events of concern. The study will be carried out in four phases, each of which will provide higher levels of analytic fidelity that focuses on those EMP/GMD sources and events that create significant consequences, or whose consequences are sufficiently uncertain, to require more in depth study. This study will leverage the best experimental data; device, equipment and system models; and simulation tools currently available. This study focuses primarily on the bulk electric system (BES) including large generating stations, large power transformers, the transmission network, and transmission system protection. Electrical distribution systems may potentially be included, if warranted, after consideration of the consequences for the bulk power system.

Phase 0 (this report) consists of several parts. In this report, we set out the following:

- Place the work we intend to perform in the context of earlier work such as the EMP Commission, Metatech and TPL-007-1
- Describe the bounding conditions of this study
- Provide an overview of the NEMP and GMD events and the environments they create
- Develop a method for parameterizing of NEMP and GMD events to determine parameter regions of concern
- Describe the critical bulk power components, with emphasis on discussing how NEMP and GMD may couple to and interact with the components
- Discuss restoration of the BES after abnormal events
- Accrue a bibliography of the works that this study will rely upon

Phase 1 will consider different NEMP and GMD event types parameterized in Phase 0 that fit within the bounding assumptions of this study as an event of concern. We will solicit input on the plausibility of such events. Along with the parameterization included in this Phase 0 report, we will begin to incorporate the initial condition of the BES as another important parameter.[1] Phase 1 will classify these parameterized events into according to the hazard that dominates the impact on the electrical infrastructure using test data, simulation results, or models from identified studies. We will further subdivide each of these classifications into events of "concern" and "no-concern" with a bias toward a "concern" classification if there is uncertainty or significant disagreement in Phase 1 of the study. Appropriate stakeholders will provide support in defining events of concern, and we may also leverage existing documents regarding BES planning to support these definitions. As an example, an NEMP or GMD event that produces impact estimates within the scope of Categories P0-P7 of Table 1 in NERC Standard TPL-001-4 on "Transmission System Planning Performance Requirements" should be classified as "no-concern". Events that produce impact estimates within or more severe than the "Extreme Events" section of Table 1 are more likely to be classified as "concern".

[1] One possible approach is to adopt the initial condition of "Normal System" as defined in TPL-001-4, Table 1 under Category P0.

Phase 2 will focus on the parameterized events of "concern", as determined in Phase 1. For each type of event, Phase 2 will develop an understanding of the important effects on electrical power systems that potentially lead to its significant failure as defined by the bounding conditions of this study. To the greatest extent possible, the impact at the electrical component or subsystem level will be characterized using effects and terminology accepted by BES transmission planners.[2] The focus of Phase 2 will be to understand the relationship of the different NEMP and GMD effects, how these interact with the behaviors and processes of the BES. Based on this understanding, the study will provide a list of available test data, modeling and simulation tools, and a description or workflow for how to use these tools to analyze the consequences of events of "concern" to BES. We will consider existing and vetted workflows and models (e.g., those suggested in NERC TPL-007-1 (NERC, 2014) for GMD events) before suggesting an entirely new workflow and models.

Phase 3 will test the key studies identified in Phase 2 via a trial implementation and provide a series of written reports that describe the viability of the workflows, consequences of NEMP and/or GMD events for the U.S. BES and a high-level summary of the parameterized events identified in Phase 1 that should be recommended for further study or may already require some form of mitigation to avoid the predicted consequences. Phase 3 will also discuss the difficulties and challenges encountered in carrying out the studies and suggestions for improvements to the study processes.

Los Alamos National Laboratory submits this draft report in fulfillment of the Phase 0 requirement for our study into the impacts of nuclear electromagnetic pulse (NEMP) and geomagnetic disturbance (GMD) on the bulk electrical system (BES). This report is a living document that we will build upon during subsequent phases of this project, altering it as a greater understanding of NEMP and GMD impacts on the BES is accrued via research.

[2] See Table 1 in NERC Standard TPL-001-4, "Transmission System Planning Performance Requirements"

2 Introduction and Context

Recent interest within government and associated regulatory agencies in evaluating the impact of an NEMP or GMD on a BES are captured in two documents: the "Report of the Commission to Assess the Threat to the United States from Electromagnetic Pulse (EMP) Attack"(EMP Commission, 2008) and the "Transmission System Planned Performance for Geomagnetic Disturbance Events"(NERC, 2014) (NERC TPL-007-1). The EMP Commission's report outlines the possible effects of a NEMP on infrastructure in the continental United States. The Commission's conclusions regarding an NEMP's impact to electrical BESs is supported by a considerable amount of literature from Metatech (Gilbert, Kappenman, Radasky, & Savage, 2010; J Kappenman, 2010; Radasky & Savage, 2010; Savage, Gilbert, & Radasky, 2010). The second document, TPL-007-1 developed by the North American Electric Reliability Corporation (NERC), outlines a workflow that evaluates the impact of a benchmark 1-in-100 year GMD to a BES. A number of power flow solvers (e.g., PowerWorld[3]) have already implemented the TPL-007-1 workflow. Figure 1 shows a generalization of the workflows in the studies mentioned above.[4]

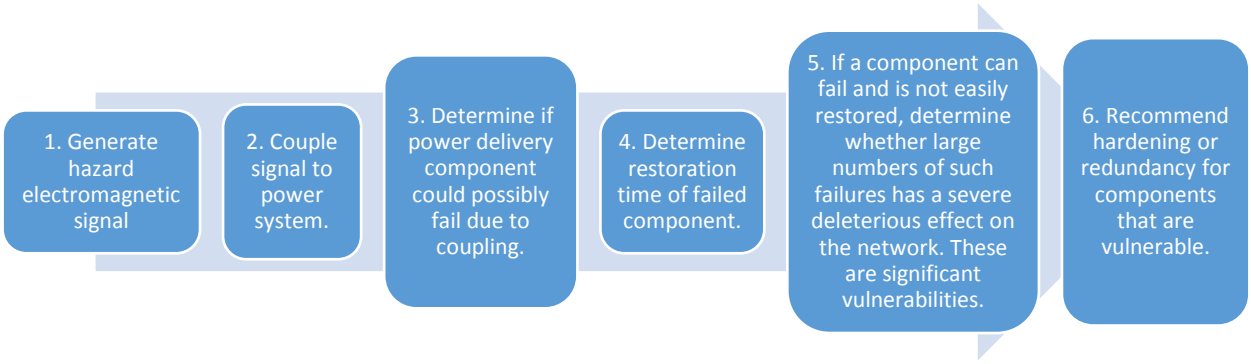

Figure 1: Generalization of the workflow used in EMP Commission report, Metatech documents, and TPL-007-1 to evaluate NEMP/GMD hazards to the BES and determine recommended hardening. This workflow does not exactly represent the workflow used in these studies and reports, rather, it is an attempt to represent the general process of each of these workflows in a single figure.

Both the Commission report and TPL-007-1 created many questions that require answers before regulators can develop appropriate regulations and the electrical power industry can implement risk screening and potentially implement efficient mitigations, such as operational procedures or system hardening. This study is a natural follow-on to these earlier documents. In this study we attempt to frame these earlier works in the context of this study's bounding assumptions and extend them by incorporating more recent measurements of grid component responses, introducing appropriate bounds and, where necessary, developing workflows whereby we can start assessing NEMP and GMD impacts as quantitatively as possible.

We begin by summarizing the Commission's report, its supporting documentation, and TPL-007-1, including what each document conveys about the particular phenomenon (NEMP or GMD) and that phenomenon's interaction with BESs. We also enumerate the workflow used in each document to reach

[3] See Powerworld, www.powerworld.com/products/simulator/add-ons-2/simulator-gic.
[4] This workflow is a simplified attempt by the authors to summarize the steps whereby the EMP Commission, Metatech and NERC evaluated impacts of GMD and NEMP to BESs, and developed hardening recommendations. It is not a product of the EMP Commission, Metatech or NERC, nor has it been verified of validated by any these groups. This workflow was developed by the authors through inspection of the various reports.

conclusions about network vulnerability and develop recommendations on network hardening. After this summary, we will place our study in the context of these earlier works.

2.1 EMP Commission Report

The EMP Commission was established in 2001. Its specific duties included:[5]

- Assess the nature and magnitude of potential high-altitude (N)EMP[6] threats to the United States
- Assess the vulnerability of United States military and especially civilian systems to an (N)EMP attack, giving special attention to vulnerability of the civilian infrastructure as a matter of emergency preparedness
- Assess the capability of the United States to repair and recover from damage inflicted on United States military and civilian systems by an (N)EMP attack; and
- Assess the feasibility and cost of hardening select military and civilian systems against (N)EMP attack.

The Commission report outlines the impact of a NEMP produced by an exo-atmospheric burst on all facets of infrastructure (e.g., power delivery, water delivery, transportation). The electrical power delivery portion of the Commission's work considered the components of power delivery and consumption infrastructure (generation, transmission, distribution, consumption, SCADA control and operations) and resulted in several specific recommendations (EMP Commission, 2008):

1. *Understand system and network level vulnerabilities, including cascading effects*
2. *Evaluate and implement quick fixes*
3. *Develop national and regional restoration plans*
4. *Assure availability of replacement equipment*
5. *Assure availability of critical communications channels*
6. *Expand and extend emergency power supplies*
7. *Extend black start capability*
8. *Prioritize and protect critical nodes*
9. *Expand and assure intelligent islanding capability*
10. *Assure protection of high-value generation assets*
11. *Assure protection of high-value transmission assets*
12. *Assure sufficient numbers of adequately trained recovery personnel*
13. *Develop and deploy system test standards and equipment*
14. *Establish installation standards*

From the presentation given within the report, the Commission developed these recommendations via a workflow that considered the NEMP vulnerabilities to several components of the electrical power system, including generation and transmission in the BES and distribution systems that move electrical power from BES substations to the end consumer. In the workflow, the component vulnerabilities were obtained through a combination of device testing and simulation. Given a vulnerable component, two questions were asked: how important is the component to power delivery operations and how difficult was the restoration of that component if it was damaged? The Commission recommend hardening of

[5] See Commission to Assess the Threat to the United States from Electromagnetic Pulse Attack, www.empCommission.org/.
[6] We have inserted (N)EMP for EMP to translate the Commission scope to our nomenclature.

the component, which might require alteration not just to the component but the power delivery system as a whole, and increased redundancy if a component was vulnerable, important to network operations, and difficult to replace.

As an example of how this workflow might be used, consider the generation constituent of the BES. The Commission notes that most of the bulk physical components are relatively robust to electromagnetic pulse, but the control systems that are critical for normal operation and component control may be vulnerable. Thus a pulse that effects control systems could physically damage the bulk generation components by forcing the plant to, for example, improperly shut down. Obviously such physical damage would result in a significant recovery time, and would constitute a significant vulnerability. Given this vulnerability, the Commission recommended a hardening of generation control and an increase in power supply redundancy and black start capability (contained in recommendations 2, 6, 7 and 10).

The Commission performed this type of analysis for the entire BES. The Commission concluded that the BES would almost certainly collapse post-NEMP insult; there would be likely widespread damage to system components, in particular to the control and communication components of the network; and, as a result, a network black-start would be challenging. An NEMP insult could result in widespread outages for extended periods of time. In particular, the Commission concluded that although the bulk power components are relatively robust to direct damage from NEMP insult, the control, protection, and communication (SCADA) components are not. One can see from a cursory review of the recommendations that the hardening and redundancy they intend is meant to minimize the insult's effects to important components of the network and to enhance the recovery capability of the network post insult.

2.2 Metatech

The Metatech Corporation produced a set of documents on NEMP that focus specifically on NEMP caused by exo-atmospheric bursts. There are four reports relevant to our discussion; two that deal with early time NEMP of an exo-atmospheric burst (Radasky & Savage, 2010; Savage et al., 2010) and two that deal with the late time NEMP an exo-atmospheric burst (Gilbert et al., 2010; J Kappenman, 2010).

Broadly speaking the first of each pair of documents describes the hazards an exo-atmospheric burst produces and the vulnerabilities of various BES components, while the second describes and/or investigates ways of mitigating the hazard. We briefly summarize both sets.

2.2.1 Early Time NEMP(Radasky & Savage, 2010; Savage et al., 2010)

The first of these reports (Savage et al., 2010) is a summary of the early time electromagnetic hazards of an exo-atmospheric nuclear burst, and the coupling of those early time NEMP effects to power delivery components. The more important sections of the document are as follows:

- Section 2: This section contains a high-level overview of the early time electromagnetic fields created by the burst and an analysis of waveforms used to represent those fields in coupling analysis to electrical components.
- Section 4: This section contains an in-depth summary of the early time electromagnetic fields created by the burst, emphasizing how those fields are ultimately simulated. The description given is essentially a more recent version of the phenomenology of Longmire (H. Longley &

Longmire, 1972; H. J. Longley & Longmire, 1973; C. Longmire, 1978; C. L. Longmire, 1978; Longmire, 1987, 1995, 2004; Longmire, Hamilton, & Hahn, 1987; Longmire & Longley, 1973).

- Section 5: This section is a very brief overview of the coupling of the early time electromagnetic fields created by a nuclear burst to electrical power lines via the Agrawal coupling model (Agrawal, Price, & Gurbaxani, 1980). In particular the section discussed how the strength of that coupling depends on burst and power line parameters.
- Section 7: This section starts with a presentation of some line coupling simulations similar to earlier work by one of the authors (Ianoz, Nicoara, & Radasky, 1996). These simulations established the voltage and current magnitudes that devices might experience at their input ports due to the early time electromagnetic fields created by a nuclear burst. These results were then supplemented by a description of some device testing, particularly relays and insulators, that Metatech performed to establish the vulnerability of these devices to such magnitudes of voltage and current. Where recent device testing was unavailable, Metatech drew conclusions from earlier work mostly performed at Oak Ridge National Laboratory (Barnes, McConnell, Van Dyke, Tesche, & Vance, 1993).

As in the Commission report, the relevant conclusions for vulnerabilities of the power delivery system, noted in Section 7 focused specifically on individual components of the power delivery system and how those components might respond to the early time NEMP. The conclusion reached echoed that of the Commission: the most vulnerable components of the power grid were the control, protection and communication components. Direct damage to these components could result in indirect damage to bulk BES devices (transformers, generators, etc.).

The second early time report (Radasky & Savage, 2010) presents protection concepts for individual components that could mitigate the vulnerabilities pointed out in Section 7 of the previous report (Savage et al., 2010). The protection concepts largely echo well known concepts for EMP hardening already present in current standards, in particular MIL-STD-188-125-1 and the International Electrotechnical Commission (IEC) standards, which we discuss later in this document. These protection concepts are described and enumerated in sections 4 and 5 of (Radasky & Savage, 2010). Section 5 of the report also includes an overview of the IEC standards.

The analysis workflow in the Metatech early time investigations utilized early time NEMP fields consistent with Longmire's work and the line coupling model of Agrawal to assess the likely voltages and currents present at the electrical ports of electronic equipment. Metatech used experiments to investigate the likelihood of damage to various components of the BES under these conditions. This work led to the proposition of hardening vulnerable components using techniques enumerated in current standards. This workflow is essentially the same as the one depicted in Figure 1.

2.2.2 Late Time(Gilbert et al., 2010; J Kappenman, 2010).

The late time reports follow the same pattern as the early time reports. The first document (Gilbert et al., 2010) describes the late time electromagnetic hazards of an exo-atmospheric nuclear burst, its eventual coupling into the BES, and resultant effects, while (J Kappenman, 2010) considers the possible reduction in effects from various blocking devices (e.g., blocking capacitors and resistors). In these documents, the characterization of the late time magnetic fields created by an exo-atmospheric burst follows from Longmire's work (Chavin, Crevier, Kilb, & Longmire, 1979; WJ Karzas & R Latter, 1962) and was simulated using HEMPTAPS. Due to the resemblance of the generated fields to GMD, the electric

field at the ground was obtained from the late time magnetic fields using a plane wave model developed in (Wait, 1953) with ground conductivities provided by USGS (Fernberg, 2012). These electric fields are finally coupled into the power grid via a steady state power flow solver.

The hazard analysis presented in (Gilbert et al., 2010) focused on the late time NEMP effects within two particular components of the BES: power transformers and circuit breakers. The deleterious effects of DC currents in transformers are well known from experience with GMDs, and the discussion in Section 3 of (Gilbert et al., 2010) largely echoes this concern with respect to late time NEMP. In particular, (Gilbert et al., 2010) determined the simulated reactive power demand, and geo-magnetically induced currents (GICs) within the transformers for several burst scenarios and found them to be large compared to measured values that have naturally occurred due to GMDs. The reactive power demands were such that it was likely the power delivery system would collapse well before the peak values were reached.

The circuit breaker investigation in Section 4 of (Gilbert et al., 2010) noted that if a large enough DC current existed on a line, the AC current would not cross zero . Such zero crossings are important for proper circuit breaker operation and current interruption. Thus, even if protection relays survive the early time NEMP effects, it is possible that the circuit breakers they control would not be able to interrupt current when receiving signals from relays due to the lack of zero crossing.

The analysis in (J Kappenman, 2010) investigates the inclusion of a variety of blocking devices intended to reduce the magnitude of currents created by the both GMDs and the late times of NEMP. Its focus is almost entirely on late time NEMP impacts to transformers. Sections 7 and 8 are the most important sections of the paper in this regard. In these sections, the number of "at risk" transformers, defined by (J Kappenman, 2010) as transformers with more than $90\ Amps/phase$ of induced geo-magnetic current, are evaluated for a variety of late time NEMP insults. This analysis is done for transformers with and without blocking resistors. Significant benefits were found with the use of blocking resistors

In (J Kappenman, 2010) there was some attempt to optimize the installation of blocking resistors, looking at the effects of installing only blocking resistors on the top 75% of transformers experiencing the largest currents. The benefits were roughly equivalent benefits to installing blocking resistors on all transformers. Section 9 also discusses engineering concerns regarding the large scale introduction of blocking resistors across the entire BES.

The workflow used in these late time documents was largely the same the workflow in the Metatech early time documents, in the Commission's report, and shown schematically in Figure 1; namely, generate electromagnetic fields representative of the late time NEMP hazard, couple the hazard to power the BES to determine voltage and current levels within devices, determine the likelihood of device failure, and recommend hardening that limits widespread device failure.

2.3 TPL-007-1

The North American Electric Reliability Corporation (NERC) developed a workflow to test the resilience of electrical delivery networks to GICs caused by GMDs, The workflow put forward was very similar to the late time NEMP workflow that appears in the Metatech documents. In particular, the workflow uses a standard benchmark wave form for a magnetic disturbance and calculates the electric and fields generated at the ground for this disturbance using the plane-wave model developed in (Wait, 1953), with ground conductivities provided by USGS (Fernberg, 2012). These electric fields are then coupled

into the BES via any number of commercially available network solvers. Finally, the workflow estimates the thermal heating in power transformers (NERC, 2014).

The major difference between TPL-007-1 and the Metatech documents is in the source that generates the magnetic disturbance—solar flares for GMD in TPL-007-1 and a high altitude nuclear explosion for late time NEMP in the Metatech work. To create a standard benchmark waveform for screening studies using their workflow, NERC selected the magnetic waveform (NERC, 2014) produced by the March 1989 storm that collapsed the Hydro-Quebec BES to represent large geomagnetic events. This benchmark magnetic waveform was scaled so that its peak amplitude was consistent with a one-in-one-hundred year solar storm, as determined by NERC based upon statistics of observed geomagnetic fields over the last twenty years. The magnetic waveform was then further scaled by geo-magnetic latitude.

Using the above techniques, the induced GIC within the transformers and the resulting the networks reactive power demands and transformer heating could be estimated. Based on this analysis, an appropriate threshold for GIC was set to indicate where further analysis is warranted.

2.4 Current Study

The workflows for the Metatech and TPL-007-01 studies are largely the same and represented by the generalized workflow in Figure 1; namely, generate an electromagnetic signal representative of the hazard due either to a NEMP or GMD; couple that signal to the power network; evaluate the vulnerability of the components to this coupling; and, if the components are considered critical to network operations and not easily restored, recomm*end hardening or increased* redundancy.

The current study builds upon this basic workflow for evaluating NEMP and GMD resilience of the BES, while simultaneously updating it with more recent scientific results and constraining its scope. We draw out gaps in our understanding of how NEMP and GMD events impact the BES and recommend targeted studies to fill those gaps. To understand this objective better, we look briefly at a few of the steps in the work flow and indicate how we might improve upon the step. This list is not intended to be and exhaustive list of all the ways in which we might improve upon a particular workflow step, rather we want to give a flavor for what we intend within phase 1. We will specifically look at a few of the improvements in workflow steps 1, 2, 5 and 6. We will not be commenting on steps 3 and 4 until phase 1 is complete.

2.4.1 Workflow Step 1

The first step in our work flow is to generate the electromagnetic hazard from the event. The TPL-007-1 standard generates a benchmark GMD hazard using a magnetic signal measured from the March 1989 event that collapsed the Quebec power system. For late-time NEMP, the magnetic signal is extrapolated from the HEMPTAPS computer code. For both of these magnetic signals, we use the plane wave model of Wait (Wait, 1953) with USGS conductivity layer data (Fernberg, 2012) to calculate the electric fields that ultimately couple into power system The ground conductivities presented in (Fernberg, 2012) are, at best, very coarse grain approximations. They are 1D models, meaning they assume that the Earth's conductivity only varies with depth, but not laterally. The plane wave model that utilizes these data assume the same homogeneity of the Earth's conductivity layers within a region.

There have been recent advances in our ability to measure the deep crust ground conductivity within a region (Yang, Egbert, Kelbert, & Meqbel, 2015). These data clearly demonstrate that there is a great degree of variability in the Earth's conductivity (see Figure 2).

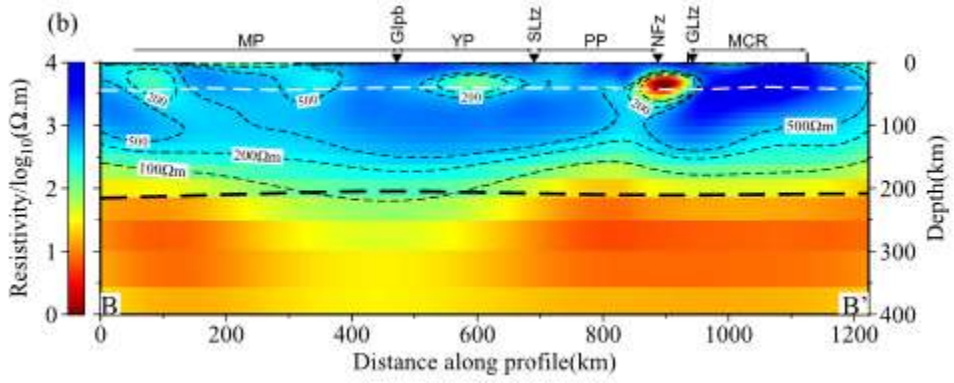

Figure 2: Cross section of the three dimensional Earth conductivity of the North Central U.S. measured by the Earth Scope project. (Image taken from(Yang et al., 2015))

The spatial variability in Earth's conductivity needs to be better accounted for in the workflow for both GMD and late time NEMP. This accounting will likely include using multi-dimensional models, rather than the plane wave approximation, to generate the ground fields. As a first step, the layer conductivity models should be replaced by a spatially averaged layer conductivity model obtained by averaging the three-dimensional conductivity data over the region of interest.[7] More detailed and computationally intensive studies could also be done on targeted regions to determine how important spatial variability of the conducting layers is to the resultant surface fields.

For early-time NEMP, an example of targeted studies that we might draw out is the effect of complex topography on the hazard. For obvious reasons, there are no tests of the electromagnetic effects of surface bursts in urban environment. However, urban environments are the most likely locations for a surface burst to occur. There are few attempts to understand how the urban landscape, with its altered ground conductivities, innumerable conductive paths, and impeding structures, would impact the electromagnetic pulse of a surface burst. Although performing such simulations is outside the scope of this study, we feel this lack of understanding is an important gap in our knowledge about the electromagnetic effects of nuclear devices that needs to be filled.

2.4.2 Workflow Step 2

In the second step of the workflow, the electromagnetic hazard environment obtained from the first step is coupled to the BES. For early time NEMP, device coupling falls within the larger field of electromagnetic compatibility (EMC), which has invested a significant amount of work focused on the coupling of stray electromagnetic fields into transmission power lines and instrumentation measurement lines and systems. Most techniques that evaluate this coupling trace their origins back to three formulations; either that of Taylor (Taylor, Satterwhite, & Harrison, 1965), Rachidi (Rachidi, 1993), or Agrawal (Agrawal et al., 1980). All three of these formulations are shown by Nucci to produce

[7] We note that the Earth Scope project has not completed its survey of CONUS. However, where such data exists, it should be substituted for the layer models presented in (Fernberg, 2012).

equivalent results in (Nucci, Rachidi, Ianoz, & Mazzetti, 1995), though the details of how the coupling occurs varies from model to model. The Agrawal model (Agrawal et al., 1980), is the most popular of these representations due to its simplicity of form and ability to incorporate non-linear effects relatively easily. (Ianoz et al., 1996; Savage et al., 2010) used this model to calculate the coupling of early time NEMP electromagnetic effects.

The Agrawal model makes some significant simplifying assumptions. In particular it only includes certain modes of propagation along the transmission line. Recently, line coupling equations have been extended to more complex geometries without significant loss of their simple form. So-called full wave transmission line theory (Chiariello, Maffucci, Miano, Villone, & Zamboni, 2008) or transmission line super theory (Haase, Nitsch, & Steinmetz, 2003) can be used to calculate the coupling to more complex geometries than can be done with the Agrawal model and with only a marginal loss in computation time; for example, lines with bends, droops, and ground wires can be analyzed via this technique. Given that such models retain the simple form of Agrawal, studies of early time NEMP coupling to power lines should compare results from these improved models with Agrawal's.

2.4.3 Workflow Steps 5 & 6

The last two steps identify important vulnerabilities in the BES based on the previous steps, and recommend hardening of the component or BES to mitigate these vulnerabilities. For early time NEMP, the Commission's report and associated Metatech documents base this recommendation solely on expert opinion; for example, detailed measurements indicated a device (e.g., a relay) was vulnerable to early time NEMP. Given this vulnerability and the importance of relays to the network, relays were considered an important vulnerability. As such, both reports recommended hardening relays.

To the best of our knowledge, neither the EMP Commission nor Metatech attempted to establish the actual system impact of unprotected relays during the early time of an NEMP. ***A primary goal of the current study is to fill this gap, and similar gaps for GMD and late time NEMP.***

Returning to relays as an example of how we might proceed in replacing expert opinion with quantitative analysis. One damage path for relays is through their communication connections (serial ports, ethernet ports, etc.). These connections are, for the most part, contained within substation control houses. Given a representation of a control house's ability to attenuate early time NEMP pulses, we can make a reasonable approximation of the current and voltage experienced at the communication ports of the relay. Using test data on relay failure for a range of current and voltage pulses, one can posit a probability of relay failure due to early time NEMP insult. Applying this model of probability of failure to all relays in the network will result in some relays failing, but not all. Following the relay failures, the system is now in an abnormal state where a portion of the relays are inoperable. In this altered state, the analysis workflow should attempt to quantitatively answer how much of the BES's power delivery capacity is lost? This analysis can be run many times using different samples of the set of lost relays to estimate the average impact to the BES and the uncertainty in that result. .

In contrast to expert opinion, quantitative analysis with uncertainty quantification enables a wider range of questions about impact and mitigation to be answered. For example, can we identify critical components of the BES by correlating large losses of BES power delivery capacity with the frequency of component appearance in such outage scenarios? Can operational changes in system state enhance resilience of the BES to GMD and NEMP? What are the optimal levels of protection to harden the BES?

2.4.4 Bounding of the Analysis in the Current Study

Nuclear detonation events of any kind are likely to have some impact on the electrical power system, however, not all of these will generate large enough consequences to be of concern. To focus the analysis of this study on events of high consequence and eliminate events that have minor fiscal impact or are of short duration, **we limit the study to events that cause $2 billion per day (2016 dollars) impact to gross domestic product from lost BES capacity for at least 3 days.** We note that the days following the 2003 Northeast U.S. blackout easily meet the $2 billion per day threshold, but the restoration was mostly completed before the 3-day threshold. In contrast the 1989 Hydro Quebec blackout due to GMD did not meet either threshold.

To make the study tractable, its scope is further limited to:

1. Generation, transmission and protection components of the BES
2. Civilian BES
3. Single detonations of stockpile weapons (for NEMP)
4. Events up to Carrington class events (for GMD)

The second bound eliminates consideration of military-hardened power networks. These are built to more exacting standards than the civilian network, both in terms of NEMP hardness as well as hardness to blast overpressure and thermal damage. The third and fourth bounds eliminate more abstract considerations such as chained multiple NEMP events or weapons specifically designed to produce NEMP.

Of the study limitations, perhaps the most critical to discuss in detail is the first, as it has important implications. First, the fact that we consider only the generation, transmission and protection components of the BES means that we consider only those physical components of the network that are critical to the ability to generate and deliver bulk power. We will not, consider SCADA[8]–the computer-based supervisory control for BESs. Similarly we will not consider telecommunication needs necessary to support power delivery in the absence of SCADA, nor will we consider whether the power industry employs the necessary personnel to black-start a network without SCADA. Although we fully recognize the need for more detailed analysis incorporating SCADA, it is outside of the scope of the current study.

Second, we do not consider the electrical distribution grid that transports electrical power from the BES delivery nodes (transmission substations) to the end consumer. Figure 3 shows a highly simplified view of typical electrical networks. The distribution grid is the load (consumption) side of the network. We focus on the supply side of the network (BES) and analyze the ability to supply electrical power after an EMP event, regardless of the ability to consume it. We are aware of the limits of this assumption. The absence of large amounts of load may make the black-start of a BES very difficult because of resulting instabilities. Regardless, analysis of the distribution grid and connected consumer loads is outside the scope of the current study and is deferred to future follow-on work.

[8] Supervisory Control and Data Acquisition.

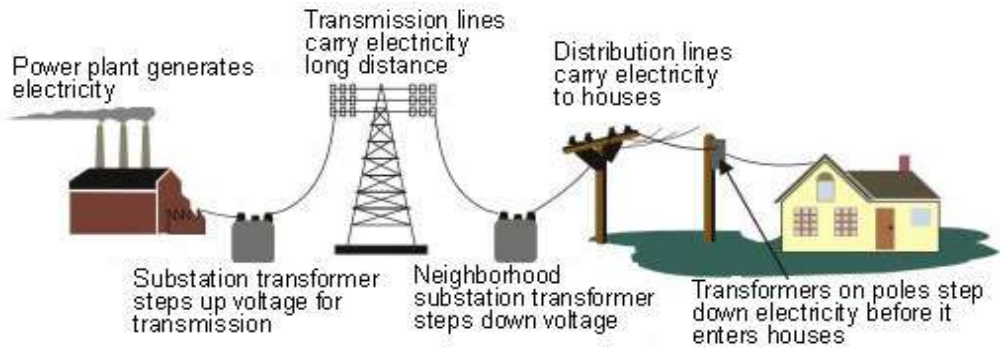

Figure 3: Branches of the electrical BES. (Credit: http://www.eia.gov/Energyexplained/index.cfm?page=electricity_delivery)

We only consider the BES and do not propagate those effects to other infrastructures and their connected electrical loads. Once electrical power is restored, transportation systems, water delivery systems, etc. are assumed to be immediately be restored to their original state, such that normal business activity resumes to the state prior to the EMP. We further assume there is no capital losses from the EMP event outside of the power system and that consumer loads are not significantly damaged. Although this assumption is crude, it serves to bound this initial study.

2.5 Summary

The simplified workflow depicted in Figure 1 is an approximate representation of the workflows utilized by the EMP Commission, Metatech and NERC in developing their standards and recommendations. The current study will supplement and enhance these underlying workflows. In particular, we anticipate a focus on quantitative analysis of system-level impacts of NEMP and GMD events coupled to the BES, within the bounding assumptions listed above.

To perform this study, we need a minimum necessary knowledge base. Along with the obvious need to simulate the generation, transmission and protection portion of the BES, we also need to understand the physics of NEMP and GMD events, how the electromagnetic fields from these events couple to the BES, and how the BES responds to and recovers from these abnormal events. To enhance our understanding of which NEMP and GMD events create impacts of concern, we develop a parameterization of the hazards generated by NEMP and GMD to classify the events into ranges of common types and make a first attempt to determine which types fall within the bounds of the study discussed above. To that end the following sections will

- Provide an overview of the NEMP and GMD events and the environments they create;
- Develop methods for parameterizing NEMP and GMD events to determine parameter regions of concern'
- Describe the critical bulk power components, with emphasis on discussing how EMP and GMD may couple to and interact with the components; and
- Discuss the restoration of the BES after abnormal events.

3 Overview of Nuclear EMP

The approximate, coarse-grained model that is thought to describe the extremely complicated environment created by a nuclear burst, and how that environment results in electromagnetic fields, is based on a handful of simple physical principles. It is important to fully understand the nuances within this statement. The use of the phrase *thought to* reflects the fact that, due to the Nuclear Test Ban Treaty, there are a relatively small number of experiments with which to validate and verify this approximate model (see (U.S. Department of Energy: National Nuclear Security Administration Nevada Field Office, 2015) for a summary list of U.S. nuclear tests). The use of the descriptor "coarse grain" is intentional. Each step in the process of coarse-graining the physics to create the approximate model is, in actuality, a very rich and deep field of active study. We cannot stress this point enough, the description of the model that follows is *by no means* a complete description—the predictions from such an approximate model should not be expected to be completely accurate. The approximate, coarse-grained model can capture certain features of the EMP created by a burst to within a factor of approximately two or so (e.g., the peak electrical field values and its time dependence). Additional certainty will require new results from important scientific research in this still fairly active field.

The current model, which is largely due to the work of Karzas and Latter (WJ Karzas & Richard Latter, 1962; WJ Karzas & R Latter, 1962) and Longmire (Chavin et al., 1979; H. Longley & Longmire, 1972; H. J. Longley & Longmire, 1973; C. Longmire, 1978; Longmire, 1974; C. L. Longmire, 1978; Longmire, 1986, 1987, 1995, 2004; Longmire & Gilbert, 1980; Longmire et al., 1987; Longmire & Longley, 1973), is accepted by the community largely due to its ability to capture both the magnitude and general temporal behavior observed during the few nuclear tests that capture NEMP data. Advances in computing are providing more and more capability to capture the physical processes at work at a level of detail that may determine if the current approximate, coarse-grained model is actually adequate to describe NEMP processes or uncover overlooked processes that may be important to a complete NEMP description.

With warnings about the limitations of the existing approximate, coarse-grained model given, we provide an overview of this model of NEMP below. As mentioned above, the model is largely due to the work of Longmire. We will begin with a description of the very early time burst for nuclear devices. We will then consider, in turn, the two types of nuclear burst that are within the scope of this study, exo-atmospheric and endo-atmospheric bursts.

3.1 The Very Early Time Burst

There are two types of nuclear devices to consider for NEMP: fission devices and thermonuclear devices. We discuss both types of device below, though we will only briefly discuss thermonuclear devices. Much of this discussion follows Glasstone's monograph, "The Effects of Nuclear Weapons"(Glasstone, 1964).

3.1.1 Fission Devices

When a neutron is absorbed by a large atomic nucleus, it is in an excited state and is unstable. The nucleus either decays to a more stable state or undergoes a reaction that causes it to fall apart into fragments. This latter process is known as a fission reaction. Along with the already-mentioned fission

fragments, fission reactions often release neutrons[9] as well as high-energy photons of light (gamma ray). Figure 4 shows a uranium-235 atom undergoing a fission reaction.

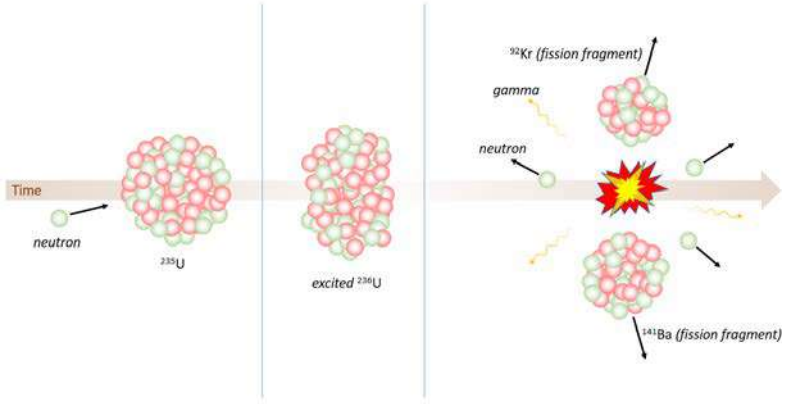

Figure 4: Fission of uranium-235 into fragments.

Explosive fission devices work on an avalanche of fission reactions, called a chain reaction. A chain reaction occurs within a mass of fissile material when enough of the neutrons that are released by a fission reaction go on to initiate further fission reactions, rather than being absorbed by surrounding material or escaping the device entirely. This condition is called “critical mass”.

The basic description of the very early time burst starts just after a mass of fissile material becomes critical. The fission chain reactions begin to build. Highly energetic fission fragments, neutrons, and gammas are ejected with each fission reaction. Because most of the reaction products are deposited within the confines of the fission device, the vast majority of the energy released with each fission reaction goes to heating up the device. This heating, along with the pressure of gammas and neutrons, causes the device to expand. This stage of the burst is depicted in the first frame of Figure 5.

As the expansion of the device continues, neutrons and gammas released by the fission reaction begin to escape the device. The leaking of gammas creates an expanding shell of gamma rays that is inconsequential to the fission reaction, although very important to EMP. The leaking of neutrons creates a similar expanding shell of neutron radiation that is consequential because it reduces the number of neutrons going on to create further fission reactions. As the device continues to expand from the pressure of hot fission fragments and radiation within it, the chain reactions begin to slow down (second frame of Figure 5).

Finally, once the device has expanded far enough, the fission chain reaction shuts down (final frame of Figure 5), which also shuts down the production of neutrons and gammas from fission reactions (though both neutrons and gammas will continue to be produced at a reduced rate by other means). At this point, both the original mass of uranium and any other material in the device has been turned into a ball of highly energetic, intensely hot plasma with temperatures reaching several tens of million degrees. Black body radiation causes the emission of X-ray radiation from the plasma ball. Within the plasma ball,

[9] As a general rule, the larger an atomic nuclei is, the greater its proportion of mass can be in the form of neutrons. Therefore the nuclei of the smaller fission fragments produced by the reaction cannot hold as many neutrons as the initial large nucleus. As a result, along with the two smaller nuclei, a fission reaction typically emits neutrons.

the pressure is many millions of pounds per square inch. A shock wave is released from the expanding plasma ball that follows the expanding shells of neutron and gamma radiation that were able to escape the device prior to the chain reactions shutting down. The end state of the very early times of a fission burst is diagrammed in Figure 6.

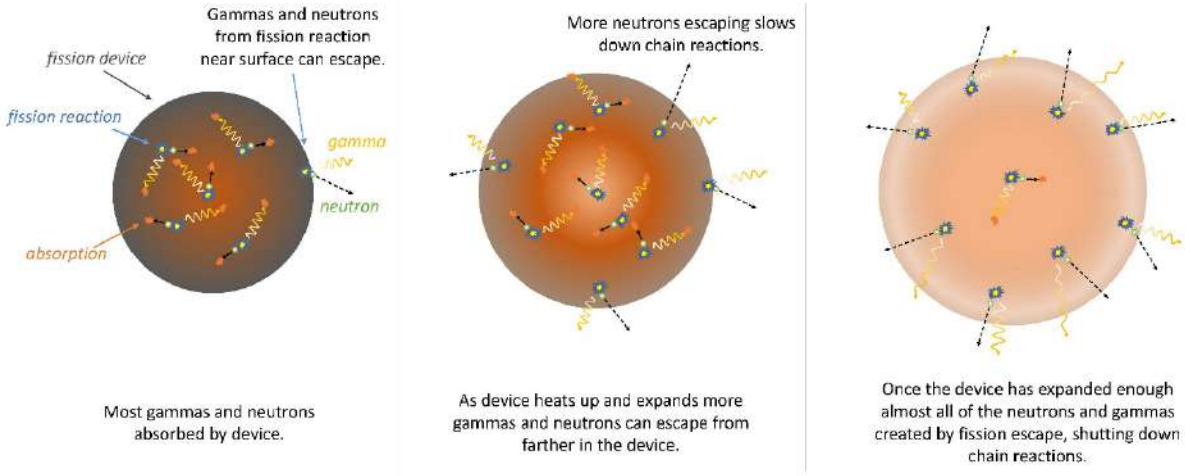

Figure 5: Stages of a fission burst. At very early times most of the fission products (neutrons and gammas) get absorbed by the device itself, heating the device up, causing it to expand and driving the fission chain reaction. As it expands, neutrons and gammas from deeper within the device can escape, slowing the chain reaction. Finally, once the device has expanded enough, most of the neutrons and gammas from the fission reactions escape, shutting down the chain reaction.

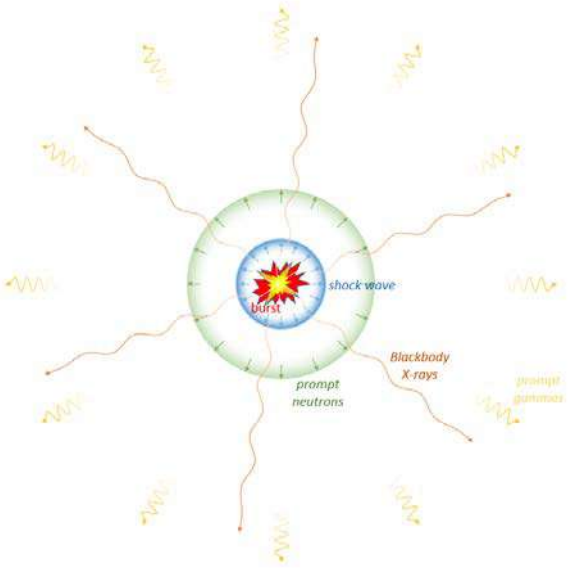

Figure 6: State of fission nuclear burst just after the bulk of the fission reactions cease.

3.1.2 Thermonuclear Devices

Because we are focusing on processes that are important for NEMP, we are able to disregard most of the details of how thermonuclear devices work. The important observations regarding such devices are that they exist as two distinct stages, the primary and the secondary. The primary stage is a fission device, exactly as described in the previous section. The secondary stage utilizes the intense heat, pressures, and radiation created by the primary fission device to trigger a fusion reaction in the secondary stage. The fusion reaction results in a release of significantly increased energy from the device compared to the primary stage. From the standpoint of NEMP, this increased energy changes only one feature when compared to the final state of the early stages of a fission device shown in Figure 6: the plasma ball at the center of the burst is significantly more energetic. As a result the shockwave and X-rays released by the plasma ball are also more energetic. Otherwise the description of the system at the end of the very early times of a burst is largely the same: a plasma ball emitting X-rays surrounded by an expanding shockwave and two shells of neutrons and gammas emitted from the primary fission device.

In summary, from an NEMP perspective, thermonuclear devices look identical to fission devices (see Figure 5), except that the plasma ball at the center of the burst is far more energetic than is its smaller fission device cousin. The higher energy also results in more energetic X-rays and a more intense shock wave.

3.2 Exo-Atmospheric Bursts[10]

In an exo-atmospheric burst, the nuclear device is detonated high above the Earth's surface at an altitude of hundreds of kilometers. Once detonated, it produces a variety of electrical effects. These physical effects are separated by the time scales over which they act. "E1" designates very early time effects at time scales less than a microsecond. "E3" designates long time-scale phenomenon resulting from magneto-hydrodynamic blast effects that span seconds to minutes.

Note that there is a gap in the above times—from microseconds to seconds. This range is designated as "E2". There is a dearth of in depth studies regarding E2; indeed none that the authors are aware of. The lack of information likely stems from the fact that the E2 has time scales and amplitudes comparable to lightning strikes. Because the electric power grid is already hardened to lightning strikes, it is theoretically already hardened to E2's effects. Although the authors tend to agree with this assessment, there are some differences between E2 and lightning: in particular lightning strikes are highly localized phenomenon wherein E2 is effectively a lightning strike simultaneous over a continental-size area. Out of an abundance of caution, the E2 effect, and its coupling to infrastructure, should be thoroughly studied.

Below we provide a high level description of exo-atmospheric bursts, and how these bursts result in electromagnetic effects. The discussion of the work that follows mirrors the work of Longmire (Chavin et al., 1979; Longmire, 1995). In particular the pictorial representations of EMP burst are, for the most part, recreations of images in the appendix of (Chavin et al., 1979).

[10] Exo-atmospheric bursts only significant damage path is through electromagnetic pulse. Thus, such bursts are frequently referred to as high-altitude electromagnetic pulse (HEMP) insults.

3.2.1 Scale and Time

To begin our description, we need an appropriate representation of the spatial scales that take place in an exo-atmospheric burst. To understand the scale of such bursts with respect to the Earth, in Figure 7, we depict a roughly scale drawing of an exo-atmospheric nuclear burst 400 km above New York in summer at midnight.

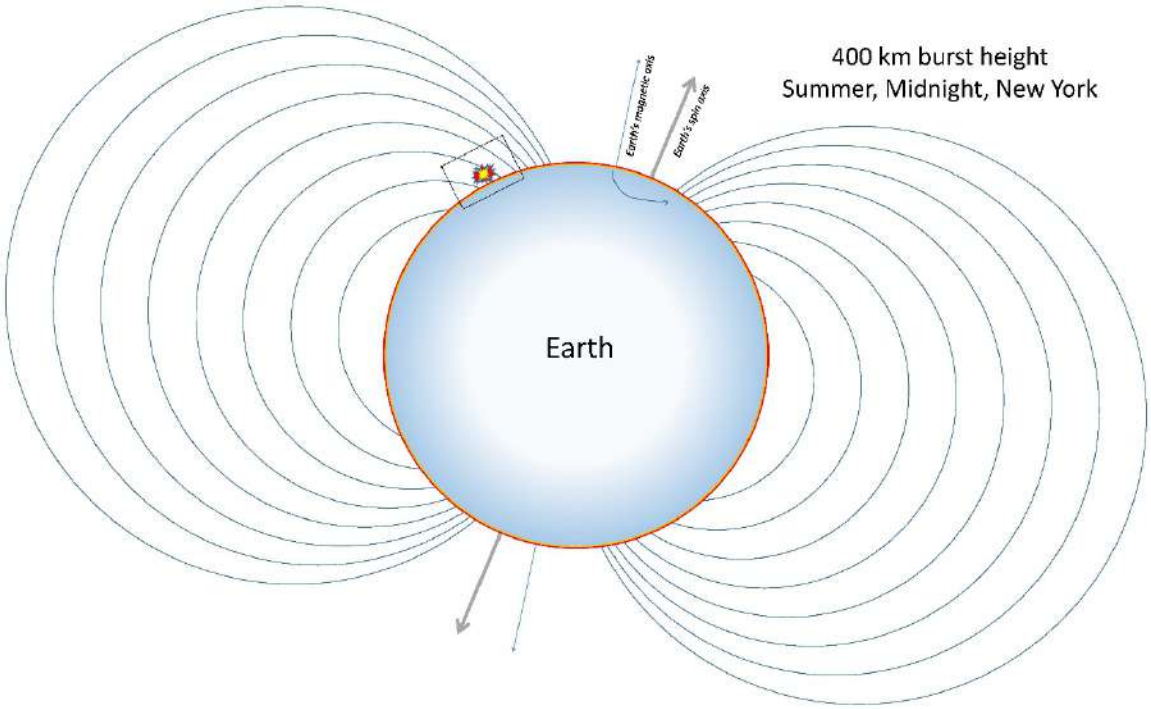

Figure 7: Approximate scale depiction of a 400-km altitude exo-atmospheric burst above New York at midnight during the summer (the sun would be to the right of the image). We do not depict the compression of the magnetic field due to solar wind. Later figures of the nuclear burst will focus on the region outlined by the box. The yellow and red bands that are barely noticeable near the surface of the Earth are scale depictions of the gamma and X-ray absorption layers, discussed below.

There are two items of note in Figure 7. First, there are layers of atmosphere in which X-rays and gamma rays emitted by the burst will get absorbed (typically around $100\ km$ and $30\ km$ elevation respectively). These layers are depicted in Figure 7 as almost imperceptible red and yellow circles near the surface of the Earth. Second, the burst is happening within the background of the Earth's magnetic field. The magnetic field points from south to north.[11] What is less well appreciated is that the field also points upward from the surface of the Earth in the southern magnetic hemisphere and downward in the northern hemisphere. Consider the field lines in the box—they point downward into the Earth's surface at a significant angle. The images of exo-atmospheric bursts that follow depict occurrences in the box of Figure 7.

Now that we have oriented the reader in terms of spatial scales, we need an appropriate timeline. We use the typical temporal representation of the electric field created by an exo-atmospheric burst at some point on the ground, shown in Figure 8. We stress that this waveform is a representative depiction

[11] The geomagnetic North Pole is a negative magnetic pole. The magnetic field lines of the Earth are directed from the South Pole to the North Pole.

only. It is satisfactory for use as a timeline, but little else. The early time peak in the diagram at around $10^{-8}\ s$ represents the E1 peak, while the double peak between $10^{0} \leftrightarrow 10^{2}\ s$ represents the E3 signal. Although E2 is not part of our discussion, it spans the $10^{-6} \leftrightarrow 10^{-2}\ s$ time scales.

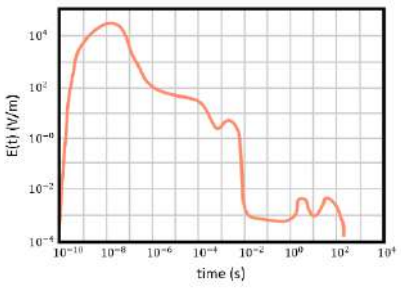

Figure 8: Representation of electric field created by an exo-atmospheric burst.

3.2.2 E1

We begin our description of exo-atmospheric bursts just after the very early time burst phenomenology described above (just after Figure 6). The plasma ball at the center of the burst region continues to expand and emit X-rays. Prompt gammas that were emitted from the fission device and were expanding in a roughly spherical shell only few meters thick have traveled from the burst point, through the intervening rarified gas at the edge of space, and begun to interact with an atmospheric layer around $30\ km$ above the Earth's surface (the yellow line in Figure 7). Similarly, the X-rays emitted by the burst have also impacted the atmosphere, but they are absorbed somewhat higher up within a layer of air about $85\ km$ above the Earth's surface (the red line in Figure 7). Following these two sets of photons is a much slower moving shell of prompt neutrons that have escaped the device (these are primarily important for E2), and finally, the blast shockwave. This process is illustrated (not to scale) in Figure 10.

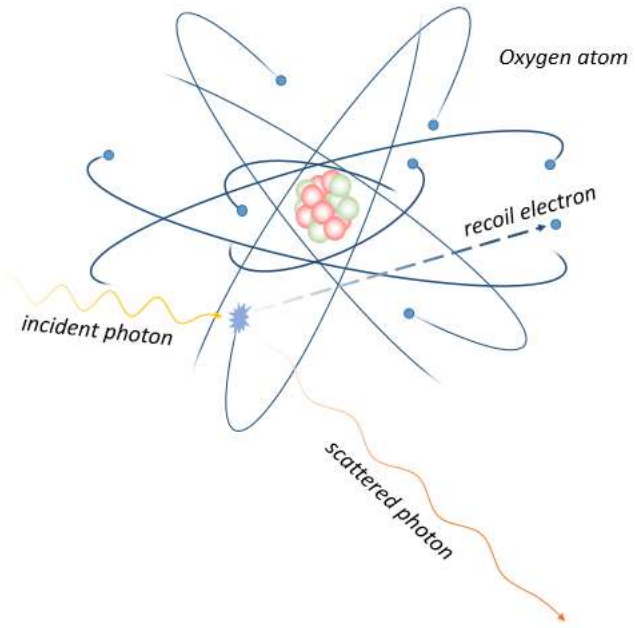

Figure 9: Compton scattering of an incident high energy photon
off one of an oxygen atom's outer electron. This positively ionizes the oxygen atom.

We focus on the gamma ray absorption layer in Figure 10 because it is the origin of the E1 pulse. We will return to the other effects when we discuss E3 in a later section. The primary interaction occurring within the gamma absorption layer is a process known as Compton scattering, which describes the interaction of photons, generally in the gamma band of the electromagnetic spectrum with electrons.

During Compton scattering with an atom, a high-energy photon transfers some of its energy and momentum to the atom's electron, dislodging the electron, now called a "recoil" electron, and scattering the now-lower energy photon at an angle that conserves momentum and energy. During this process the atom becomes positively charged, also called positively ionized, because it no longer has the same amount of negatively charged electrons in orbit around the nucleus as positively charged protons in the nucleus. This process is shown in Figure 9. Because Compton scattering is a quantum mechanical process, the result of any particular Compton scattering event is an inherently statistical process; however, the probabilities are well defined and display two important trends.

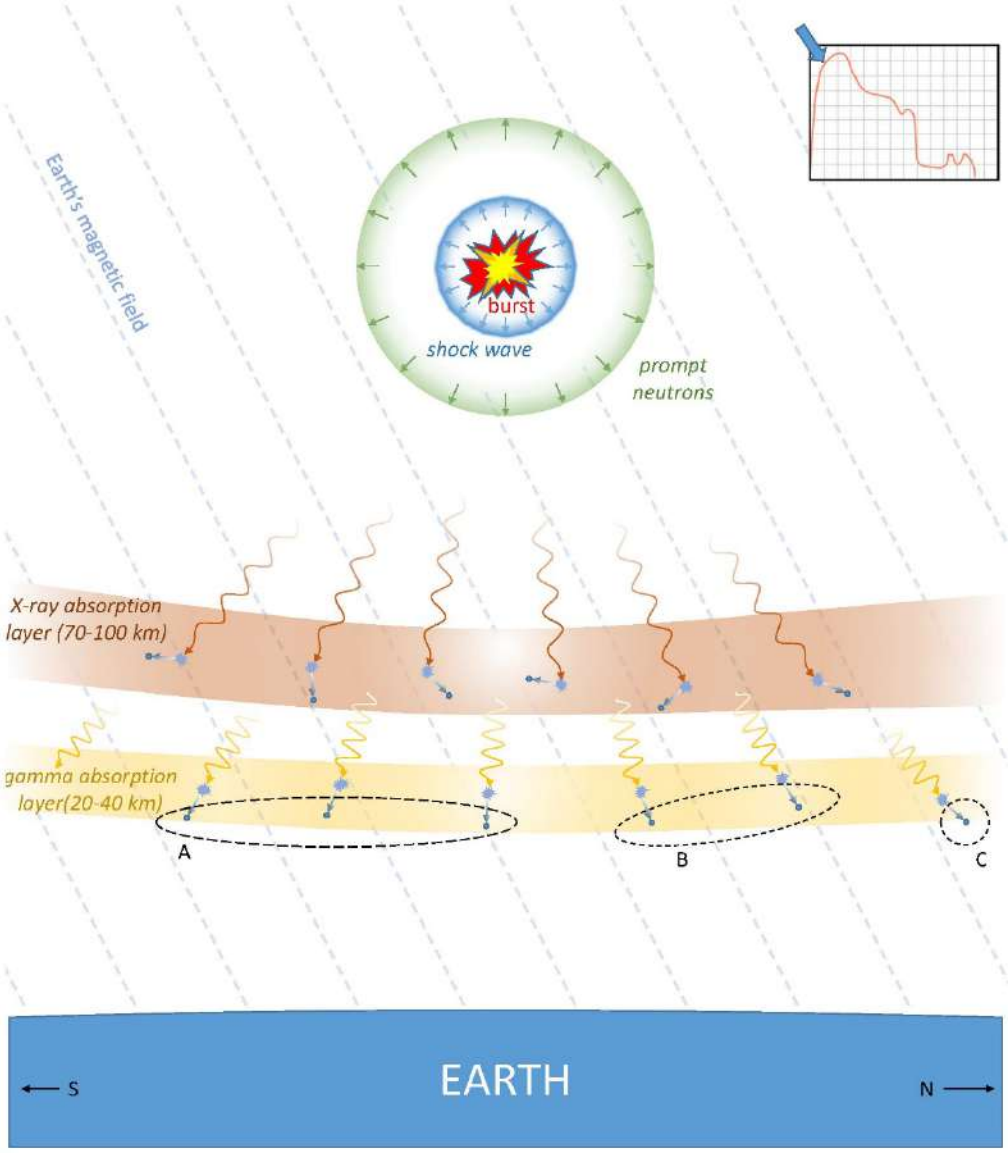

Figure 10: Early time in exo-atmospheric burst (note timeline in upper right corner) for the region indicated by the box in Figure 7. X-rays are represented by reddish waves, gammas by yellow waves. Electrons freed by X-rays and gammas from air molecules through various processes described in the text are indicated by blue circles.

The first trend is that the recoil electron and scattered photon are more likely to be emitted in the "forward" direction as the energy of the incident photon increases. Here, the forward direction means along the same path and in the same direction that the incident photon was traveling. The counter argument is also true; as the incident photon energy decreases, the scattered photons and recoil electrons are less directed and will deviate more from the forward direction.

The second trend is that as the incident photon becomes more energetic, it transfers more of its energy to the electron in the collision, causing the electron to recoil at higher velocities. As such, a low energy photon, when Compton scattered, will retain most of its energy and the electron will gain only a small amount of energy. A high-energy photon like the prompt gammas in Figure 9, on the other hand, will lose the majority of its energy and cause the electron to recoil at velocities approaching the speed of light.

The gamma rays emitted by nuclear devices are highly energetic. Following the second trend mentioned above, about half of a gamma's initial energy is transferred to the first recoil electron in the gamma absorption layer by Compton scattering. The recoil electron is emitted at about 90% the speed of light. Following the first trend mentioned above, the recoil electron is generally emitted in the forward direction. Because the prompt gammas travel radially away from the burst, the recoil electrons, on average, initially travel radially away from the burst. Compton scattering is indicated in Figure 10 at the end of the gammas (the yellow waves) by a light blue star with the resultant recoil electron indicated by a dark blue circle with blue arrow indicating direction of motion. We omitted the scattered gamma and ionized atom for simplicity.

Now consider what happens to one of the recoil electrons once it is freed from its now ionized atom. The first effect to consider is that the recoil electron is moving in the Earth's magnetic field, which points north and into the Earth (for the location of the box (Figure 7). If the electron moves along the magnetic field, such as the electrons in the dashed oval labeled B in Figure 10, it feels no magnetic force. If the electron moves across the field line, it feels a magnetic force perpendicular to both its motion and the magnetic field line. The electrons in the dashed oval labeled A will feel an initial deflection towards the west (into the page, recalling that the electron is negatively charged), while the electron in the dashed oval labeled C will initially deflect east, opposite from the electrons in A because it crosses the field in the opposite direction. This motion shown for an observer looking upward along the field lines in Figure 12. If there were no other effects the electrons would continue to deflect and eventually orbit around the field lines in a circle with about a $85\ m$ radius[12] on their way down to the Earth.

There are other effects however, because the recoil electrons are not in a vacuum. They are traveling through a layer of air and interacting with surrounding air atoms. Ignoring the Earth's magnetic field for the moment, when a recoil electron travels through matter, it interacts with surrounding atoms. This is illustrated in Figure 11. The recoil electron does not have to "collide" with an atom to transfer energy because the recoil electron and the electrons bound to the atoms in the matter are both negatively charged, so they feel a repulsion. In a very real sense, the electron produces a wake, much like a boat in the ocean.

Atoms caught in the recoil electron's wake will receive some energy from the electron, thereby slowing the recoil electron down. Sometimes in this interaction, sufficient energy is transferred to cause one of the atom's electrons to become excited enough to become free, thus creating a second lower energy free electron moving through the air. Free electrons created in this way are called secondary electrons. Sometimes just enough energy is transferred to excite the atom and have it release a low wavelength photon. In either case a small amount of energy is transferred from the recoil electron to the surrounding air, heating up the region in the recoil electrons wake and slowing the recoil electron down. This process continues until the recoil electron does not have enough energy left to remain free and is recaptured by an atom. Depending on whether the recapture atom was already ionized, this final step in the process results in either a neutral atom or negatively charge ion. For the recoil electrons created by Compton scattering in the gamma absorption layer of Figure 10, the density of the air and the electron's initial energy is such that recoil electrons can travel about $170\ m$ before losing the majority of their energy. During this transit, the recoil electrons free $20{,}000 \leftrightarrow 30{,}000$ secondary electrons.

[12] Their Larmor radius for an electron traveling in a $0.8\ Gauss$ field at 90% the speed of light. The exact radius depends on the angle with which the electrons cross the magnetic field lines. The Larmor radius applies for particles initially crossing the field lines at right angles.

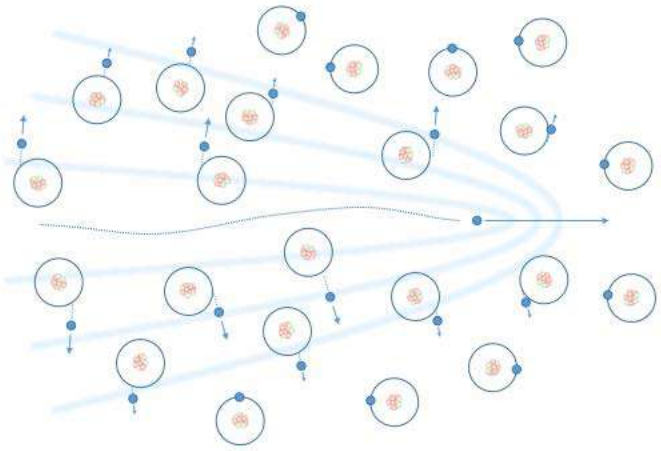

Figure 11: Recoil electron moving through air, interacting with surrounding atoms and creating secondary free electrons.

Recall that the radius of the electrons orbit due to orbiting the Earth's magnetic field lines is around $85\ m$. To complete a full orbit around the magnetic field lines, the electron must travel at least $534\ m$. Due to the interaction with air molecules described above, the recoil electrons only travel about $170\ m$ before being recaptured. The recoil electrons that get both deflected by the Earth's magnetic field and interact with surrounding air molecules travel, at most, about one-third of the way around an orbit before losing their energy.

To summarize, the incident gammas traveling radially from the burst point interact via Compton scattering with atoms in air molecules creating recoil electrons that travel at velocities approaching the speed of light radially away from the burst point. Depending on the orientation of the Earth's magnetic field with respect to the recoil electron's velocity, the recoil electron's motion is deflected into an orbit around the magnetic field lines as it travels. During their travel, the recoil electrons interact with surrounding atoms within the atmosphere and free secondary electrons, heat up the gamma absorption layer, and lose the energy they gained from the gamma during Compton scattering. Over about one-third of an orbit around the Earth's magnetic field, the recoil electrons lose all of their kinetic energy and are recaptured by air molecules, forming neutral atoms or negative ions.

An observer on the ground looking upwards along the magnetic field lines will see a brief but intense electrical current within the layer that initially travels radially away from the burst point, which is deflected by the Earth's magnetic field, and quickly dissipates. This current, called the Compton current because it was created by Compton scattering, is the total motion of the recoil electrons. It is illustrated for an observer looking up along the Earth's magnetic field lines in Figure 12 for the three regions indicated in Figure 10. The observer will also see the gamma absorption layer heat up and become conductive; a result of the recoil electrons interacting with surrounding matter and freeing secondary electrons.

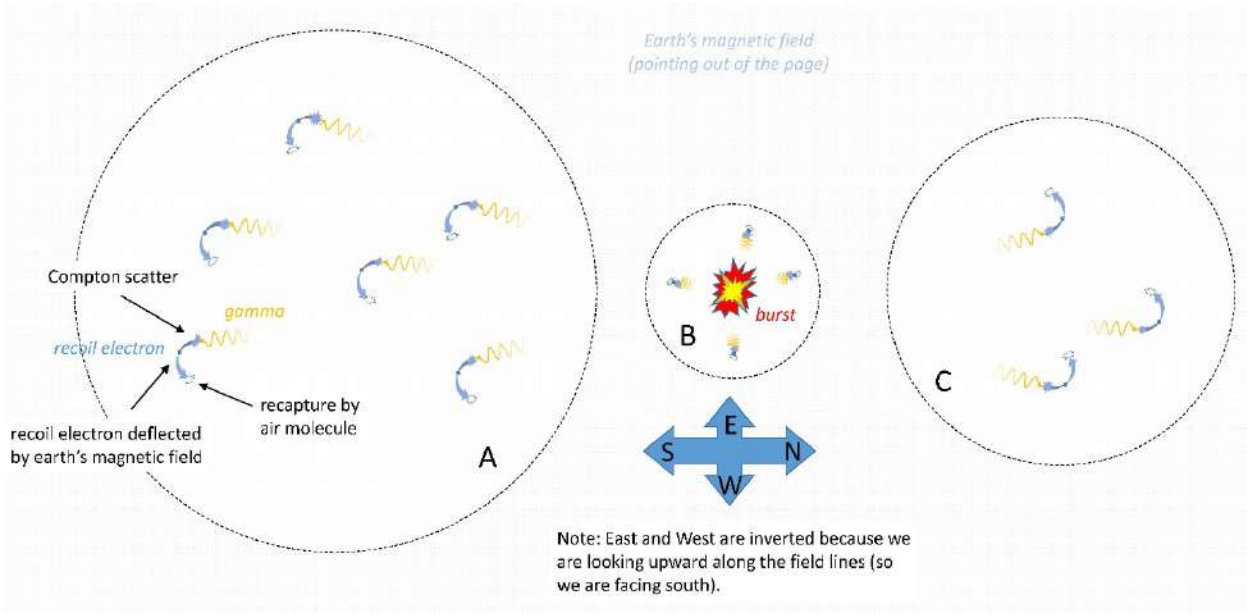

*Figure 12: Electron motion for the three regions indicated in Figure 10. The viewpoint is an observer on the surface of the Earth looking upward **along the Earth's magnetic field lines** (along the light blue lines in Figure 7 and Figure 10). For all regions there is an average electron motion out of the page (i.e., away from the burst), and therefore a vertical Compton current directed into the page[13]. Along with this motion, electrons in region A are deflected westward resulting in an eastward lateral Compton current. Electrons in region C are deflected eastward resulting in a westward lateral Compton current. Electrons in region B are not deflected at all resulting in no lateral Compton current.*

The intense Compton current generated within the gamma absorption layer is time varying because it starts at zero, grows rapidly in strength as the number of Compton recoil electrons increase and finally dissipates back to zero once all of the gammas have scattered and the recoil electrons recombine with atmospheric atoms. The recoil electron current within the gamma absorption layer behaves like an enormous radio antenna that broadcasts a short electromagnetic field pulse towards the ground.[14] This broadcast is the E1 electromagnetic pulse created by the nuclear burst. Like the current that produced it, the pulse strength starts off at zero, rapidly rises as the current grows stronger with more Compton scattering, and dissipates back to zero once the gammas have all scattered and the recoil electrons recombine with atmospheric atoms.

Figure 13 depicts the electron motion in the gamma absorption layer and the E1 pulses they create. Note that only regions A and C emit an E1 pulse traveling towards the ground. Going back to the antenna analogy, the bulk of the electromagnetic energy emitted by a radio antenna travels perpendicular to the antenna axis, in this case, perpendicular to the motion of the Compton current. The electrons, and thus the Compton current, in regions A and C in Figure 13 have considerable horizontal motion, so they emit E1 pulses that travel vertically towards the ground. We note that the Compton currents in A and C are directed in the opposite directions, with A predominantly eastward (into the

[13] The Compton current is opposite the direction of electron motion due to the electrons negative charge.
[14] Another way of thinking about this is to consider each recoil electron as an infinitesimally small radio antenna and an observer on the ground receives the total broadcast from the sum of all of these little radio antennas.

page) and C predominantly westward. This means that though both regions A and C emit pulses that travel vertically, the electromagnetic fields they emit are of opposite sign.

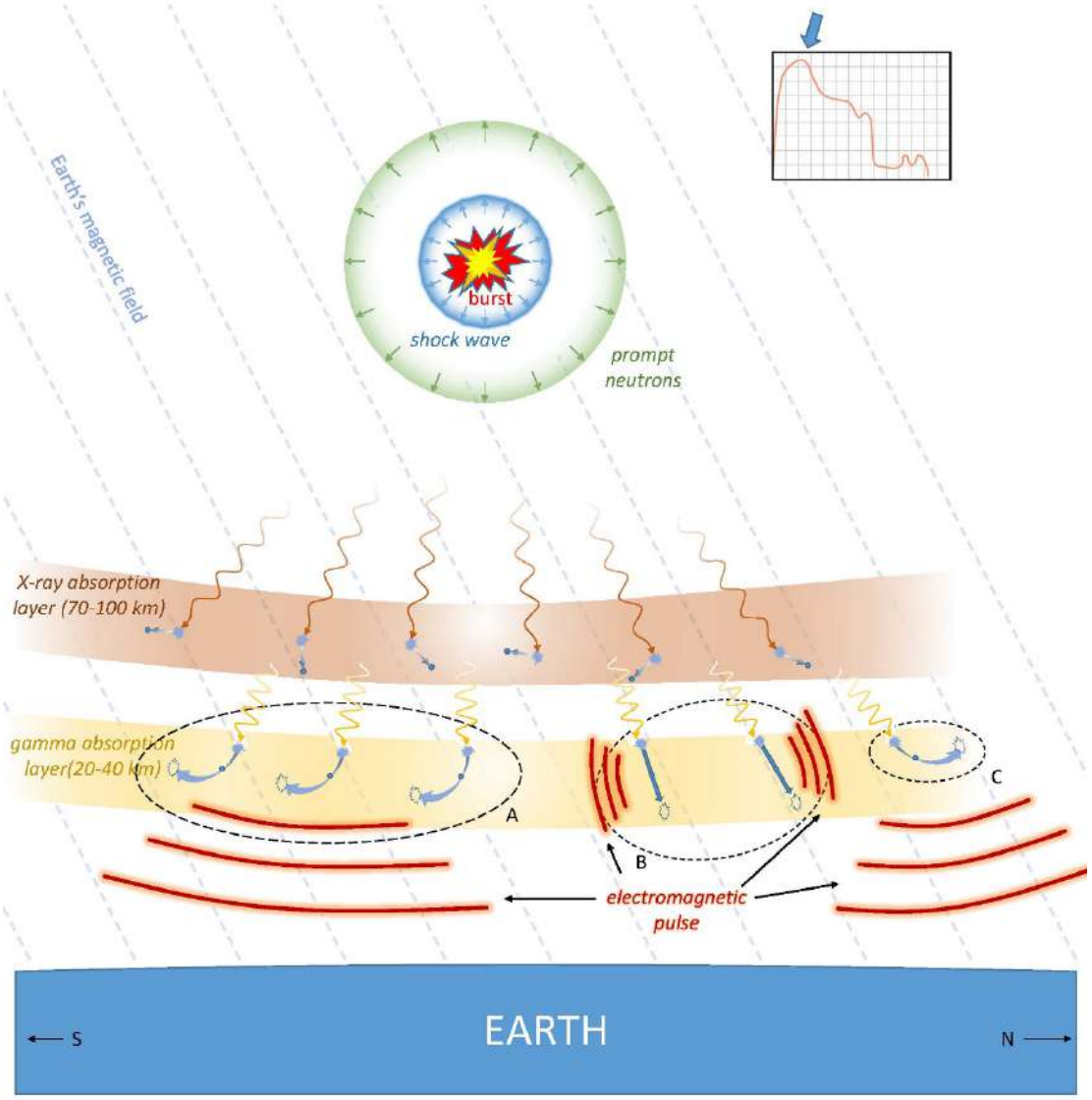

Figure 13: Depiction of the E1 pulse created by the deflected Compton electrons in the gamma absorption layer. Pulses created by patch A and C travel toward the ground and create the early time E1 pulse. Patch B electrons do not deflect and produce a pulse that travels parallel to the ground. This pulse does not build because it travels perpendicular to the gamma wave moving through the absorption layer and quickly dissipates due to the conductivity of the layer.

In contrast to regions A and C, electrons, and thus the Compton current, in region B of Figure 13 have predominantly vertical motion, so they emit an E1 pulse that travels horizontally. This horizontal pulse does not build because it moves perpendicular to the motion of the gammas through the layer. What little pulse does get emitted quickly dissipates within the gamma absorption layer by conductivity effects described below.

As we conclude the description of how the E1 pulse is generated, note that along with the basic generation mechanism, we are also able to understand the temporal behavior and some of the spatial behavior of the pulse. For the temporal behavior, the pulse rises exponentially fast as the expanding shell of gammas emitted by the fission device impacts the gamma absorption layer and generates Compton current. It then decays as the gammas become exponentially attenuated by Compton scattering. This time dependence forms the common "double exponential" used to describe E1 NEMP (an exponential rise followed by exponential decay).

For the spatial behavior, we expect little to no pulse along the Earth's magnetic field lines below the pulse, and oppositely directed fields north and south of this location. The strongest fields should be roughly were the Compton currents intersect the Earth's magnetic field perpendicularly. The result is the so called "smile" diagram shown in Figure 14.

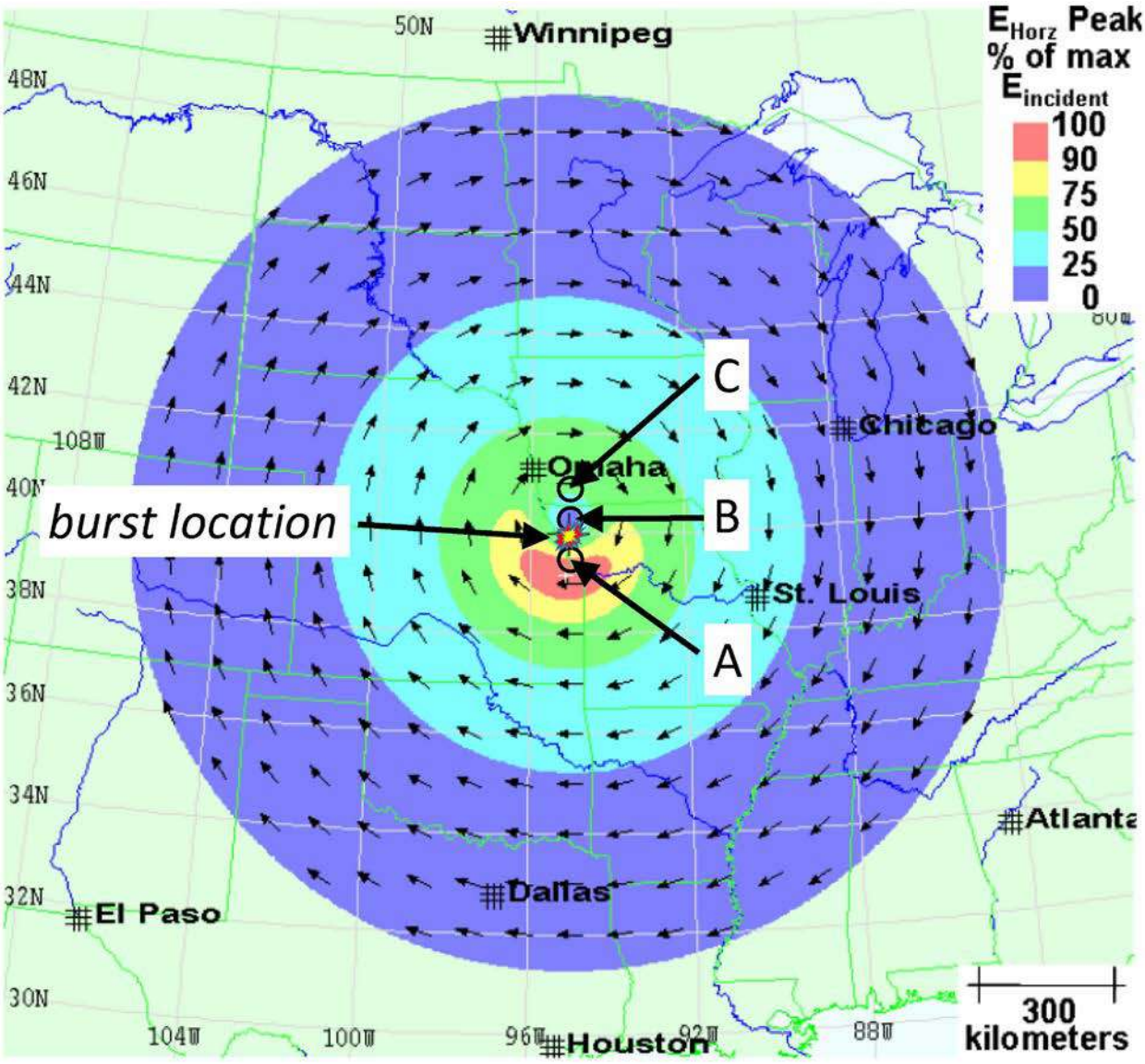

Figure 14: "Smile" diagram of the horizontal electric field component of E1 pulse (the vertical component is significantly weaker). We have indicated the burst location (yellow and red explosion) as well as regions A-C from

Figure 12 and Figure 13 on the diagram. The original smile diagram is copied from (Savage et al., 2010). This diagram should be compared to the electron motion/Compton current displayed in Figure 12.

As described above, the model could be used to estimate field strengths, but it would overestimate the pulse's strength by a considerable amount. To understand why requires discussion of the charge separation created by the motion of the recoil electrons.

As the gammas released from the fission burst travel through the gamma absorption layer, they generate recoil electrons that travel radially away from the burst with a spiral motion caused by the magnetic field as discussed above. This motion continues until the electron is eventually recaptured by an air atom. From a large-scale point of view, a region of neutrally charged matter loses electrons, becomes positively charged, and the freed electrons are deposited some distance way, creating a spatial charge separation.

A charge separation generates an electric field pointing from the region of positively charged matter to the region of negatively charged matter. Figure 15 depicts this separation for a small region in the gamma absorption layer. The electric field attempts to pull electrons in the direction opposite to the field direction. This pull has little effect on the recoil electron due to its very high energy. There is, however, a bath of relatively low energy secondary electrons that can be pulled by the electric field. Recall from our earlier discussion that each recoil electron created $20{,}000 - 30{,}000$ secondary electrons as depicted in Figure 11, which are pulled in the direction opposite the electric field creating a return current.

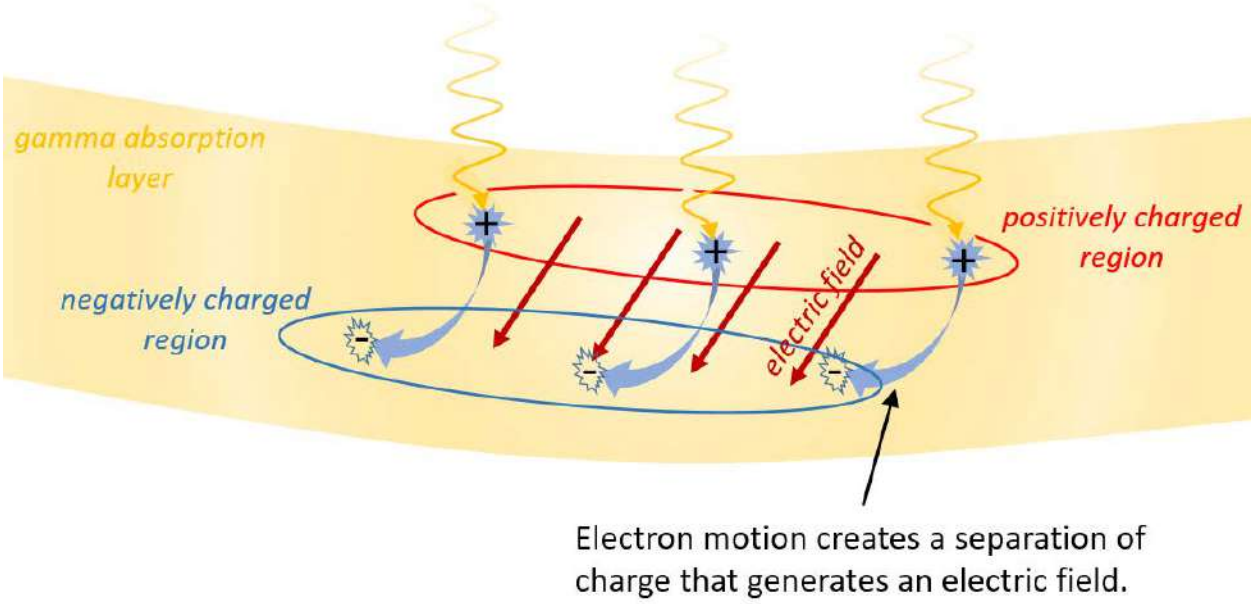

Figure 15: Separation of charge caused by the motion of recoil electrons within the gamma absorption layer. This separation of charge generates an electric field in the direction of the electron motion.

To summarize this part of the process, the when the gammas from a fission burst create recoil electrons through Compton scattering, the resulting motion of recoil electrons causes a separation of charge and generates secondary electrons. The separation of charge creates an electric field. This electric field pulls the secondary electrons along a return path creating a return current in the opposite direction to the original motion of the recoil electrons.

The return current is moving in the opposite direction of the recoil electrons average displacement and spirals around the Earth's magnetic field in the opposite direction as the Compton current. The resultant current (the Compton current plus the return current) tend to cancel one another out limiting the magnitude of the E1 pulse. At first, there are not many free secondary electrons to produce a return current, and the E1 pulse can build because there is only a small return current to balance the Compton current. Eventually, as more secondary electrons are created by recoil electrons, the return current builds until it balances the Compton current. At this point there is no net current, therefore, the magnitude of the EMP cannot increase.

This limiting feature results in a very counterintuitive conclusion: the magnitude of the pulse created by a fission device depends only weakly on the device yield; doubling the fission devices yield, e.g., going from $10\ kTon$ to $20\ kTon$, does not double the size of the E1 pulse. Although a larger device results in more gammas and, thereby, more recoil electrons and larger Compton current, it also means there are more secondary electrons, a larger separation of charge and a larger return current. A larger device does not net a proportional increase in the E1 pulse magnitude as both the Compton current and opposing return current have increased.

To conclude the discussion of E1, we repeat the warning noted in the introduction to this section—the description given above is only a crude model of what actually occurs to generate E1 NEMP. To aid in the understanding of the phenomena, a number of simplifications have been made in the discussion above that are technically inaccurate. We have omitted many subtleties because they are entire active fields of research. Moreover, although we have presented the above as if it was "settled" science, by no means is this the case. Models of the E1 pulse incorporating more physical effects and more detail on the effects we described above are still being developed to this day.

3.2.3 E3

By the time the E3 phase of an exo-atmospheric burst begins, the Compton currents and conductivity within the gamma absorption layer have dissipated and play no further role. The later time electrodynamics of exo-atmospheric bursts are driven by altogether different physical effects than create E1. The primary physical effect at work in the E3 phase involves the motion of plasma, ionized weapon debris, and ionized atmosphere within the Earth's magnetic field. However, we first return to Figure 10 and consider the X-ray absorption layer of the atmosphere.

The X-rays from the nuclear burst are produced from the plasma ball by a process called blackbody radiation. Blackbody radiation links the frequency of light emitted by an object to its temperature (hotter objects emit higher frequency light). Because the plasma ball created by a nuclear burst is very hot, it emits X-rays. It will continue to emit these X-rays as long as the plasma ball remains hot. For an exo-atmospheric burst, this can be a few to tens of seconds. These X-rays continue to affect the X-ray absorption layer for a few seconds after the burst, which is in contrast to the gamma absorption layer,

which dissipates quickly because the burst only produces significant numbers of gammas in the very early stages,

Within the X-ray absorption layer, X-rays are interacting with air atoms by a process known as the photoelectric effect. Specifically, the photoelectric effect describes the interaction of photons, generally in the low energy (soft) X-ray band and ultraviolet band of the electromagnetic spectrum, with electrons bound to atoms. Unlike the prompt gamma rays, the energy of the X-rays is not much larger than the binding energy of an electron in an atom in an air molecule, meaning that the fact that electrons are bound to atoms cannot be ignored. Depending on the energy of the incident photon, the coarsest representation of the photoelectric effect can be either a one- or two-step process (see Figure 16).

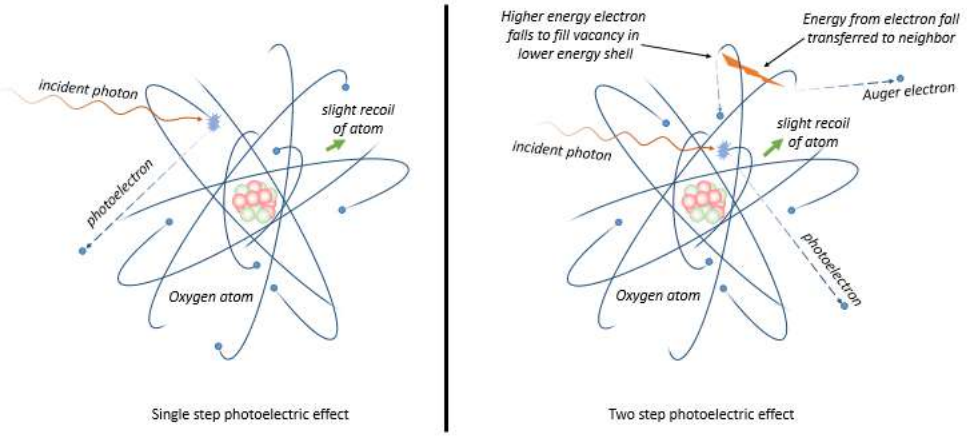

Figure 16: A single step, and two-step photoelectric effect for small atoms (heavy atoms would have a two-step process as well that emits X-rays and, possibly, Auger electrons).

In either the one- or two-step process, the first step of the photo-electric effect involves the incident photon interacting with an atom's electrons by annihilating itself and transferring all of its energy to the atom's electron. The electron (now called a photoelectron) gains enough energy to be liberated from the atom. To conserve momentum, a small amount of energy and momentum is also transferred to the atom's nucleus, although this latter effect is ignored except insofar as it is required to balance energy and momentum equations. Just as in Compton scattering, the photo-electric effect results in a free electron and a positively ionized atom.

If the incident photon is of high-enough energy to create a photoelectron from one of the electrons closer to the atom's nucleus, then the result of the photoelectric effect is an ionized atom in an excited state; i.e., the atom has electrons in orbits farther away from the nucleus and an electron "vacancy" in an orbit closer to the nucleus. In this case the photoelectric effect has a second step, during which the atom relaxes from its excited state. The relaxation process depends significantly on the size of the atom. For lighter atoms, such as those that occur in air, an electron falls to fill the vacancy left by the photoelectron by transferring its energy to a neighboring electron. This neighboring electron, called an Auger electron, is then ejected from the atom as well, doubly ionizing the atom. For heavier atoms, such as metals, the excited atom emits a photon of light (a fluorescence X-ray) as it relaxes to the ground state. In so doing an electron falls to fill the vacancy left by the photoelectron. Auger electrons may also be emitted in this process.

A direct consequence of the complete annihilation of the photon in the first step of the photo-electric effect is that pure forward scattering of the photoelectron is not allowed, regardless of energy. For X-ray photons emitted from the hot plasma ball, only half of the ejected photoelectrons in the X-ray absorption layer are within 60° cone of the forward direction.

The wide angle of photoelectron emissions within the X-ray absorption layer results in little coherence of motion of photoelectrons, which is in contrast to the recoil electrons in the gamma absorption layer. There is no pulse generated from the X-rays, nor a significant separation of charge. The X-ray layer does, however, heat up and become highly conductive due to the number of free photoelectrons and Auger electrons within the layer. This conductivity, unlike in the gamma absorption layer, does not dissipate quickly because the layer continues to be bombarded by X-rays from the hot plasma ball for seconds after the burst. We saw in the previous section that conductivity of the gamma layer played an important role in limiting the E1 pulse. We will see later in this section that the conductivity in the X-ray layer plays a related role in the E3 phase.

There are two stages of the E3 magneto-hydrodynamic electromagnetic pulse portion of an exo-atmospheric burst: the blast stage and the heave stage. The combination of these stages constitutes the E3 pulse that last from seconds to a few hundred seconds. In Figure 8, the blast stage is the small pulse between $10^0 s \leftrightarrow 10^1 s$ and the heave stage is the small pulse between $10^1 s \leftrightarrow 10^2 s$.

3.2.3.1 E3 Blast

During the blast stage of E3, the bomb debris, which is a plasma at this point and, therefore, a very good conductor, begins to expand away from the burst point. This material is initially traveling at radial speeds of $10^2 - 10^3 km/s$. Within a second after the burst, the plasma ball grows to hundreds of kilometers across. As such, the nuclear burst creates a rapidly expanding conductive plasma bubble embedded within the Earth's magnetic field, high in the upper atmosphere. This expanding plasma ball is displayed as the round red shape in Figure 17.

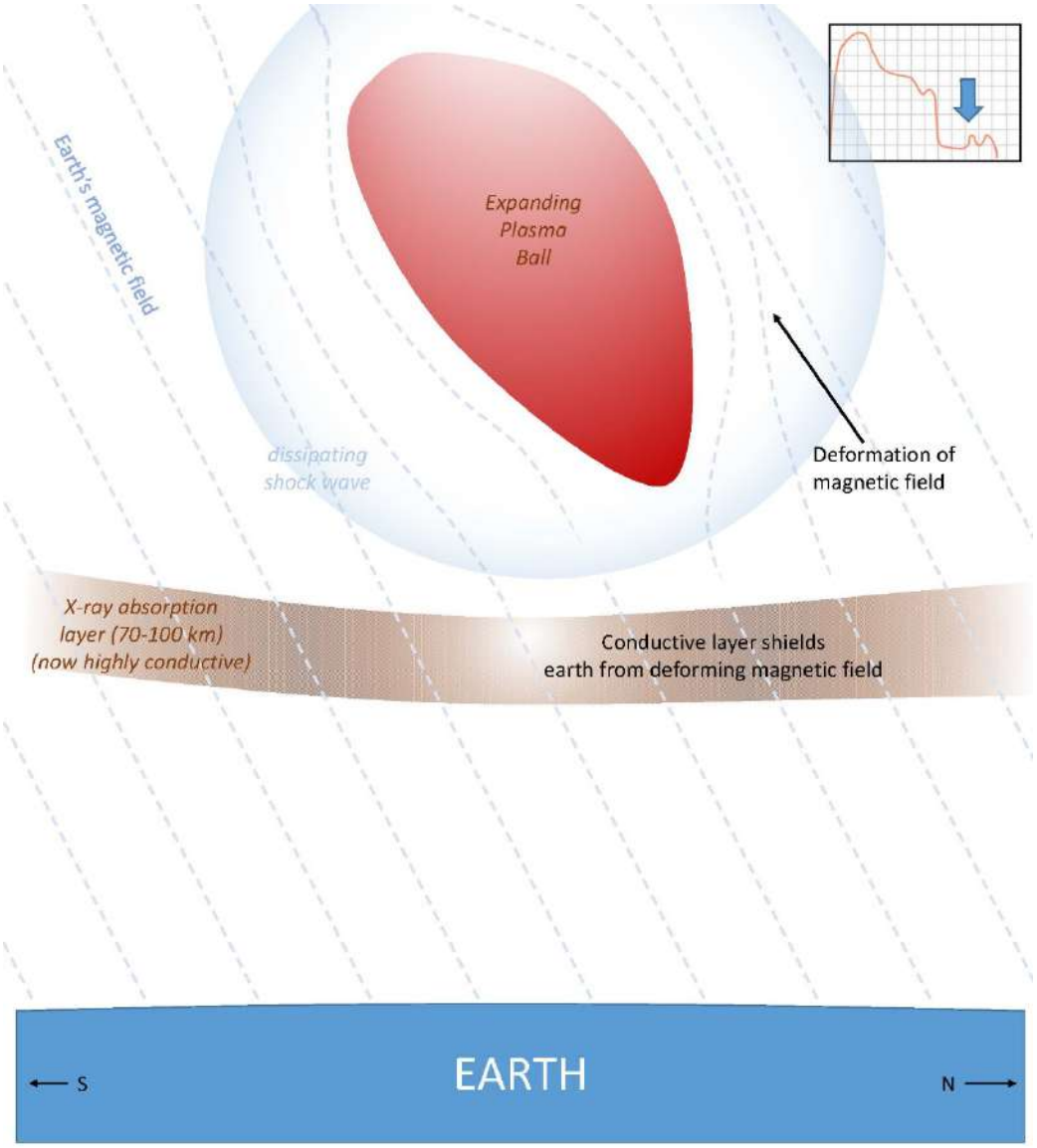

Figure 17: E3 blast stage of an exo-atmospheric burst. The expanding plasma bubble expels the Earth's magnetic field lines causing the magnetic field to deform. This deformation would cause significant ground fields were it not for the highly conductive X-Ray layer pinning the field lines and shielding the ground from the fluctuations.

Conductors in magnetic fields try to keep the total number of magnetic field lines (called the magnetic flux) penetrating their surface fixed by generating internal currents to oppose any magnetic field changes. In the case of a nuclear burst, the total amount of the Earth's magnetic flux that penetrates the plasma ball starts out very small, effectively zero because immediately after the burst the plasma bubble is only a few meters across. As the plasma bubble expands, internal currents create a magnetic field within the conductive plasma bubble that cancel the Earth's magnetic field and effectively expel the Earth's magnetic field from the expanding bubble, causing the Earth's field lines to deform around the plasma bubble. This is diagramed in Figure 17. The time-evolving deformation of the Earth's magnetic field lines by the plasma ball creates electrical fields at the Earth's surface in way equivalent to geo-magnetic disturbances caused by coronal mass ejections. These surface fields constitute the blast phase of the E3 pulse.

The size of the plasma bubble and its distance from the Earth determine the magnitude of the blast phase of the E3 pulse, because larger plasma bubbles result in larger deformations of the Earth's magnetic field and the proximity to the Earth's surface affects the geomagnetic field magnitude at the surface. The two main factors that determine the size of a plasma bubble are the yield of the device that created the burst and the altitude of the burst. In the first case, larger yield devices create more energetic and larger plasma ball and create larger disturbances to the magnetic field; a tenfold increase in device yield will create a tenfold increase in the E3 blast pulse magnitude.

The effect of the altitude of the burst is somewhat more complicated. Altitude determines the degree that dissipative effects slow the plasma bubble expansion. There are two such dissipative effects: magnetic pressure due to the plasma bubble's expelling of the magnetic field lines and frictional effects from bomb debris moving rapidly through the atmosphere.

In the first of these effects, the expelling of the Earth's magnetic field lines, the expanding plasma bubble transforms some of its kinetic energy of expansion into internal electrical currents. The resulting "magnetic pressure" slows the expansion, and effect that is stronger for expansion perpendicular to the field lines than parallel to the field lines. This asymmetry explains why the red region in Figure 17 is elongated along the Earth's magnetic field.

The second dissipative effect that slows the expanding plasma bubble of ionized debris is the friction with the atmosphere through which the debris moves. The atmosphere at these altitudes is very low density, however the bomb debris moves at considerable speed, so the frictional force is also considerable. Moreover, the force is asymmetric because the air above the blast point has a lower density than the air below, thus the bubble expands upward faster than downward, which produces the top heavy egg shaped plasma bubble drawn in Figure 17.

As mentioned earlier, these two dissipative effects depend on altitude. At low altitudes, both dissipative effects are present, but the frictional effect is by far the dominant effect. As the altitude increases, the frictional effect of the atmosphere becomes less important because the density of the atmosphere decreases. For bursts altitudes in excess of $300\ km$, the magnetic pressure becomes the dominant dissipative effect. Thus nuclear bursts at higher altitude result in a larger plasma bubble and a larger deformation of the Earth's magnetic field.

The larger plasma bubble at higher altitude is balanced by a decrease in the effect at the Earth's surface when the plasma bubble is more distant. Plasma bubbles that are farther away create smaller magnetic field variations at the Earth's surface. As a result, for a given device yield there is an optimal altitude for which the bubble can grow as large as possible while still strongly coupling to the surface of the Earth.

If the expanding plasma ball from the E3 blast phase was the only physical effect, it would be capable of generating very strong electrical fields on the Earth' surface. There is, however, a compensating effect created in the highly conductive X-ray absorption layer between the expanding plasma ball and the Earth's surface.

Like the plasma ball, the X-ray absorption layer is a very good conductor and it will oppose changes in the magnetic flux that penetrates it by generating internal currents. As a result, the X-ray absorption layer pins the Earth's magnetic field so that deformations caused by the plasma bubble on the upper side of the layer are incapable of passing through to the surface (see Figure 17). In a very real sense, the

X-ray absorption layer shields locations below the burst from significant ground fields from the E3 blast phase. If the plasma bubble grows large enough, the fluctuations caused by the deformation of the Earth's magnetic field may be able to impact the Earth around the edges of the X-ray absorption layer "shield". This effect is shown in Figure 18 (taken from (Gilbert et al., 2010)), where one can see that the most intense fluctuations are just to the north of the X-ray patch indicated by a solid black line.

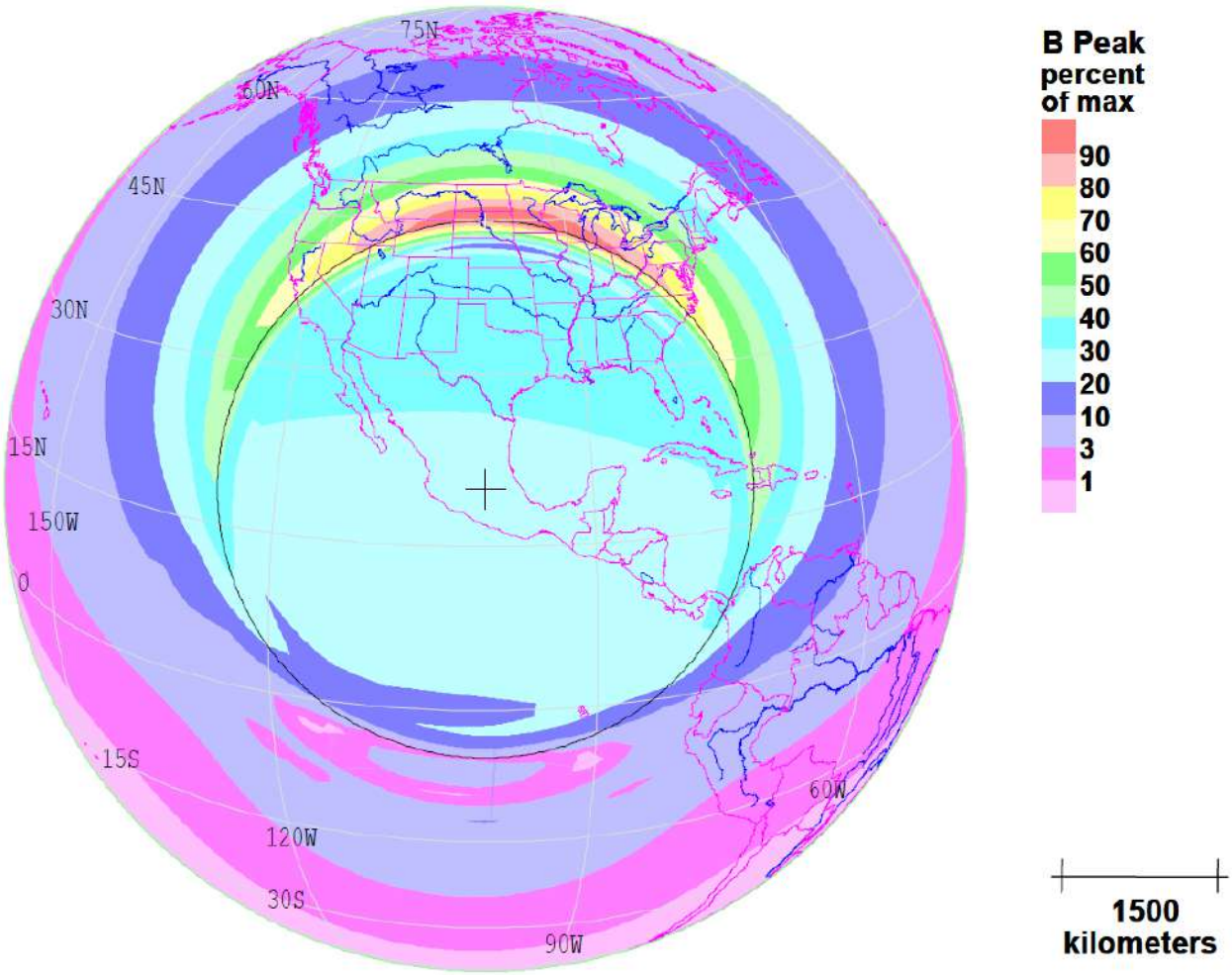

Figure 18: Magnetic field fluctuations caused by the blast phase of E3 (copied from (Gilbert et al., 2010)). The detonation location is indicated by the black cross. The X-ray absorption region extends out to the black circle.

3.2.3.2 E3 Heave

The heave stage of E3 begins as the blast stage begins to subside. The hot plasma ball that drove the E3 burst deformations of the Earth's magnetic field has expanded to its greatest extent. The cooler plasma ball emits fewer blackbody X-rays, and the conductivity in the X-ray absorption region falls. Although the plasma ball has cooled, it is still much hotter than the surrounding atmosphere, so it begins to rise. Over the next few seconds, three things will happen simultaneously: the Earth's magnetic field returns to normal following the E3 blast, the last of the conductivity in the X-ray adsorption patch subsides, and a new conductive patch of ions builds up (see Figure 19). The new conductive ion patch is created in the

upper atmosphere from a combination of super-heated ionized remnants of bomb debris and shock-heated atmospheric ions that spiral down the Earth's magnetic field lines, raining on the upper atmospheric layers. If the burst altitude is somewhat lower than two hundred kilometers, this ion rain is supplemented by ultraviolet radiation from the somewhat cooler plasma ball.

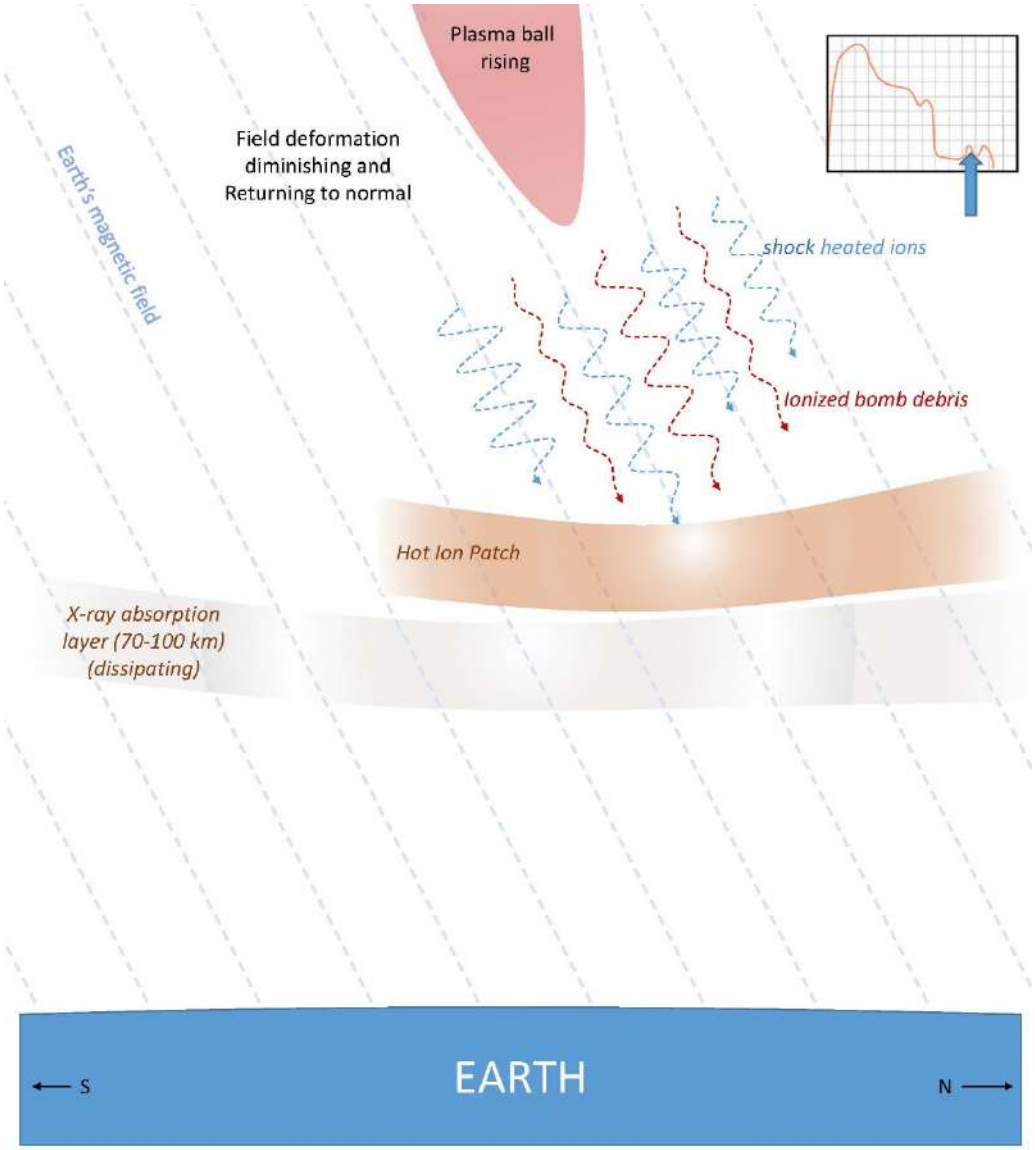

Figure 19: Beginning of the heave phase. Hot ions from bomb debris or due to air atoms being heated by the shockwave from the blast heat up a patch of atmosphere called the hot ion patch.

As the hot ion patch heats up, it expands. As with the plasma ball in the E3 blast stage, the hot ion patch is a good conductor that will try to maintain the magnetic flux penetrating its surface. Unlike the plasma ball, the hot ion patch was formed with a significant amount of the Earth's magnetic field already penetrating its surface. To maintain this flux while expanding, the hot ion patch must generate internal currents that compress the Earth's magnetic field lines downward and expand them laterally outward. This action is illustrated in Figure 20. The downward compression and outward lateral expansion of the

field lines generate magnetic fluctuations at the Earth's surface, which themselves create electric fields. These fields constitute the beginning of the E3 heave pulse.

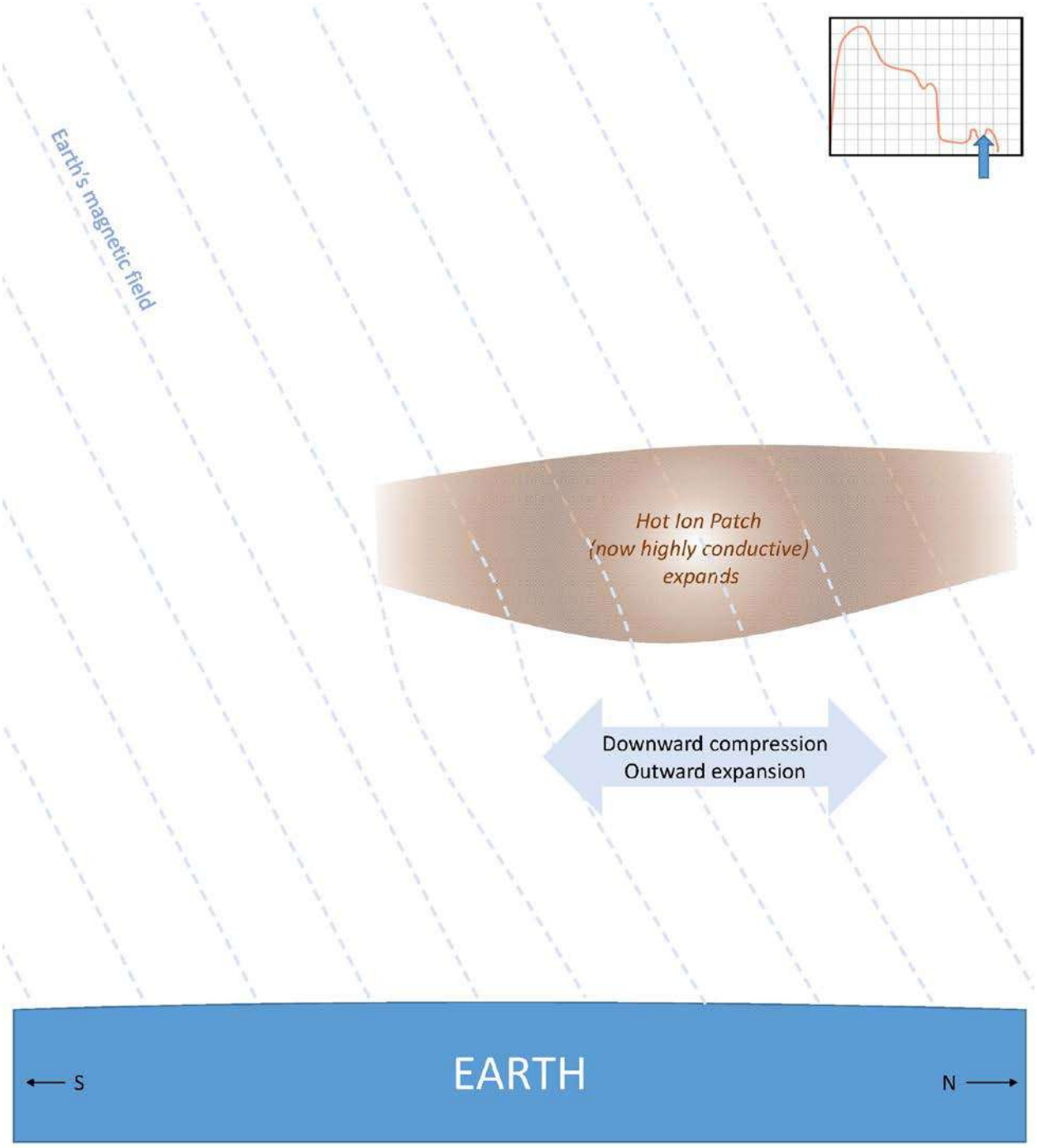

Figure 20: The hot ion patch which is now highly conductive begins to expand. This compresses the Earth's magnetic field downward and outward generating the initial stages of the E3 heave

The beginning of the E3 heave pulse is extended as the hot ion patch begins to rise. The now super-heated layer of air is significantly less dense than the surrounding atmosphere, and begins to rise due to buoyancy. The layer is still highly conductive and continues to generate internal currents that keep the

field lines penetrating its surface constant. As it rises, the hot ion patch pulls the Earth's magnetic field lines up with it along with an inward lateral compression, as illustrated in Figure 21. At this point the magnetic deflections experienced at the Earth's surface are changing rapidly, resulting in the largest electric fields. This process constitutes the peak of the E3 heave phase.

Eventually the hot ion patch rises and cools, and the magnetic fluctuations at the Earth's surface dissipate, concluding the E3 stage as well as the immediate time exo-atmospheric burst event.

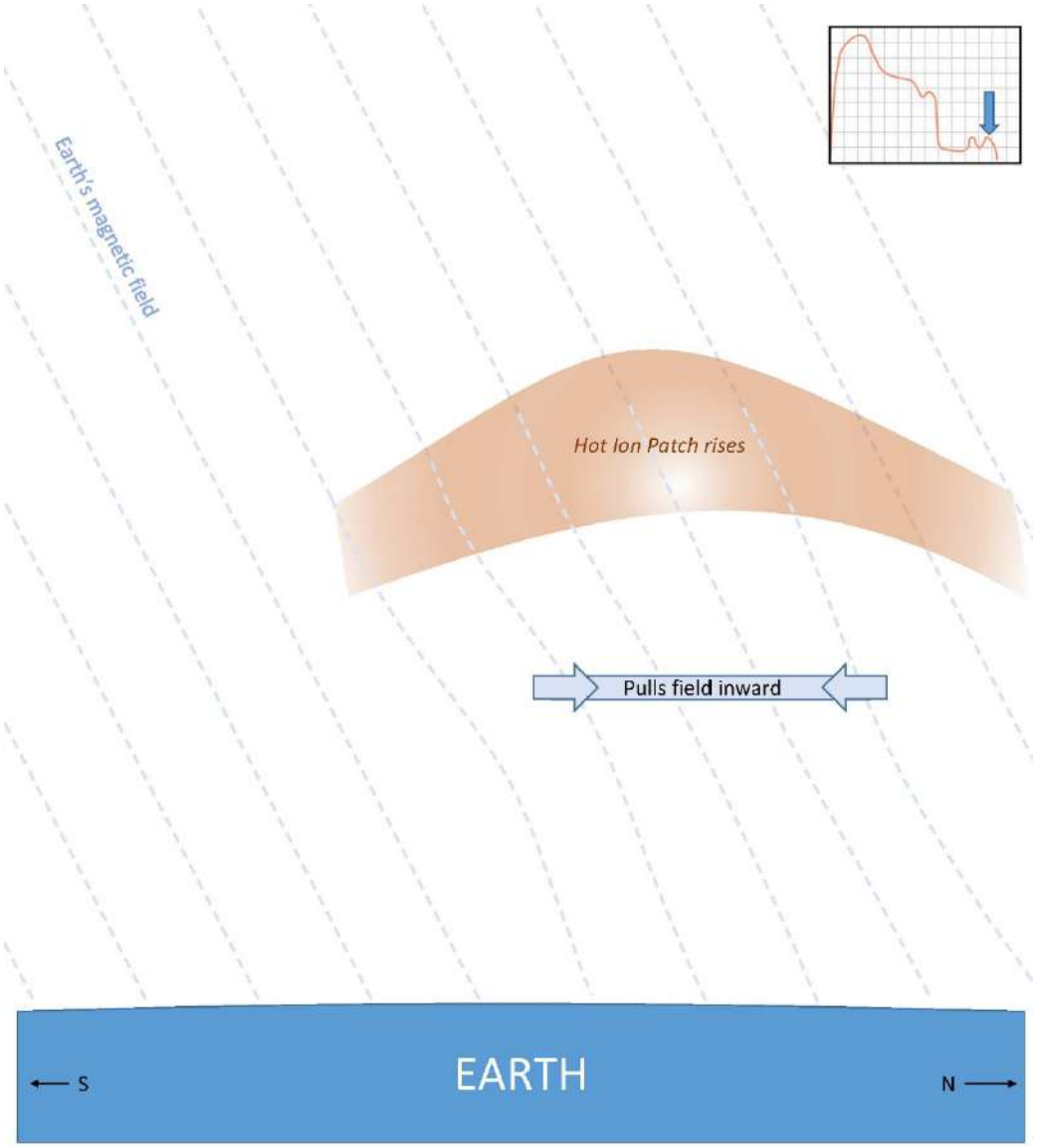

Figure 21: Due to buoyancy effects, the hot ion patch rises. Because it is still conductive it pulls the magnetic field upwards with it. This is the final part of the E3 heave phase.

3.2.4 Exo-Atmospheric Event Parameterization

With the electromagnetic effects of an exo-atmospheric burst now described, we can describe the electrical hazard environment of a nuclear explosion using a low-dimensional parameterization

consisting of the yield of a fission or thermonuclear device and its burst altitude. There are three main hazards we wish to parameterize: the E1 pulse, and both the blast and heave of the E3 pulse.

The behavior of the E1 pulse is dependent on the flux of gammas hitting the gamma absorption layer in Figure 15. The gamma flux itself depends both on the total gamma yield of the device and the degree of spreading of the gammas before they reach the gamma adsorption layer. Therefore the E1 peak electric field will depend on the yield of the fission device (or the fission primary of a thermonuclear device) and the burst altitude.

The dependence of the peak E1 electric field on these two parameterization variables has been explored in simulations performed by Seiler (Seiler Jr, 1975) (see Figure 22). It is important to note that the yield in this figure is actually gamma yield, i.e., the number of gammas emitted by the device. For the range of burst altitudes considered, the peak E1 electric field at the strongest point in the smile diagram (see Figure 14) increases from approximately 10 *kV/m* to 40 *kV/m* as the gamma yield increases from 10 *Tons* to 10 *kTons*. A change in gamma yield of 1,000 only increases the peak E1 field by a factor of approximately four. This weak dependence on gamma yield is due to the significant "self screening" of the initial Compton recoil electron current by a return current of secondary electrons (see Figure 15).

Figure 22 also shows that for a particular yield device, there is an optimal altitude of burst. For example, a $1\ kTon$ yield finds its optimal burst height on the $100\ km$ curve, while the 10 $kTon$ yield is optimal at $200\ km$. The existence of an optimal burst height for each gamma yield can also be traced back to the changes in the flux of gammas hitting the gamma absorption layer. If a given yield device is at a lower altitude than the optimal altitude, the device's interaction with the gamma absorption layer (which is between 20 to 40 km) disrupts the E1 pulse, dropping the magnitude of the pulse. If the device is higher than optimal, the geometric spreading of the expanding gamma ray shell also reduces the gamma flux. The optimal altitude for E1 peak field generation for a fission device burst, and the extrapolation for the fission primary of a thermonuclear device, is shown as a band in Figure 23. We stress this band is meant to be indicative, rather than quantitative.

To summarize for the E1 pulse, the magnitude of the pulse is only weakly dependent on device yield. For a given yield there is an optimal burst height that tends to increase with yield. Devices detonated at heights above or below the optimal height experience a reduction in their generated E1 pulse.

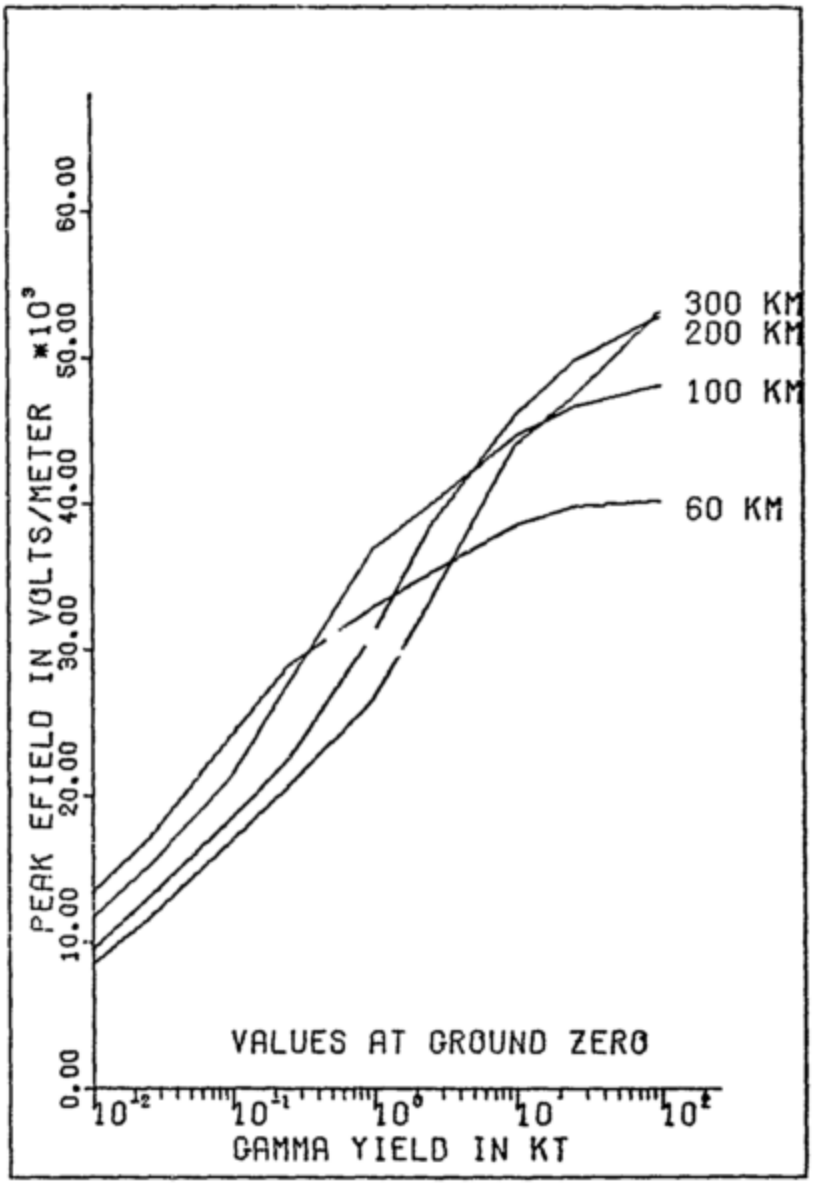

Fig. 6. Peak Electric Field as a Function of Burst Height

Figure 22: Dependence of the peak electric field for the E1 phase of an exo-atmospheric burst on the gamma yield for different burst altitudes. Gamma yield is not necessarily linked to device yield, in particular as one crosses from fission devices to thermonuclear device. Taken from (Seiler Jr, 1975).

We have already discussed the strong dependence of the E3 blast field on device yield and altitude. Figure 23 shows the approximate dependence E3 blast field on the same low-dimensional parameterization as used for the E1 pulse. Unlike the E1 pulse, the pulse created by the E3 blast is proportional to device yield. Below approximately 100 kTon, no substantial E3 blast pulse is generated at any altitude (yellow region in Figure 23). The conductive plasma ball created by this relatively low yield is not large enough to sufficiently disturb the Earth's magnetic field. At lower altitudes the friction

drag from the denser atmosphere slows the plasma ball expansion requiring a larger yield to cross the threshold of substantial E3 blast field. The effect causes the border between yellow and orange regions in Figure 23 to bend to high yield at lower burst altitude.

These same effects also create and optimal burst height for the E3 blast field shown as the upper horizontal green band in the orange region in Figure 23. Burst heights below the optimal height have a reduced E3 blast pulse magnitude due to the plasma bubble being slowed excessively by friction. Burst heights above the optimal height have a reduced E3 blast pulse magnitude due to smaller coupling to the Earth's surface.

The E3 heave pulse can be described using the same low-dimensional parameterization in Figure 23. The E3 heave pulse magnitude increases strongly up to about $10\ kTon$ devices, however, at this relatively low yield, the area of the hot ion patch in Figure 19 is not very large. Above this yield, the magnitude of the E3 heave pulse does not increase much, however, the area of the hot ion patch and the eventual area of hazard on the surface of the Earth increase. Considering these two combined effects, for this Phase 0 report we use the same boundary in Figure 23 between substantial E3 (yellow) and no E3 (orange) for E3 heave as for E3 blast.

As with its earlier counterparts, the E3 heave pulse has an optimal height of burst for a given yield device. As the burst altitude is lowered, ultra violet radiation also contributes to the heating of the ion patch in Figure 19 increasing the effect of convection and a higher E3 heave pulse. Below this burst altitude, the device's interaction with the hot ion patch disrupts the convection process and reduces the E3 heave pulse.

Figure 23 summarizes the Phase 0 parameterization of NEMP hazards from exo-atmospheric nuclear bursts that occurs above an altitude of approximately 20km. For lower burst altitudes, the physics of the interaction of the products of the nuclear explosion is different than described here and will be discussed in the subsequent sections on endo-atmospheric bursts. For all exo-atmospheric bursts, substantial E1 peak field magnitudes are created (yellow and orange regions in Figure 23), and there exists an optimal burst altitude shown by the "optimal E1" band. Below a lower altitude-dependent yield limit, the energy in the burst is insufficient to generate substantial E3 (yellow region in Figure 23). Above this threshold (orange region in Figure 23), competing effects on the conductive plasma ball expansion or atmospheric heating create independent optimal burst altitudes for E3 blast and E3 heave fields.

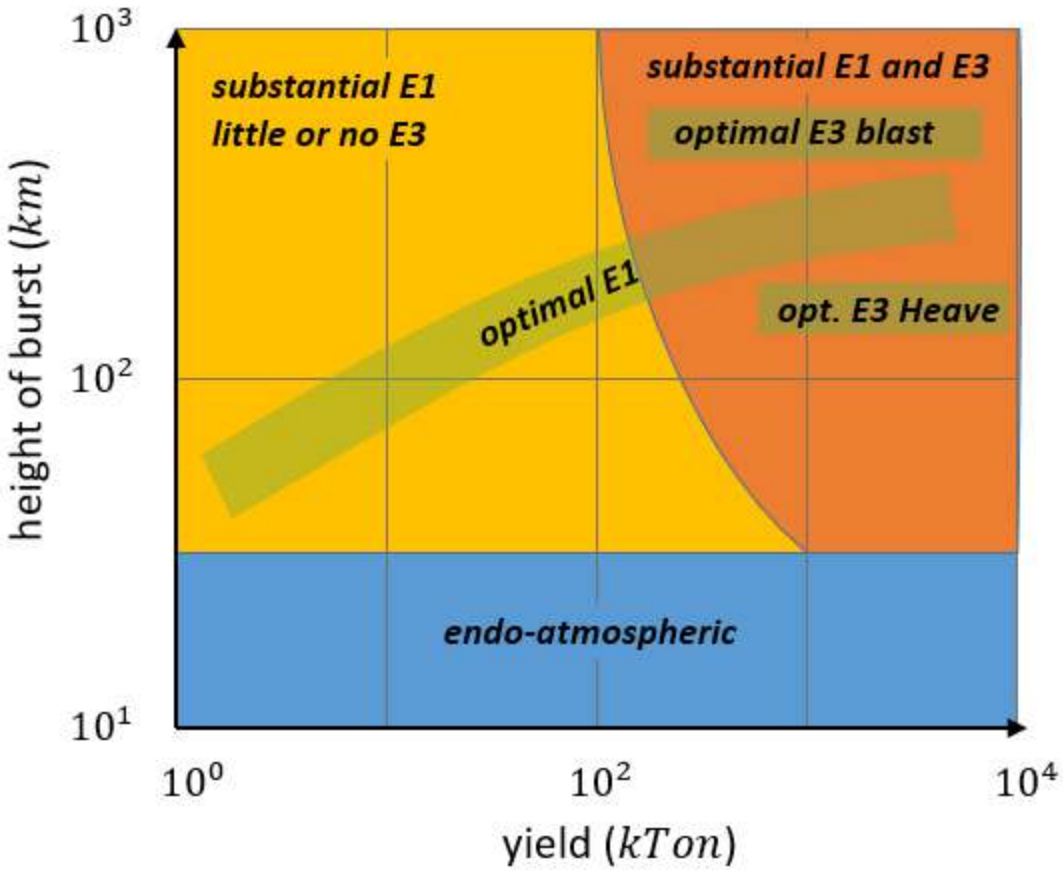

Figure 23: Hazard parameterization of exo-atmospheric burst. The blue region denotes endo-atmospheric bursts, which will be parameterized in a later section. The yellow region corresponds to bursts that create a considerable E1 pulse, but little E3 pulse. The orange region denotes bursts that create both E1 and E3 pulses. The green bars denote optimal burst altitudes for a given yield device to achieve a particular effect. These bars are meant to be indicative rather than quantitative.

3.3 Endo-Atmospheric Bursts

Devices that detonate within the atmosphere in relatively close proximity (within 1 km) to the surface of the Earth are called endo-atmospheric bursts. There are many hazards associated with such a burst—pressure waves, thermal effects, and radiated hazards are the most obvious. Along with these hazards, there are a variety of electrical hazards. The type and severity of these electrical hazards depend on the degree of interaction of the plasma ball and radiation with the Earth's surface. In contrast to exo-atmospheric bursts, the endo-atmospheric events interact with a dense atmosphere, which greatly limits the expansion of the plasma ball.

As with our discussion of exo-atmospheric bursts, we start the description of endo-atmospheric burst just after the very early time burst phase as the shell of prompt gammas is expanding away from the burst (Figure 6). Because the processes that are occurring (e.g., Compton scattering, electron recapture, charge separation, etc.) are now familiar, rather than enumerate each temporal step in detail, we consider what electromagnetic effects occur for a series of endo-atmospheric bursts that are increasingly close to the ground.

3.3.1 Burst in Uniform Air

We first consider an endo-atmospheric burst at a “high enough” altitude that there are no interactions with the ground, as well as at an altitude such that there are almost no gradients in atmospheric density. Of course no such altitude exists that satisfies the latter condition, for the moment let us assert that this is true at some “high enough” altitude, but not so high that the burst becomes an exo-atmospheric burst. Figure 24 depicts the relevant physical processes for such a burst.

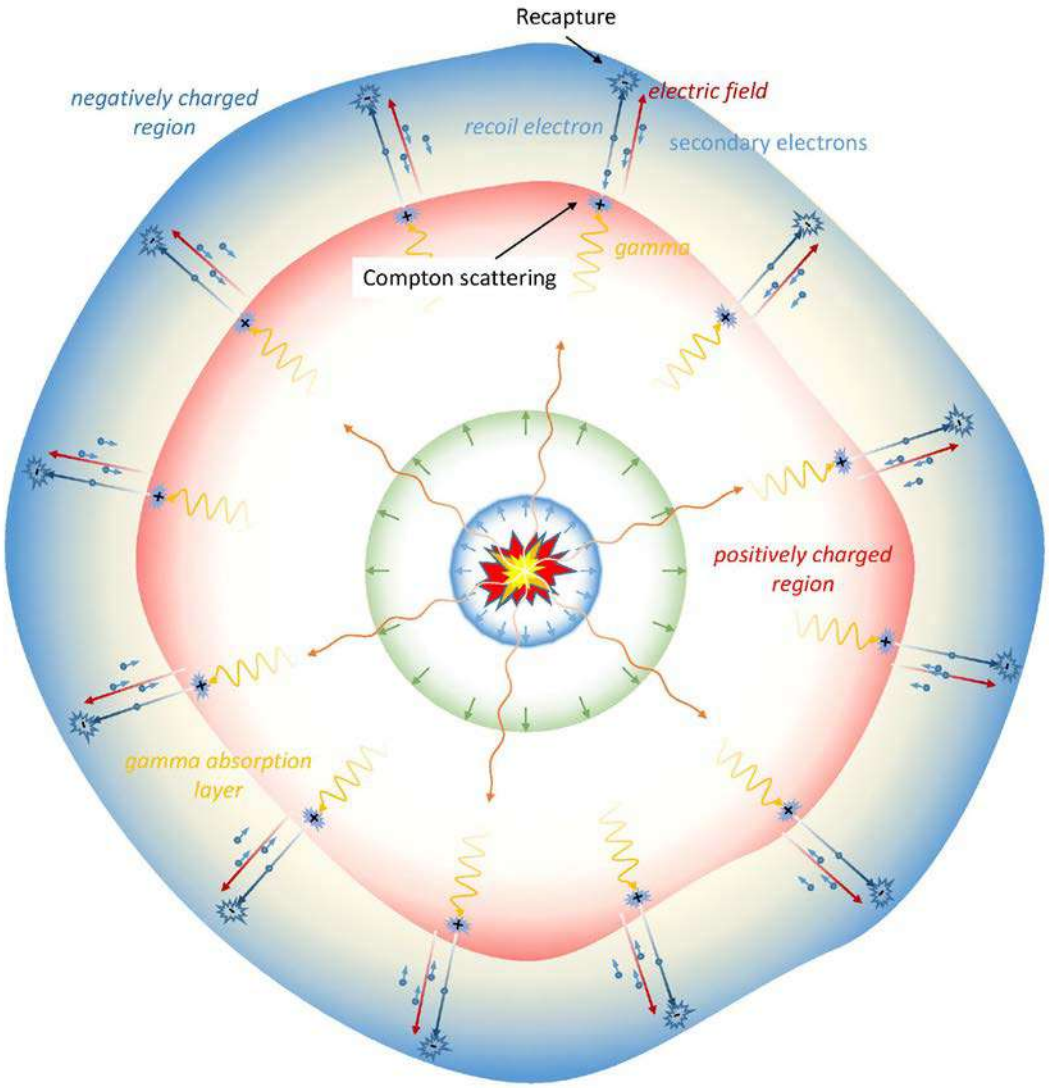

Figure 24: Depiction of the physical processes at work in an endo-atmospheric burst within a fictional layer of uniform density air. The processes are, for the most part, identical to the E1 phase of an exo-atmospheric burst. Unlike the exo-atmospheric burst, the X-rays are absorbed almost immediately by the atmosphere and will play no role in our discussion. Similarly we will be ignoring effects of the neutrons (green shell) and the shock wave (interior blue shell).

The physical processes for this endo-atmospheric burst are almost identical to exo-atmospheric bursts. Compton scattering frees high-speed recoil electrons, which themselves free many secondary electrons. This process turns the gamma absorption region into a highly conductive bath of secondary electrons. The recoil electrons also generate a separation of charge that causes an electric field. This electric field causes the secondary electrons to begin to move in a direction opposite to the recoil electrons. Eventually the system achieves a balance between Compton current and secondary electron return current, at which point the field can grow no larger. Once the driving gammas are all absorbed, the separation of charge and conductivity of the region subside.

The only real difference from the E1 phase in the exo-atmospheric burst is that instead of a more or less flat gamma absorption layer (as depicted in Figure 10), the gamma absorption layer for this endo-atmospheric case is a shell surrounding the burst. For endo-atmospheric blasts, this layer is frequently referred to as the "source region".

The most significant electromagnetic field created by a burst at this fictitious altitude is the electrical field caused by charge separation within the source region. The temporal behavior of this field is quite similar to its exo-atmospheric E1 counterpart. Despite being confined to a comparatively small region of space, the pulse for this burst is frequently denoted as an E1 pulse as well. It is also frequently referred to as a source-region EMP (SREMP). This field will be present for all of the endo-atmospheric scenarios that we consider here, and it is by far the largest field present in all such bursts.

Outside the source region, the situation is somewhat more complicated. Because the source region is a shell rather than a flat layer (as is present for exo-atmospheric bursts), there is quite a bit of cancellation of electromagnetic fields outside the source region; fields produced by currents on one side of the source region are reduced by the fields produced by oppositely directed currents on the opposing side of the source region. This weakens electromagnetic effects outside the source region considerably. This cancellation is by no means perfect, however. As a result, for any endo-atmospheric burst, a weak electromagnetic pulse quite similar to the E1 pulse of exo-atmospheric bursts is generated for observers outside the source region. Due to its relative weakness, however, we ignore this pulse in the discussion that follows.

Air Burst (Atmospheric Density Gradient but No Ground Interaction)

We now consider an endo-atmospheric burst somewhat lower down in the atmosphere—10 kilometers above the ground. At this altitude the ground is not close enough to play a significant role. There are, however, significant gradients in the density of the air. These gradients will deform the shell that primarily confined electromagnetic effects to the gamma absorption layer in the previous scenario. Such bursts are called air bursts. The relevant effects are depicted in Figure 25. We have omitted return current, etc. for simplicity.

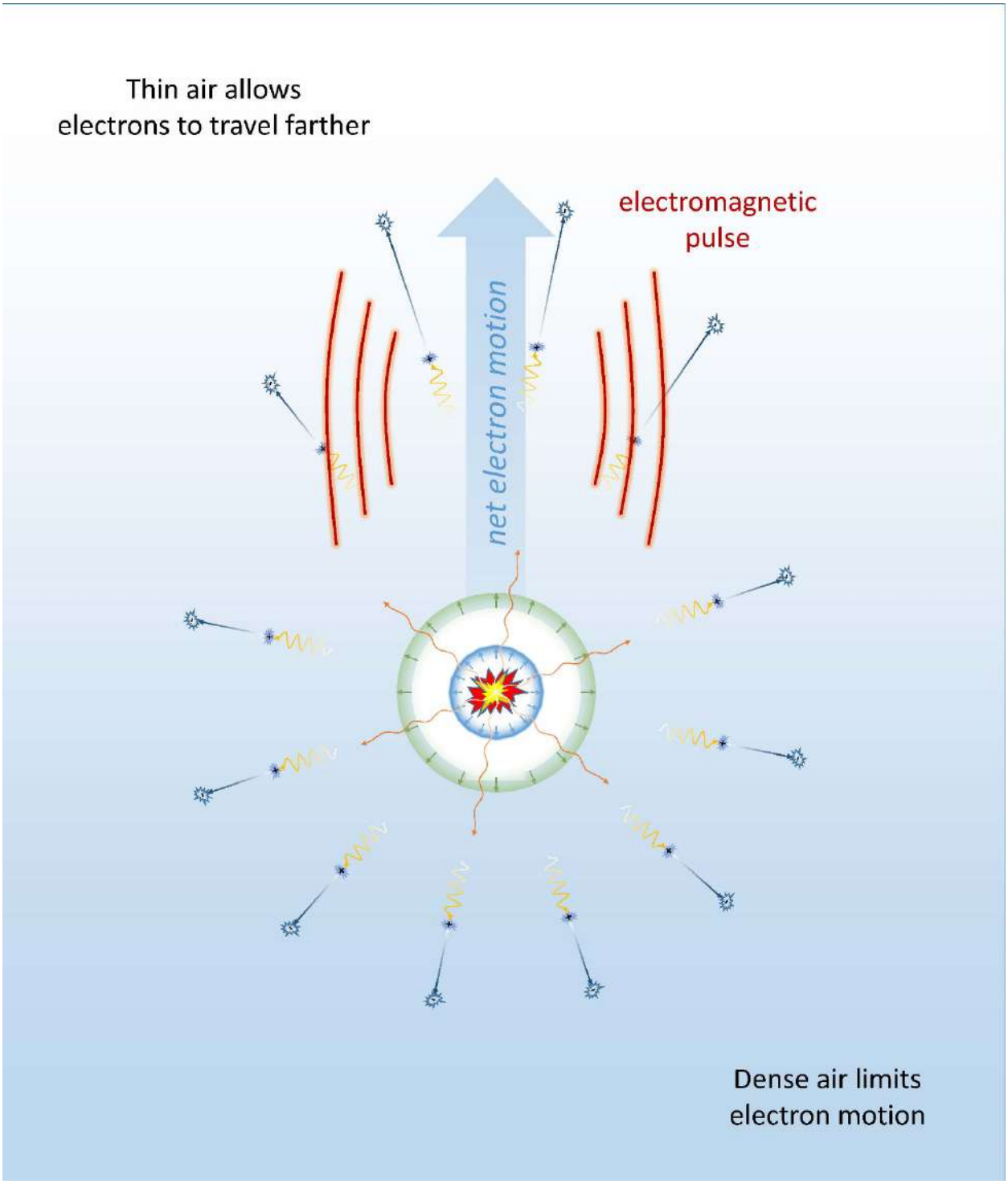

Figure 25: Relevant physical processes for an air burst. Due to the density gradients in the air, Compton recoil electrons can travel farther upwards then downwards, which causes a net electron motion (blue arrow) resulting in an "asymmetry" pulse.

In the air burst, recoil electrons scattered upwards into less dense air are able to travel farther than those scattered downward into more dense air. As a result, there exists a net upward pulse of electrons and a net downward current pulse. This current pulse behaves identically to a radio antenna and emits

an electromagnetic pulse, primarily in the direction perpendicular to the current. Unlike the electric field confined to the gamma absorption layer (the SREMP), this asymmetry electromagnetic pulse can travel significant distances away from the burst point. The magnitude of this "asymmetry" pulse, however, is extremely small in comparison to the SREMP.

3.3.2 Ground Burst (Strong Ground Interaction)

We consider one final endo-atmospheric burst scenario at a low enough altitude where the ground plays a significant role. In a ground burst, the interaction with the ground creates strong asymmetry and generates additional secondary effects.

The first effect is that the ground absorbs gamma rays much more readily than air. The source region is truncated in the downward direction so that instead of a sphere surrounding the burst point, the source region of gamma absorption in the air is now a hemisphere. The net of the Compton and secondary-electron return electrical currents is now strongly directed downward, which increases the magnitude of the electromagnetic "asymmetry" pulse in Figure 25.

The second, and far more complex, effect arises because the ground is a good conductor and provides a return path for the recoil electrons. The resulting toroidal current loop drives a magnetic field on the ground in a circle about the burst point. Like the SREMP, this "ground return" electromagnetic pulse is confined to the source region and the ground immediately below the source region.

We note that the SREMP described in the section on a spherically symmetry burst is still present. The two more complex pulses described above for a ground burst are in addition to the SREMP.

3.3.3 Endo-Atmospheric Parameterization

With the electromagnetic effects of an endo-atmospheric burst now described, we can effectively parameterize the electrical hazard environment. There are three electromagnetic effects of concern: SREMP, the ground return pulse, and the asymmetry pulse. These effects are important only if they are able to couple to the power system. SREMP and the ground return pulse are confined to the source region and can only couple if the source region touches the ground. The asymmetry pulse is too weak in air burst scenarios to cause significant impact to electrical devices on the ground. Therefore, the only endo-atmospheric bursts of interest for this study are ground bursts (less than 1 km in altitude) that have significant interaction with the ground.

For ground bursts, as reported in Longmire (Longmire & Gilbert, 1980), the SREMP can reach considerable magnitudes, with peak electric fields reaching $200\ kV/m$ roughly 20 nano seconds after the burst (see Figure 26). These fields are a significant hazard only if the source region extends beyond the damage radius of the device.[15] This situation can occur for small yield devices, in the $1kTon \leftrightarrow 10kTon$ range. Increasing device yield increases both the radius of the source region and the damage radius of the device, however, the damage radius grows faster than the source region. For thermonuclear devices, the damage radius exceeds the source region; as a result SREMP is no longer important for civilian systems. For a military system that may be designed to withstand such nuclear

[15] It matters little if a power delivery component is damaged by SREMP if, moments later, it is destroyed by a blast wave. There is a possibility that coupling to transmission lines within the damage radius might matter if the pulses created by such coupling can travel significantly far enough away before the damage pulse destroys the line. This possibility will be explored further in phase 1.

blasts, however, SREMP remains important, although understanding the impacts of SREMP on military systems is outside the scope of this study.

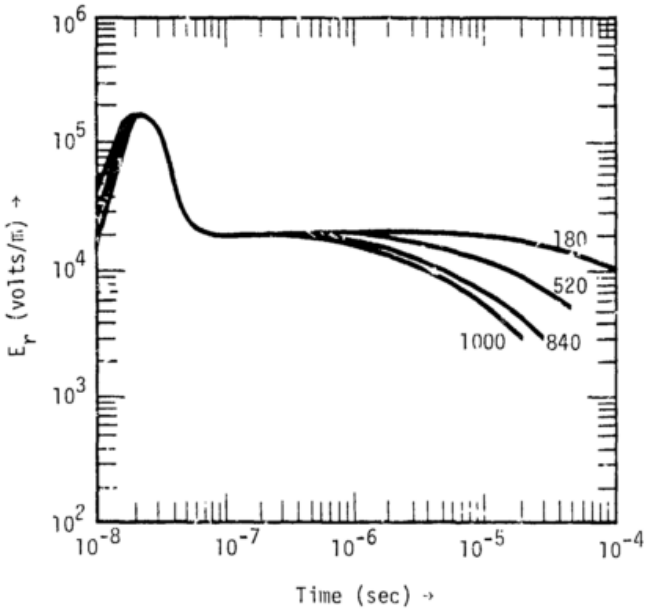

Figure 26: The peak SREMP field magnitude for a 3 $MTon$ burst versus time for several ground ranges (indicated on the plot in meters) as reported in Longmire(Longmire & Gilbert, 1980).

The ground return pulse is confined to the source region. Although it may reach considerable magnitudes, its magnitude is almost certainly small compared to the SREMP, thus, we ignore it in our studies as a minor perturbation to the SREMP in the source region. More quantitative comparisons of these pulses will occur in phase 1 of the study.

Finally there is the asymmetry pulse; the only pulse created by an endo-atmospheric blast that can extend beyond the range of the source region via propagation through the air. In (Dolan, 1972), estimates are given for asymmetry pulses having magnitudes of around $1kV/m$ at the edge of the source region for very large ground bursts ($10\ MTon$). This magnitude of electric field level for a very short burst is analogous to a weak lightning strike (much like the E2 component of an exo-atmospheric burst). In addition, the pulse magnitude is expected to decrease as the inverse of the radial distance from the burst. Considering all of these effects, the asymmetry pulse is expected to have little impact on the electric power system.

From a comparison of the relative magnitudes and spatial extents of the different electromagnetic hazards, a ground burst SREMP is the only electromagnetic pulse created by an endo-atmospheric burst that is important for the current study. The primary parameters that determine the importance of this hazard are the yield of the device and the ground range to the burst. Figure 27 displays the ground ranges for direct damage from the physical effects (blue region, the boundary of the blast zone) and direct damage from SREMP (yellow region, the boundary of the source region). Although SREMP of significant magnitudes are contained to the orange region in Figure 27, the SREMP can also couple to

and propagate along power system transmission lines and reach ranges in the white “conducted region” in Figure 27. This propagation and its impacts is discussion in later sections.

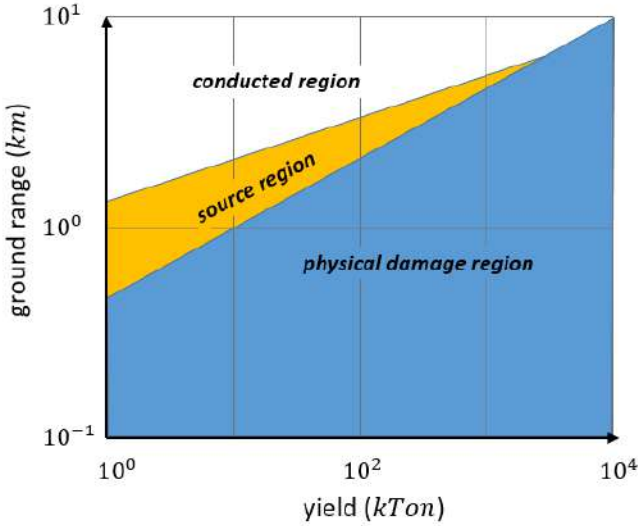

Figure 27: Parameterization of endo-atmospheric hazard. The blue region indicates extensive physical damage to BES components and subsystems. The yellow region is the source region where very high SREMP fields are expected to directly damage BES components and subsystems. The SREMP may also couple to BES transmission lines and conductively propagate along these lines into the white region potentially damaging other BES components connected to the transmission lines.

4 Overview of GMD

Before discussing the effects of severe geomagnetic storms, we clarify what we mean by a "severe" geomagnetic storm.

4.1 Measures of Storm Strength and Storm-time Geomagnetic Activity

Because geomagnetic storms are actually a constellation of phenomenologies, there is no single metric that perfectly describes storm intensity and the severity of storm effects. However, it has become standard to use the Disturbance Storm Time (D_{st}) Index as a proxy for describing storm severity. Because D_{st} has a limited history (1957-present), it is occasionally necessary to use other measures, such as the Antipodal Index (*aa*), to enable comparison of storms in the pre- and post-1957 eras.

4.1.1 Disturbance Indices (D_{st} and D_{cx})

Values of D_{st} are determined from a weighted average of measurements from four equatorial geomagnetic observatories. This index was first calculated in 1957, but a recent effort has extended this data set back to 1932, resulting in a similar index known as D_{cx}. D_{st} and D_{cx} that measures the strength of the terrestrial ring current, a population of charged particles that becomes strongly enhanced during geomagnetic storms. Specifically, D_{st} is the magnetic perturbation at the center of the Earth due to the ring current particles; it is proportional to the amount of energy stored in the ring current particles, much like energy is stored in a battery. (Loewe & Prölss, 1997) introduced a classification scheme for geomagnetic storms based on the D_{st} index (see Table 1) that is now used widely.

Table 1: Geomagnetic Storm Classifications from (Loewe & Prölss, 1997)

Dst (nT) Range	Classification
-30 > Dst > -50	Weak
-50 > Dst > -100	Moderate
-100 > Dst > -200	Strong
-200 > Dst > -350	Severe
-350 > Dst	Great

Usually larger (i.e., more negative) values of D_{st} are associated with larger GMDs; however, this is not a hard and fast rule. Instead, larger values of D_{st} are indicative of the magnetosphere being pushed further away from a nominal equilibrium state; there is a greater likelihood of an energetic relaxation of the magnetosphere back towards its pre-disturbance state.

4.1.2 The Antipodal Index (aa)

A distinct drawback to the D_{st} index is that it has been available since 1957. As discussed later, many of the largest and most severe observed geomagnetic storms predate the usage of D_{st}. Historically, the geomagnetic antipodal indices, which are based on measurements from two antipodal geomagnetic observatories, have the longest continual coverage. The *aa* index has 3-hour resolved measurements back to 1868, with an extension back to 1847 via historical data from other observatories (Nevanlinna, 2004). Because of its limited spatial coverage, interpretation of *aa* is subject to some caveats, which we discuss later. We also note that because *aa* is based on two observatories at fixed latitudes (around ±50° geomagnetic latitude), it may not fully capture geomagnetic storms whose peak disturbances are at different latitudes.

4.2 Occurrence Frequency of Severe Geomagnetic Storms

The statistical distribution of geomagnetic storms and their effects are not well established at present. Some of this confusion is due to how geomagnetic activity is characterized. For example, (Love, Rigler, Pulkkinen, & Riley, 2015) used the peak value of D_{st} during a given storm; (Pulkkinen, Pirjola, & Viljanen, 2008) used the peak daily geoelectric field; (Thomson, Dawson, & Reay, 2011) used a thresholding technique with full 1-minute cadence time to estimate extreme GMD amplitudes; and (Backhaus & Rivera, 2015) used autocorrelation times to determine statistically independent peaks. If we are concerned with the occurrence probability of a storm (as parameterized by D_{st}) only, then considering storms stronger than what have occurred since 1957 (D_{st} < -589 nT) requires extrapolation. (Tsubouchi & Omura, 2007) used extreme value statistics for storms with D_{st} < -280 nT to show that that the 1989 storm was a 1 in 60-year event. (Love et al., 2015) considered an expanded data set consisting of storms with D_{st} <-63 nT. Their findings also predict a 1 per 60-year frequency for the 1989 storm; by carefully fitting a log-normal distribution to their data, they were also able to predict that a 100-year extreme storm should have -660 ≥ D_{st} ≥ -900 nT (see Figure 28). Based on these two studies, we can be reasonably certain that we have not experienced the effects of a 100-year storm since 1957 (the beginning of the space age). There are indications that we have previously experienced such storms, however.

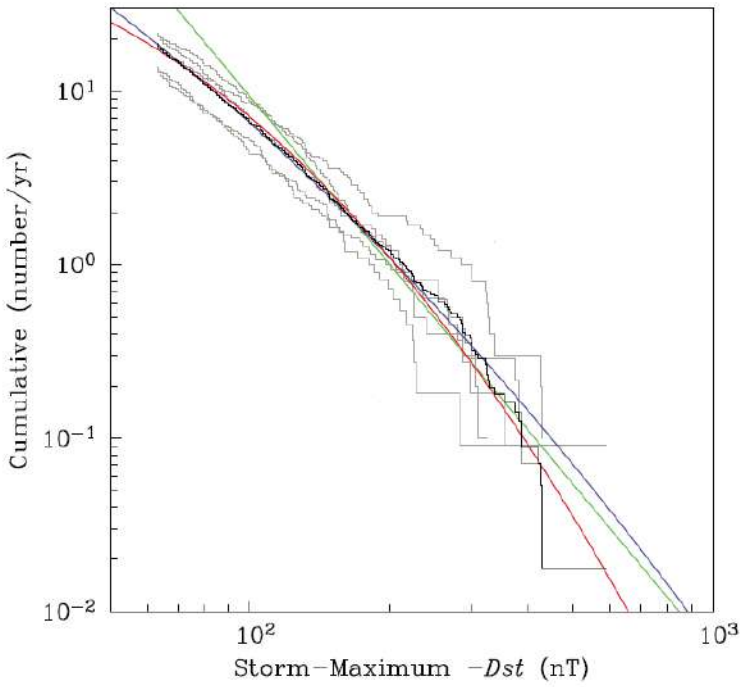

Figure 28: Cumulative probability of occurrence for geomagnetic storms at a given Dst index (Love et al., 2015)

4.3 Important Historical Storms

The modern D_{st} index that we use to characterize storm severity was developed in 1957. Since that time, the strongest observed storm had D_{st} = -589 nT. There are historical accounts, however, that suggest storms that were much stronger, with an estimated value of D_{st} = -1760 nT in one case. Care must be taken in assessing the intensity of storms without proper instrumentation, but it is nevertheless necessary to assess storm intensity to predict what we should expect from truly severe storms.

4.3.1 March 1989 "Quebec" storm (D_{st}=-589 nT, aa=441)

With peak D_{st} = -589 nT and extreme ground-level impacts in Canada – including a 9-hour blackout of the entire Quebec power grid, the March 1989 storm is frequently cited as an example of what should be expected for the most severe storms. (NERC, 2014) uses the Quebec storm as its template for a 1-in-100 year event, but it is highly debatable whether this template is an accurate assessment of the likelihood of an event like Quebec. Although the Quebec storm is undeniably the largest storm since 1957, there was a comparable storm (*aa*=429, D_{cx}=448) in September 1941. A similar but nominally weaker storm (*aa*=377, D_{cx}=-355) in March 1940 was reported to have burnt out lightning arrestors in Bangor, ME, and to have caused "complete fusing" of the Fargo-to-Winnipeg cable at Neche, ND (Odenwald & Green, 2007).

Although this storm was quite severe from the perspective of D_{st}, its most famous consequence, the HydroQuebec failure, may have been less of function of storm intensity than limited awareness of the potential impacts, limited forecasting, and lack of operational mitigations. As noted in (Gilbert et al., 2010), the ground-level effects of this storm were not exceptional (the Hydro-Quebec collapse was due to a *dB/dt* = 6 nT/s signal).

4.3.2 May 1921 "Railway" storm (D_{st}=-900 nT, aa=356)

At first glance, the antipodal indices for this event suggest that this event was weaker than the Quebec storm. However, it is important to note that the antipodal configuration is extremely sensitive to localization effects and that the observing stations used in the measurement of the antipodal index are located around λ=±50° geomagnetic latitude – precisely the latitude at which Quebec was known to maximize, but poleward of the observed auroral oval for this event. Using the scaling proposed in *NERC* [2016], the actual perturbations would be expected to have been around 40% larger: *aa*=508.

Based on the statistical study of (Love et al., 2015), this is a true 1-in-100 year event. The auroral oval was observed to be directly overhead at λ=48° geomagnetic latitude, with the lower boundary of the oval close to λ=41°. Strong GMDs were recorded at very low latitudes, including magnetic field fluctuations in excess of 1000 nT at Apia, Samoa (λ=13°) (Silverman & Cliver, 2001).

Numerous ground-level events were associated with this storm. The "Railway" nickname of this storm was given because of two particularly striking events that occurred during the storm

- A fire destroyed the Central New England Railroad station after a telegraph operator was driven away from his switchboard by a "flare of flame" that proceeded to ignite the building.
- The entire signal and switching system of the New York Central railroad below 125th Street was rendered non-operational and the 57th Street control tower caught fire from a spontaneous short circuit.

Telephone engineers, who measured excess voltages above 1 kV on the Chesapeake to Potomac line, provide a few quantitative measurements of the ground-level effects. Assuming that the affected line ran from Washington, DC, to Baltimore, MD (a distance of 40 miles), this implies a 15 V/km geoelectric field.

4.3.3 August 1859 "Carrington" storm (D_{st}=-1200, aa=400)

Based on limited historical data, the Carrington event may have been as strong as D_{st} = -1760 nT (Tsurutani, Gonzalez, Lakhina, & Alex, 2003). As with the Railway storm, it is probable that the *aa*

underestimates actual intensity due to the peak of activity being equator-ward of the antipodal stations; in fact, the effect should be more pronounced, as *aa* prior to 1868 was calculated using only a single station at Helsinki (Nevanlinna, 2004), which is at higher magnetic latitude than the traditional antipodal stations.

According to eyewitness accounts, dynamic auroral forms were visible overhead on the Iberian Peninsula (with confirmed observations as far south as Seville), placing the auroral oval somewhere near 40° (Farrona, Gallego, Vaquero, & Domínguez-Castro, 2011), although auroral signatures were visible as far as λ=23° (Kimball, 1960).Using a more conservative estimate of λ=42° and applying the (NERC, 2014) latitudinal scaling to bring the signal to λ=50°, we find that *aa* would have been closer to 1000. It is questionable whether or not this latitudinal scaling is valid over such a large range of latitudes, but even *aa*=700 would far exceed any other storm ever measured. Because the observing station at Helsinki is actually closer to λ=55°, the large *aa* value is even more remarkable.

All of the caveats associated with the Railway storm extend to the Carrington storm. Although there was little in the way of "vulnerable" infrastructure, there were still many accounts of storm-related effects. For example, telegraph wires in Spain were interrupted by electricity overloads (Farrona et al., 2011); in Baltimore, a telegraph operator reported that "the intensity of the spark at the instant of breaking the circuit was such as to set on fire the wood work of the switch board"; and at telegraph office in Springfield, MA, "the heat was sufficient to cause the smell of scorched wood and paint to be plainly perceptible" (Shea & Smart, 2006).It is not clear whether this burning was due to Joule heating or the Peltier effect, but it is impossible to draw quantitative conclusions from this observation because they would require knowledge of the electrical characteristics of the telegraph apparatus, as well as the duration of time over which the heating occurred.

There are other observations that are more amenable to quantitative assessment. According to one observer, the effect on telegraph lines was estimated to be "at times equal to that of 200 cups of Grove's battery"(Shea & Smart, 2006). This reference allows us to make a quantitative estimate of the excess voltage in this instance: the Grove cell used as a power source for telegraph systems at this time had a voltage of about 1.8-1.9 volts (Boteler, 2006), so if we assume that 1 cup refers to the standard volume of a Grove cell, this measurement would suggest an excess of 360–380 V. It is not clear which lines were subjected to this additional voltage, but given the unreliability of telegraph operation beyond 100 miles (longer transmissions required repeater stations), this implies a geoelectric field somewhere in the range of 2 to 20 V/km.

Magnetometers at the Kew Observatory, UK, were saturated at 700 nT (Tsurutani et al., 2003), and measurements from Russian magnetic observatories were similarly saturated at 1000 nT (Tyasto, Ptitsyna, Veselovsky, & Yakovchouk, 2009). Where magnetometers were not saturated, perturbations of 3000 nT were measured at Rome (λ=39°) (Cliver & Dietrich, 2013), and magnetometers in Bombay (λ=10°) measured perturbations of 1700 nT.

Interestingly, there were more reports of destructive effects (e.g., fires) from the 1921 storm than from the 1859 storm, despite the latter's much greater intensity. As noted in (Cliver & Dietrich, 2013), this is best regarded as evidence of an increased vulnerability of the evolved infrastructure to the inductive effects of space weather.

4.4 Assessment of Ground-Level Hazard

Our understanding of the severity of the ground-level hazard from GMDs and it connection to metrics like D_{st} is limited by observations of these effects. This limitation is partially due to a mismatch between the sophistication and availability of observing technologies and the occurrence of extreme space weather events, and to the fact that many space weather effects—particularly those responsible for the production of large GMDs—are not globally uniform.

Even with storms in the modern era, these connection can be difficult. (John Kappenman, 2010) presents the results of the Metatech Corporation study sponsored by Oak Ridge National Laboratory. This study was very comprehensive in its investigation of potential storm-related effects on the US power grid, but its conclusions were on proprietary simulations whose capabilities and shortcomings are not known. For example, Kappenman presents results from simulation of the March 1989 geomagnetic storm but gives no indication of the inputs or boundary conditions for this simulation. We note that simulations of this type typically require data from solar wind monitoring spacecraft, and there is a notable lack of such data for this storm because the appropriate spacecraft, IMP-8, was in the Earth's magnetotail for much of the event. Given this limitation, we will not quote results from Kappenman unless they are providing actual measurements that are unavailable elsewhere.

Both observations and theory show that GMDs exhibit latitudinal and local time variability, and it is well known that induced geo-electric fields are dependent upon local ground conductivity structure. In the sections to follow, we discuss the effects that produce spatial variability in GMD signatures and ground-level hazards.

4.4.1 The Magnitude of Extreme GMDs

As mentioned above, there have been a variety of different attempts to quantify the severity of geomagnetic activity using a variety of different measures. Most of these attempts limit the analysis to GMDs occurring after 1957 so that we may use D_{st} as a uniform index. In doing so, these studies ignore other periods during which extreme behaviors can occur.

(Thomson et al., 2011) used 1-minute time series from a network of 28 magnetometers in Europe to estimate the magnitude of extreme (100-year) GMDs. Based on their analysis, which in some cases covered over 30 years' of data, 100-year levels at λ=55° were $2000 \leq \Delta B \leq 5000$ nT and $17 \leq dB/dt \leq 67$ nT/s. (Woodroffe, 2016) showed that there are two primary effects of increased storm intensity (D_{st}) on GMDs: an increase in the typical geomagnetic field and an equatorward migration of the affected region. Consequently, we might expect that the 100-year levels experienced at higher latitudes are also representative of what would be experienced at lower latitudes during a 100-year storm when the mechanisms of extreme GMD production (e.g., the auroral electrojets) are themselves pushed to lower latitudes. This expectation is consistent with observations from Norwegian magnetometer stations at λ=62°, which routinely observe *dB/dt* > 5 nT/s, typically sees *dB/dt* > 30 nT/s at least once per year, and which experienced *dB/dt*=77 nT/s during the D_{st}=-383 nT "Halloween" storm of 2003 (Myllys, Viljanen, Rui, & Ohnstad, 2014).

(Woodroffe, 2016) discovered that an extreme GMD of a given magnitude is equally likely to occur during a storm of D_{st} = -100 nT as it is during a storm of D_{st} = -300 nT because the increased frequency of storms compensates for the decreased average severity of GMDs. The implication of this finding is that a 100-year storm that pushes the auroral ovals down to λ=45° should have GMD effects comparable those

experienced at higher latitudes during weaker storms. Based on the extreme event analysis of (Woodroffe, 2016), this observation would suggest that a 100-year storm would have a median of *dB/dt* > 20 nT/s and geoelectric fields in excess of 8 V/km (see data in Figure 29); this latter value is in line with the proposed magnitude from TPL-007-1.

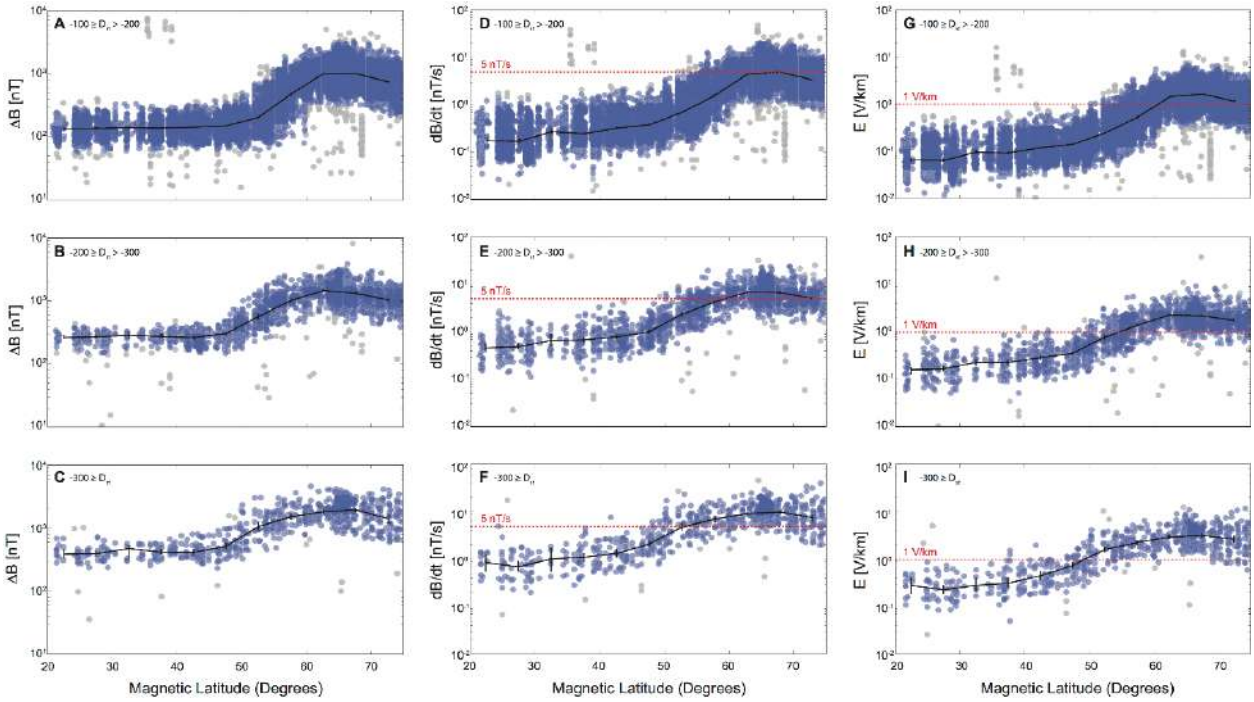

Figure 29: Latitudinal distribution of peak GMD amplitudes for different ranges of D_{st} [Woodroffe et al., 2016]. Each blue dot represents the largest GMD of a given type measured at a single observatory during a single geomagnetic storm.

4.4.2 Latitudinal Variability

It is vitally important to recognize that the region that is susceptible to storm-time GMDs expands equatorward with increasing storm severity. This equatorward expansion is clearly seen in data from weaker storms (Backhaus & Rivera, 2015; Starkov & Feldstein, 1967; Woodroffe, 2016), and it is also demonstrated by the limited data available from historical storms. The equatorward motion of the auroral oval is related to the inward motion of the Earth's magnetopause and the associated enhancement of the terrestrial ring current. Although it can be explained using a simple physical model of the Earth's magnetosphere *(Schulz, 1997)*; it has not been explicitly discussed in recent attempts to characterize the latitudinal variation of GMDs. This omission appears to stem from a paper by *(Ngwira, Pulkkinen, Wilder, & Crowley, 2013)* that posited the existence of a "threshold barrier" at λ=50°, below which only weak GMDs were observed. Although this threshold was a legitimate feature of their data, there is no *a priori* reason to believe that this barrier should persist in larger storms. Indeed, simulations presented in a follow-up paper (Ngwira, Pulkkinen, Kuznetsova, & Glocer, 2014) directly contradict the notion of a threshold barrier at λ=50°. A recent statistical study by (Woodroffe, 2016) identified *Ngwira's* threshold barrier as the location of the auroral electrojets, thus, explaining the D_{st}-dependence of this barrier as well as its apparent λ=50° limit in (Ngwira et al., 2013): no storms that were sufficiently strong to push the electrojets below that latitude have occurred since 1957.

A recent paper by *Love et al.* [2016] used a lognormal fitting procedure to estimate the magnitude of GMDs as a function of latitude for given frequencies of occurrence. Although the applicability of a lognormal model in this case is debatable, the application of a different model would change the magnitude rather than the morphology of the results shown in Figure 30. There is clearly a latitudinal peak that moves equatorward with decreasing event frequency, which in turn corresponds to increasing severity of geomagnetic activity. The equatorward shift of the curves with increasing return period is an expression of the equatorward motion of the auroral oval, because the auroral electrojets are the primary source of intense GMDs at these latitudes. These results are in qualitative agreement with those of This equatorward motion is also found in the earlier work of (Backhaus & Rivera, 2015) and (Woodroffe, 2016), who identified a similar trend in the median values of GMDs (the black lines in Figure 29).

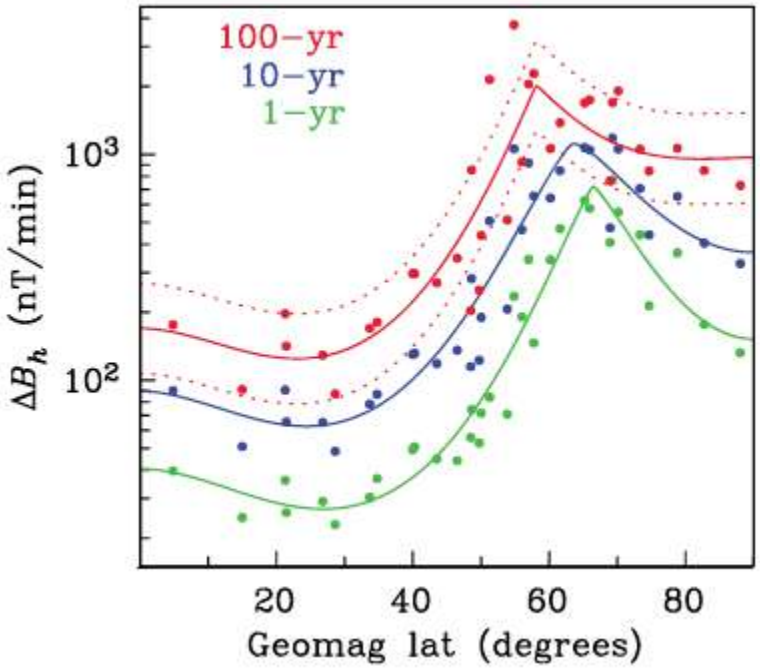

Figure 30. The latitudinal variation of $\Delta B_h = dB_h/dt$ *for different recurrence times (Love, Coïsson, & Pulkkinen, 2016).*

For the purposes of GMD impacts on infrastructure, latitudinal variation is a crucial issue. The 1989 storm has been erroneously cited by some as a 100-year event, whereas the statistics of such storms indicate that the Railway storm is much more representative of a 100-year event. Because the locations at risk from the most intense storm-time effects are dependent on the level of geomagnetic activity, adopting the wrong model will provide a poor indication of the regions that are actually in danger. In this case, the 1989 storm was most intense over Canada and near the US-Canada border (λ=50°), but the ground-level effects mentioned above and observed brilliance of the aurora over New York City are both consistent with the electrojets being at or near λ=45° during this storm:

> "Until after midnight crowds stood in Broadway watching the phenomenon. The flashes extended from the north to the zenith, and a bright star overhead was dimmed by rays of flickering light that showed all colors of the rainbow… Even the intense lights of the

electric signs along Broadway could not dim the brilliance of the flaring skies that appeared to spring from the flashing signs…"

The New York Times, 15 May 1921

The proposed TPL-007-1 standard assumes that GMDs will peak at λ=60°, and that the magnitude of GMDs decreases as an exponential function of geomagnetic latitude. Even if the proposed magnitude of GMD is correct, latitudinal scaling will produce erroneously small results if we do not account for the equator-ward displacement of the GMD peak.

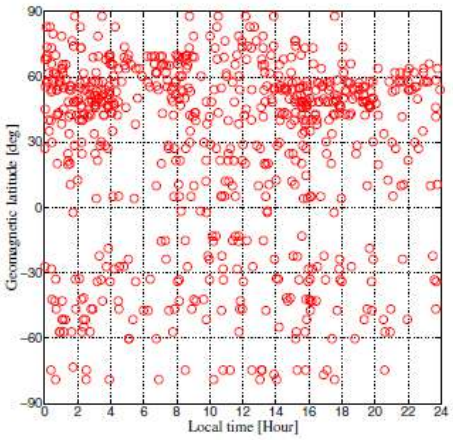

Figure 31. Local time distribution of peak GMD occurrence during 12 large storms (Ngwira et al., 2013).

4.4.3 Magnetic Local Time Variation

To our knowledge, the first systematic study of global GMD distributions was carried out by(Ngwira et al., 2013). Although they focused primarily on the latitudinal distribution, they also briefly mentioned local time distribution, suggesting that there was no apparent preference for GMDs to occur at any given magnetic local time based on the data shown in Figure 31. We believe this claim is incorrect in two ways: first, there is a clear clustering of large GMDs at certain local times; and second, the strength of GMDs is already known to exhibit a magnetic local time[16] (MLT) dependence (Tomita et al., 2010).

The local time distribution shown in Figure 31 is due to the distribution of source currents. There is a clustering of peaks near 2 MLT and 16 MLT rather than at noon—MLTs that correspond almost perfectly to the known peaks of the Westward and Eastward auroral electrojet currents (Guo et al., 2014) supporting our prior assertions that these intense GMDs are associated with electrojet activity, particularly at higher latitudes. Indeed, there is considerable evidence that GMDs are correlated with activity in the auroral current systems (see e.g., (Viljanen, Nevanlinna, Pajunpää, & Pulkkinen, 2001)). Figure 32 shows a global image of the aurora taken by the DE-1 satellite during the March 1989 storm that collapsed the Hydro Quebec power systems. Auroral activity is indicated by an orange color (brighter color corresponds to greater intensity). There is a clear band of intense auroral activity stretching across the Atlantic that weakens and becomes sporadic across North America. It is highly probable that observers would have seen very different ground level effects if this storm had occurred a

[16] At night, when you and your nearest magnetic pole and the Sun are on the same plane, you are at local magnetic midnight. From that point in time you measure local magnetic time in the normal manner of one hour per 15° of longitude. Reference https://www.physicsforums.com/threads/magnetic-local-time.738028/

few hours later, when a peak of auroral activity was located over the continental United States. As noted by (John Kappenman, 2010), the largest GMDs from the March 1989 storm (*dB/dt*=33 nT/s) were actually observed over the southern Baltic region, far removed from the region where the most damaging ground effects were observed, likely because the electrical infrastructure in the Baltic region is much less complex and therefore much less susceptible to space weather effects. Had these effects occurred over North America, it is probable that power grid disruptions would have been even more severe.

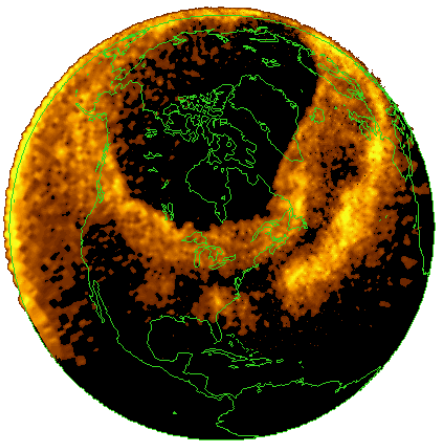

Figure 32. Auroral image from the DE-1 SAI instrument during the March 1989 storm.

4.4.4 Spectral Content and Geographic Variability

Existing analysis methods (NERC, 2014) use a regional conductivity map (Fernberg, 2012) based on physiographic regions of the United States to determine the local magnitude of the induced geo-electric field from a given geomagnetic source. However, these models are typically very coarse and have traditionally been derived based on assumptions of local geological structure rather than geo-electric sounding. The EarthScope[17] project has undertaken a more comprehensive efforts to examine geo-electric sounding, and their findings underscore the necessity of properly characterizing the detailed spatial variability of the frequency-dependent electromagnetic response of the Earth.

The geomagnetic field disturbance time series interacts with the frequency-dependent Earth response making the frequency content of the driving geomagnetic time series another important determinant in the generation of the geo-electric field. Existing analysis methods (NERC, 2014) use a single measured geomagnetic field time series from the March 1989 event, but the direct applicability of this signal to other locations is questionable. First, the total geomagnetic field measured at a given point is a function of both the source (e.g., the electrojets) and the local ground conductivity structure—both incident and reflected waves contribute to the observed signal. Thus, the proposed waveform already has been modified by local (Quebec) geology. Moving this waveform to another location, especially one with different geology, leads to a confusion of Earth response and input signal. As noted by (Bedrosian & Love, 2015), the failure to properly account for the frequency-dependent response of the local conductivity can strongly influence GMD magnitudes.

[17] http://www.earthscope.org/

Reinforcing the need for better characterization of local geological features and spectral content of the magnetic field disturbance, (Bedrosian & Love, 2015) have identified regions in Minnesota where the estimated GMDs can be wrong by a factor of 100 if the correct anisotropic conductivity model is not used. If both the wrong frequency and conductivity profiles are used, (Bedrosian & Love, 2015) found that the induced geoelectric field could range from 0.05 mV/km/nT to 79 mV/m/nT depending on frequency and local conductivity, i.e., a 1000 nT input signal could induce a geo-electric field of anywhere from 0.05 V/km to 79 V/km depending on its spectral content and the assumed conductivity profile.

Finally, we note that it is also important to recognize that the induction of geo-electric fields is not entirely local. As mentioned above, the depth-resolved structure of the conductivity is very important; however, transverse variation in structure can also contribute to localized GMD enhancements, changing GMD amplitudes by an estimated 20% in some cases (Bo, Ze-Zhong, Lian-Guang, Li-Ping, & Chun-Ming, 2015). This enhancement can be interpreted as a generalization of the well-known geomagnetic "coast effect" (Parkinson & Jones, 1979), but is not well-understood in the context of storm-associated GMD threats.

4.5 GMD Event Parameterization

The scientific understanding of GMD and its coupling to the Earth and built infrastructure is still emerging. A quantitative parameterization of the threat beyond existing methods is not possible in Phase 0 of this work and is deferred until Phase 1. Phase 0 has, however, identified several of the factors that should be accounted for in a determining an improved benchmark threat event in Phase 1:

Modifying the proposed latitudinal scaling to account for the equatorward motion of the sources responsible for intense GMDs:

Existing analysis methods (NERC, 2014) address many important issues related to GMD parameterization, however, there are still a number of shortcomings that could potentially—and adversely—impact its effectiveness. Existing benchmark magnetic time series are based on the March 1989 event. Although the March 1989 storm was undeniably the largest storm ever observed post 1957, there is an apparent consensus that this was not a 100-year event, but rather something closer to 50- or 60-years. Eyewitness accounts from a likely 100-year event, the 1921 "Railway" storm, indicate that larger GMDs have more severe effects at lower latitudes. Recent statistical analysis of historical data (Backhaus & Rivera, 2015; Love et al., 2016; Woodroffe, 2016) also indicate that larger GMD have their greatest impact at lower latitudes than assumed in existing analysis methods (NERC, 2014). Revised benchmark events and analysis methods are needed to better characterize the spatial distribution of the GMD hazard and to avoid underestimating the severity of the impacts.

Using correct local conductivity models and include anisotropy effects whenever possible and considering the introduction of a new multiplicative factor to represent the effects of close proximity to strong conductivity gradients:

Existing analysis methods recognize the spatial inhomogeneity of ground conductivity, however, better characterization of the Earth's electromagnetic response are now available from EarthScope, although not yet uniformly across the entire United States. Where and when these data are available, they should be incorporated into the analysis.

Using multiple different input signals with similar amplitudes but different spectral content (these may be either real or synthetic):

By using a single magnetic disturbance waveform, the existing analysis methods do not account for the inherent variability in the disturbance and the frequency dependence of the Earth's electromagnetic response. A more comprehensive benchmark for analysis of GMD should include many different possible waveforms or alternative methods for bounding the variability of the geo-electric response at specific locations.

Recognizing that there are certain MLT sectors where GMD amplitudes are known to be larger, possibly by including an additional MLT-dependent multiplicative factor:

Assumptions of local time invariance are not supported by either theory or observation, as the physical drivers of GMDs have well-known spatial variations that are associated with enhanced GMD power at certain magnetic local times.

5 Potential Impacts on Devices and Power Systems

With an overview of the electromagnetic environments created by nuclear bursts and GMD now complete, we consider how these environments couple into the BES. This discussion is broken into two sections. The first section discusses the coupling of fast effects (E1) and is denoted as high-frequency device coupling. The second section discusses the coupling of slower effects (E3 and GMD) and is denoted low-frequency device coupling. In this section we will focus only on the components of the BES that fall within the scope of the study and are at risk. We conclude this section with a discussion of current standards that are related to NEMP and GMD.

5.1 High Frequency Device Coupling

This section is applicable solely to NEMP; in particular coupling to NEMP from the E1 (and E2) phases of exo-atmospheric bursts. The device coupling described here is not applicable to GMD or the E3 phase of an exo-atmospheric burst.

5.1.1 NEMP Radiated vs Conducted Hazard

There are two ways that high-frequency NEMP effects are a hazard to ground devices: radiation and conduction. Radiation refers to a direct coupling of a device to effects produced by a nuclear detonation. For example, a device could act as a receiving antenna that directly "picks up" the EMP pulse released by a nuclear detonation, and, as a result, generates anomalous internal currents that could lead to damage. Conduction, on the other hand, is when the device does not experience a direct effect from the detonation, likely because it is well shielded or far enough removed from the blast epicenter, but is electrically connected to components that are affected. In this case deleterious effects are conducted through the connection points and may eventually damage the device or cause it to engage in unexpected behavior, regardless of shielding. The presence of a conducted hazard requires at least one component to couple through radiative effects (i.e., if everything was perfectly shielded, there would be no conductive effects). Generally speaking, the components that are the main culprit in this regard are power transmission lines and measurement and control cables which are, from the point of view of this discussion, large receiving antennas for high-frequency NEMP effects. For that reason we will discuss in some detail radiative coupling to measurement and transmission lines later.

The radiated hazard can further be broken into two general types: source region and free-field coupling. Source region coupling is an issue only for SREMP in endo-atmospheric bursts and requires accounting for the huge electrical fields generated within the source region and the change in electrical properties of the surrounding environment, as well as the gamma rays and associated free-space current of Compton scattered electrons. Free-field coupling is much simpler; one need only account for electrical fields and their coupling to devices. Free-field coupling is the primary type of radiated hazard in the early stages of exo-atmospheric bursts. It is also present from the asymmetry EMP of endo-atmospheric bursts at ground range distances well outside of the source region (although for the latter the source region coupling is by far the most important).

In the following sections, we will focus on free-field radiative coupling and conducted coupling. For the most part, we will not discuss source region coupling due to its complexity. Interested readers should reference the works of Longmire (Longmire & Gilbert, 1980).

5.1.2 Transmission and Measurement Lines

5.1.2.1 Radiative Coupling

Transmission and measurement lines are the primary components of BESs that directly couple to the radiated hazard of a NEMP. Although this coupling does not have any deleterious effect on the line itself, it generates a considerable pulse of current and voltage on the line, which is conducted to other BES components. Thus, along with being the main source or coupling to NEMP-radiated hazard, measurement and transmission lines also generate the NEMP conducted hazard.

The fact that electromagnetic effects caused by a nuclear detonation would likely couple to electrical cables with deleterious effects to the attached equipment was realized as early as the Trinity test (Bainbridge, 1976). Since that time there has been significant development in the ability to calculate both the coupling of EMPs to transmission lines and the propagation of the current surge along these lines. Although there are many notable reports on the subject matter (Agrawal et al., 1980; Rachidi, 1993; Taylor et al., 1965), much of the current academic literature tends to point to the work of Agrawal.

To understand the coupling, consider what occurs when an E1 pulse wave created by an exo-atmospheric burst encounters a conductive line. For the moment we ignore the ground and assume the line is freely floating in space. This NEMP wave along with a plot of current in the line is diagrammed in Figure 33. Note that, although we are considering a horizontal line in the following discussion, a similar model exists for vertical lines.

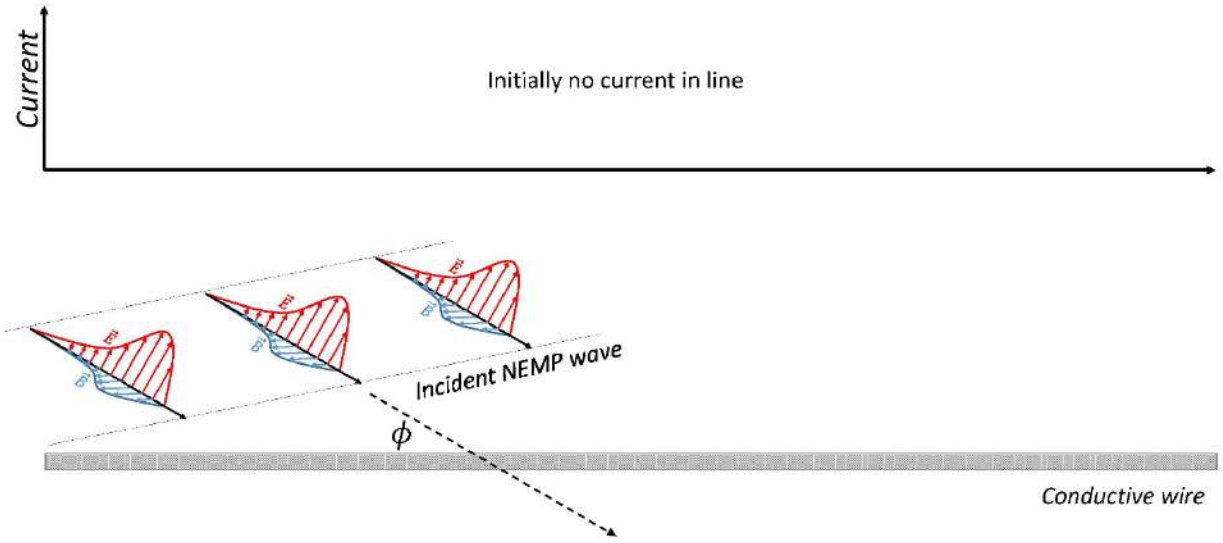

Figure 33: NEMP wave incident on conductive wire (e.g., a transmission line or measurement cable). The pulse wave has electric (red) and magnetic (blue) components that are perpendicular to each other as well as the direction of travel (dashed black arrow). A plot of the total current in the wire is above the image (initially there is no current in the line). The angle ϕ is the incidence angle of the wave relative to the wire.

Initially we assume there is no current in the line—an assumption that changes once the pulse wave impacts the line. When the pulse wave impacts the line, the portion of the electric field that is directed *along the line* will begin to generate a current pulse within the line (see Figure 34). This current pulse occurs over a region of the line that we call the current generation zone (CGZ). It is important to stress

that only the component of the electric field (the red vectors in Figure 34) that lie *along* the conductor contribute to current generation.[18] So, for example, if the angle ϕ in Figure 34 was zero, all of the red electric field vectors would be pointing vertically. This is perpendicular to the horizontal conductive line, not along it, therefore a $\phi = 0$ incident wave would *not* couple to the line and create a current. For any other incidence angle, however, at least a small part of the electric field lies along the line and will create a current.

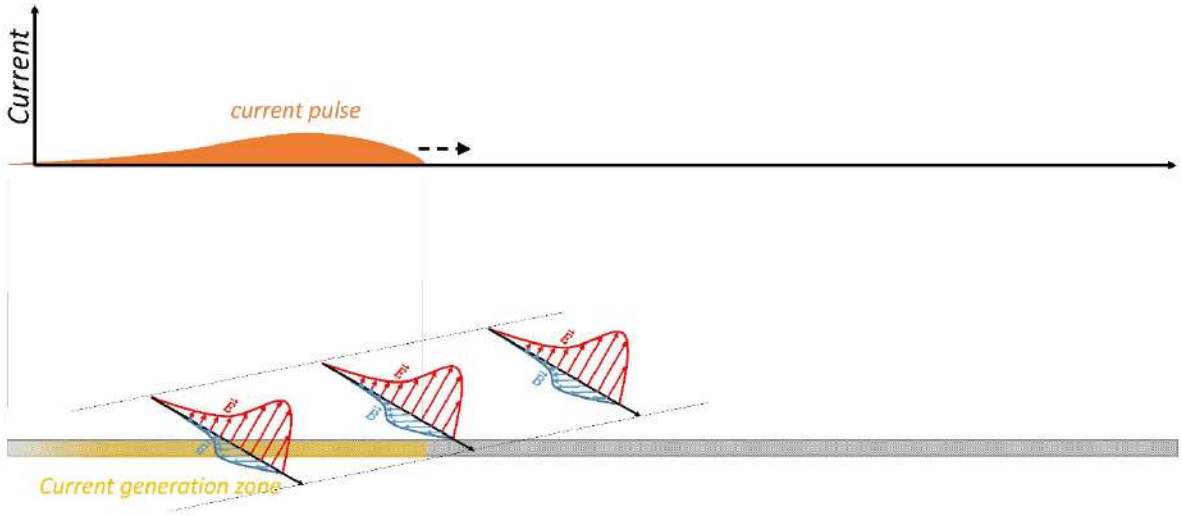

Figure 34: Once the NEMP pulse wave begins to intersect the conductor, the component of the electric field (red vectors) that lie along the conductive line begin to generate a current (the current generation zone is indicated by a yellow bar). The resultant current pulse (orange pulse) begins to travel down the line.

Once generated, the current pulse will begin to propagate down the line. The CGZ also moves down the line, but this is due to the propagation of the NEMP pulse. The current created by the pulse, however, travels more slowly down the line than the CGZ and may become spatially separated from the CGZ. Thus there are two regions of current on the line. Inside the CGZ, the ongoing current generation is continuing to build on top of the current generated at earlier times. This situation is diagramed in Figure 35. Outside the CGZ, the current pulse within the line continues to propagate, however, the magnitude of this current is rapidly decreasing due to the finite resistance of the line.

[18] This is a highly simplified point of view.

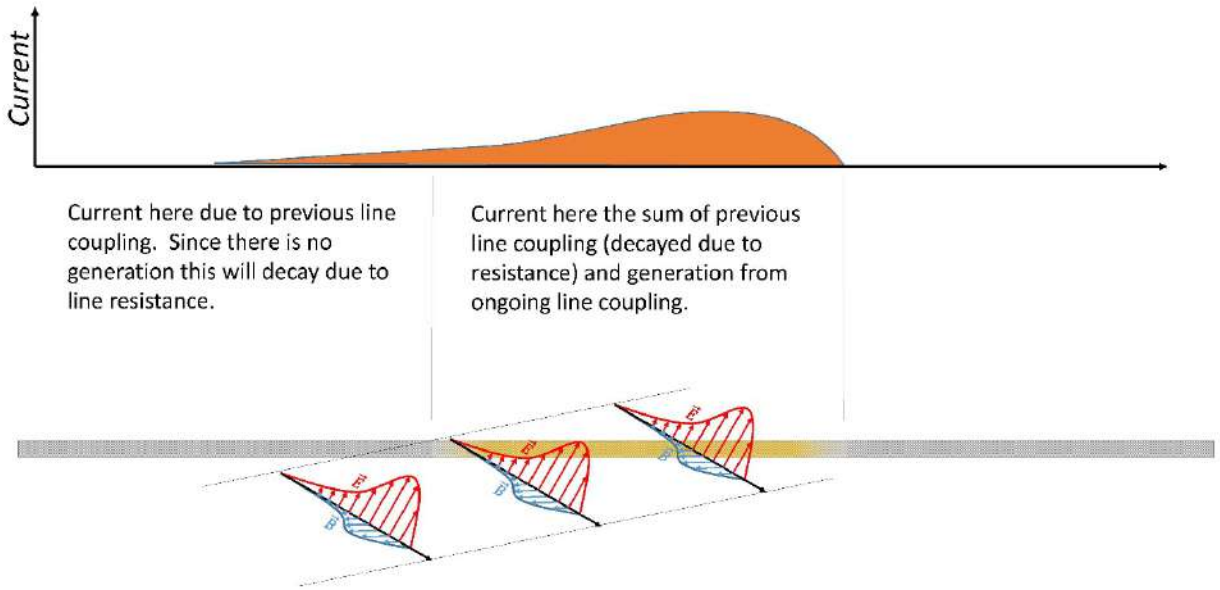

Figure 35: The current pulse (orange) and current generation zone (CGZ, yellow) travel down the conductive line, however the CGZ outpaces the current pulse such that the regions of current on the line can be broken into two categories: inside the CGZ where current generation continues, and outside the CGZ. Outside the CGZ, the current pulse dissipates from line resistance. Inside the CGZ, current generation will replenish the current dissipated by line resistance as well as continue to build the current wave.

This process continues to build the magnitude of the wave in the CGZ until resistive losses in the line balance the ongoing current generation. At this point, called the “effective couple length”, the current in the line will become no larger. This is shown in Figure 36.

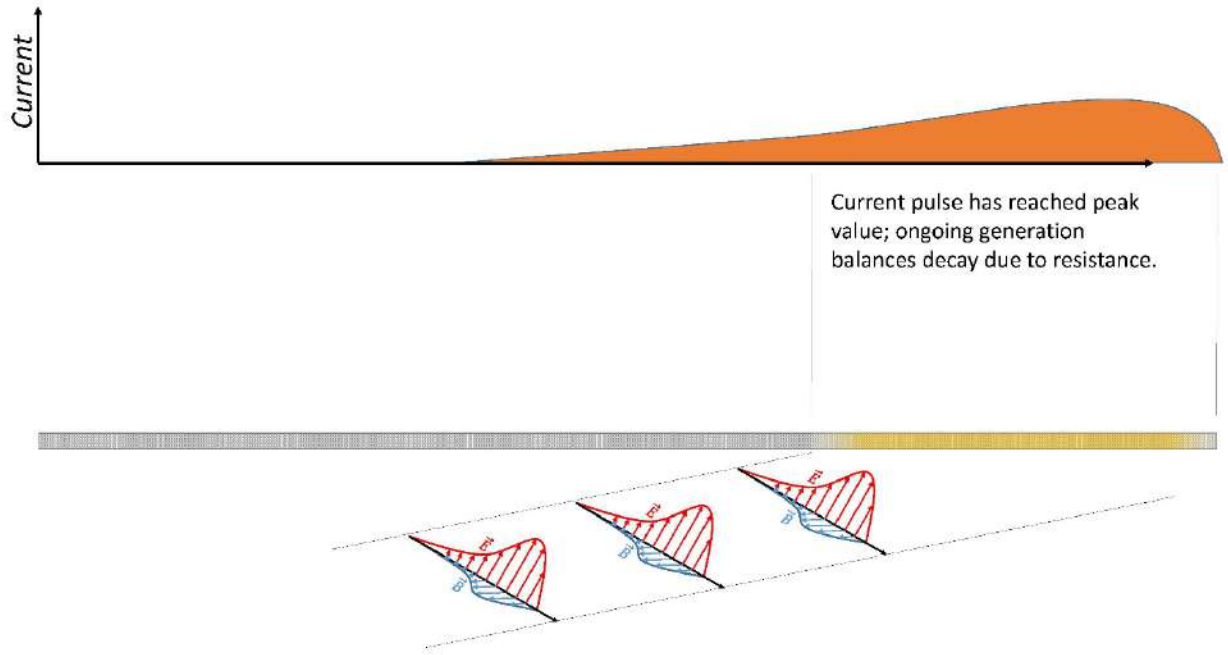

Figure 36: The current pulse within the conductive line has built to its highest possible value. At this point current generation in the yellow current generation zone exactly balances resistive losses.

Normally a discussion of coupling to lines indicates that longer lines couple more strongly to high frequency NEMP pulses. From the above discussion, however, one can see that this coupling holds true only up to the effective coupling length, after which the coupling has reached a maximum amplitude. For very long lines, it is coupling only within the effective coupling length to the ends of the lines that ultimately generates a current pulse creating a hazard to attached devices. The effective coupling length was briefly discussed in the early time pulse Metatech document (Savage et al., 2010) on page 5-6 (item #7) as well as on page 7-2.

The early time pulse Metatech document (Savage et al., 2010) suggests effective coupling lengths of about $1\ km$. A more recent set of documents (Xie et al., 2015; Xie, Li, Qiao, & Wang, 2016) agrees with this general assessment both numerically and experimentally, although they obtain somewhat shorter effective coupling lengths. The concept of an effective coupling length is very important for the analysis we intend to perform on the system-level effects of an NEMP. It allows us to treat entities on the BES as essentially independent where high frequency coupling occurs since they are generally separated by more than $1\ km$. This vastly simplifies the system wide analysis.

The model described above does not consider the ground (recall the cable was essentially floating in space). In the simplest approximation, the ground has two effects that both tend to attenuate the current pulse in the line. First, it increases current losses from the line through a very small amount of current leakage to ground. Second, the ground reflects the EMP wave creating a second interaction between the EMP wave and the line. After reflection, the EMP wave is attenuated and the horizontal component of the electric field (the component along the line) is oriented in the opposite direction (see Figure 37). For a perfectly horizontal line and ignoring the attenuation of the EMP wave, the reversal of the horizontal component creates another moving CGZ that effectively cancels the action of the initial

CGZ. The details of the attenuation and actual orientation of real transmission line relative to the reflected wave relative create a complex interaction that can only be addressed through system specific numerical calculations. Both of these ground effects, however, effectively attenuate the initial current pulse.

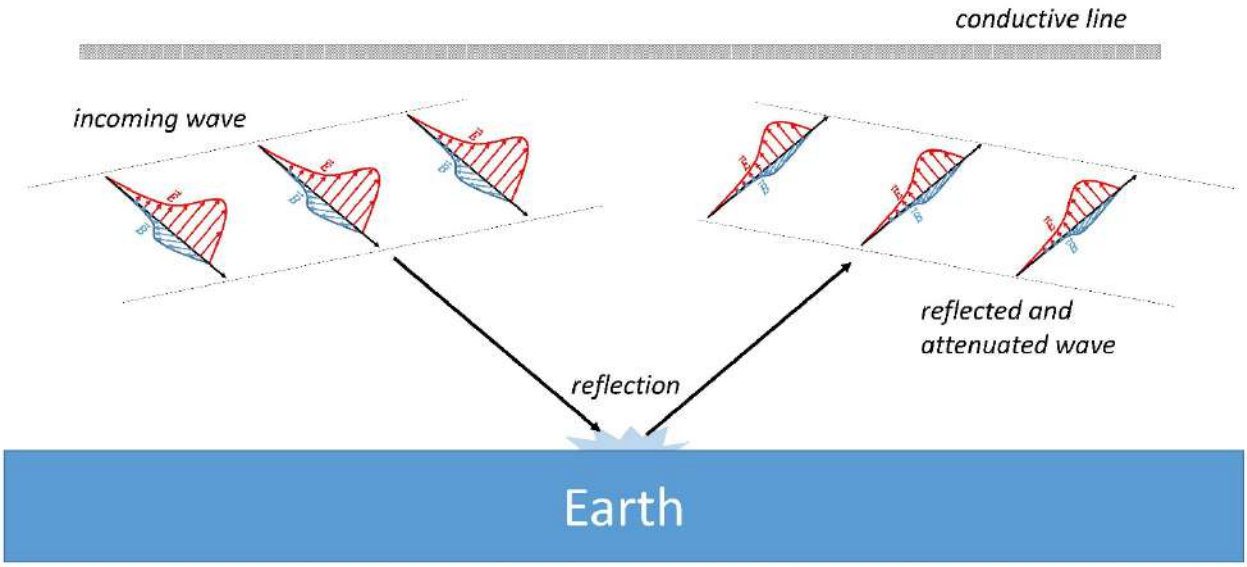

Figure 37: EMP wave reflected and attenuated by the ground. Note that the direction of the electric field along the conductive line reverses from pointing to the right to pointing to the left.

In summary, high frequency, free-field pulses generated by NEMP couple to conductors and drive currents within them. The degree of coupling depends on many variables, including: the angle of incidence of the pulse wave, the resistance of the conductors, the resistance of the ground, the height of the conductor above the ground, etc. A wave that hits a long conductor has an effective coupling length, which is a length of conductor after which the peak pulse current generated within the conductor can grow no larger due to the balance of current pulse generation with losses.

5.1.2.2 Conducted Coupling

Transmission and measurement lines can conductively couple. As in the case of radiative coupling, conductive coupling poses little threat to the transmission line itself. Rather, conductive coupling through transmission and measurement lines allows the high-frequency effects of NEMP to travel to other devices and potentially cause damage.

5.1.3 Power Transformers

5.1.3.1 Radiative Coupling

Transformers in a BES are generally housed in grounded, thick metal casing. This metal is more than thick enough to attenuate any significant radiative coupling to the internal components.

5.1.3.2 Conducted Coupling

The primary hazard generated to power transformers by the high-frequency effects of NEMP is conducted hazard from attached transmission lines.

When a high-voltage, high-current pulse passes from the transmission line into the terminal of a transformer, the first component it reaches is the bushings. Bushings are insulators with a conductive core that allow electrical current to pass through the grounded transformer case and into the transformer without arcing to the case. Lower voltage bushings utilize porcelain as an insulator, while higher voltage designs use oil and paper. When a bushing experiences a high voltage, the insulator may begin to break down, allowing an arc to pass from the conductive core, across the insulator, to the transformer casing. The ability of the insulator to withstand voltage surges degrades over time, which makes it difficult to determine the probability of a break down in a bushing. For oil bushings, for example, products of aging are known to build up in areas of high electrical stress, reducing the bushing's capacity to insulate against surges.

Assuming the pulse generated from the transmission line passes through the bushing without arcing, the pulse then passes into the transformer windings. One might expect that the transformers inductance would naturally attenuate or reflect such high frequency pulses but this is not the case because the pulse is so short in duration it does not significantly magnetize the transformer core. The windings in the transformer are insulated from each-other by paper/press board insulation that, just as in the case of the bushings, can break down and arc when subject to such high frequency pulses. This breakdown could happen between primary and secondary windings or between conductors within the individual windings, depending on the transformer design.

If the pulse does not cause an electrical break down within the core or at the bushings, the pulse can be efficiently transmitted from one winding to the next (effectively one winding "broadcasts" the signal to the other) and the pulse will pass through the transformer, possibly damaging substation equipment on the other side of the transformer.

In summary, power transformers can be damaged by high-frequency NEMP effects. The most likely damage occurs due to insulation breakdown, either within the bushings or between transformer windings. If no breakdown occurs within the transformer, it is possible for the pulse to travel through the transformer from one winding to the other with little attenuation.

5.1.4 Generation facilities

The major hazard to generation facilities is radiated coupling to measurement lines that causes conducted pulses to low-voltage control and protection electronics, resulting in misoperation and damage to generation capital equipment. The academic literature covering the interaction of generation facilities with fast transient voltages is almost nonexistent. Recently there has been some numerical research into the susceptibility of power plants to lightning strikes and switching transients (Yeo & Kim, 2012). The conclusion in that paper made the above assertions more quantitative, namely that the susceptible devices are low-voltage electronic protective and control equipment that are potentially damaged from high-voltage transients in the grounding system.

There are a host of IEEE standards and recommendations on grounding and lightning surge protection in generation facilities that were outside the original scope of Phase 0 and that have not been reviewed. As such, we do not know to what extent these standards and recommendations are implemented in actual generation settings. These standards are listed in Table 2. In Phase 1 of this work, we anticipate reviewing these standards to determine applicability and potentially aid in quantifying the high frequency hazard.

Table 2: IEEE standards for grounding and lightning surge protection

Standard number	Title
IEEE Std 80-2000	IEEE Guide for Safety in AC Substation Grounding (ANSI)
IEEE Std 81-1983	IEEE Guide for Measuring Earth Resistivity, Ground Impedance, and Earth Surface Potentials of a Ground System (ANSI)
IEEE Std 81.2-1991	IEEE Guide for Measurement of Impedance and Safety Characteristics of Large, Extended or Interconnected Grounding Systems
IEEE Std 142-1991	IEEE Recommended Practice for Grounding of Industrial and Commercial Power Systems
IEEE Std 367-1996	IEEE Recommended Practice for Determining the Electric Power Station Ground Potential Rise and Induced Voltage from a Power Fault (ANSI)
IEEE Std 487-2000	IEEE Recommended Practice for the Protection of Wire-Line Communication Facilities Serving Electric Supply Locations (ANSI)
IEEE Std 665-1995 (R2001)	IEEE Guide for Generating Station Grounding
IEEE Std 666-1991 (R1996)	IEEE Design Guide for Electrical Power Service Systems for Generating Stations
IEEE Std 998-	IEEE Guide for Direct Lightning Stroke Shielding of Substations
IEEE Std 1100-1999	IEEE Recommended Practice for Powering and Grounding Electronic Equipment
IEEE Std 1050-1996	IEEE Guide for Instrumentation and Control Equipment Grounding in Generating Stations (ANSI)
IEEE Std C37.101-1993	IEEE Guide for Generator Ground Protection (ANSI)
IEEE Std C62.23-1995 (R2001)	IEEE Application Guide for Surge Protection of Electric Generating Plants
IEEE Std C62.92.1-2000	IEEE Guide for the Application of Neutral Grounding in Electrical Utility Systems, Part I-Introduction (ANSI)
IEEE Std C62.92.2-1989 (R2001)	IEEE Guide for the Application of Neutral Grounding in Electrical Utility Systems, Part II-Grounding of Synchronous Generator Systems (ANSI)
IEEE Std C62.92.3-1993 (R2000)	IEEE Guide for the Application of Neutral Grounding in Electrical Utility Systems, Part III-Generator Auxiliary Systems (ANSI)

5.1.5 Relays

5.1.5.1 Radiative Coupling

Although protective relays are more susceptible to radiated hazard than well-shielded transformers, the relays' resilience is augmented due to its location in control housing, which is generally metallic, as well its location within racks, which further attenuate the radiated hazard. IEC-61000-2-11 (Commission, 1999) classifies these layers of protection into "concepts". Most modern concepts reduce expected peak radiated voltages by a factor of 10 or more, however, these modern concepts may not be in general use in older facilities.

Moreover, relay manufacturers design their relays with radiated hazards in mind because there are a large number of transient fields generated during normal operation in switchyards. Relays must pass

testing against electromagnetic compatibility standards (EMC) in order to demonstrate their suitability for use in switchyards. For example, Schweitzer Engineering Laboratories (SEL) reports that their SEL-411L relay withstands $5\ kV/m$ (one-tenth the peak magnitude of the exo-atmospheric E1 pulse) without incident and remains undamaged for pulses up to $34\ kV/m$[19].

There is a small probability of relay failure due to radiative coupling that will need to be accounted for in future phases.

5.1.5.2 Conductive Coupling

The primary conducted hazard to relays is not through their voltage and current sensing ports, which are already designed with surges caused by the switchyard operations in mind. This fact is echoed in (Savage et al., 2010) on page 7-9. Rather, the relay's low voltage communication and control ports seem to be the most susceptible to upsetting and, possibly, damaging the relay. If a control house does not provide adequate attenuation of the radiated hazard, it is possible for the early time E1 pulse created by an exo-atmospheric burst to couple to communication lines *within* control houses. Surges produced on these lines would enter, almost unfiltered, into the relay's control and communication ports, possibly damaging the components. As an example, SEL tests their relays against IEC-60255-26 for surge and conducted radio frequency interference hazards. A review of this and related standards will be performed in Phase 1 of this work to determine if such testing is adequate to draw conclusions about a particular devices resilience to NEMP early time conducted hazards.

5.2 Low Frequency Device Coupling

This section is applicable to the coupling of magnetic field fluctuations created by GMD or late time exe-atmospheric NEMP to the BES. It does not apply to high-frequency effects created during the early time, E1 phase of NEMP.

5.2.1 Transmission Lines

Magnetic field fluctuations caused by GMD or late time NEMP alter the direction and field strength of magnetic field lines (i.e., the magnetic flux) penetrating the surface of the earth. The Earth is a reasonable conductor, and as we saw in much of the discussion in section 3.2.3, when a conductor is subject to changing magnetic flux it generates internal currents that create their own magnetic fields in opposition to the magnetic flux changes. In the Earth, these currents are called telluride currents. Given the finite conductivity of the Earth, the telluric currents cannot perfectly oppose the fluctuations induced by the GMD or late time NEMP.

At the surface of the Earth where our BES system resides, the total magnetic field fluctuations are the sum GMD or late time NEMP magnetic field fluctuations and the opposition field fluctuations generated by the telluric currents. The resultant low-frequency fluctuations in the surface magnetic field generates electrical fields at the Earth's surface.[20] These electrical fields can couple into conductors (and any other structure) on the Earth's surface and drive a geomagnetically induced current (GIC).

Surface electric fields generated by the above effects for large geomagnetic disturbances are on the order of $1\ V/km\ \leftrightarrow 10\ V/km$. To have a significant GIC within a structure from this low level of electric

[19] https://cdn.selinc.com/assets/Literature/Miscellaneous/EMP-Threats_20150408.pdf?v=20151024-141016
[20] By Faradays law of induction.

field, the structure would have to be kilometers-large and a fairly good conductor. Most components in the BES are not that large, thus they will not experience a direct coupling to the surface field. Transmission lines, however, generally span $50\ km \leftrightarrow 100\ km$ or more, and are good conductors, which makes them particularly efficient coupling structures for the low frequency fluctuations caused by GMD and late-time NEMP.

As with high-frequency coupling, the current driven in the transmission line will have almost no effect on the line itself. It is the BES components at the ends of the line that are most susceptible to damage. The BES components on either end of transmission lines are power transformers.

5.2.2 Power Transformers

When the surface electric fields caused by GMD or late-time NEMP drives currents through a transmission line, the transmission line pulls that current from the nearest available source of free electrons at one of its ends and dumps the current out at the opposing end into the nearest available sink of electrons. As stated above, transmission lines are connected at either end to power transformers. Three-phase wye connected transformers and autotransformers have a grounded neutral. Such grounds tap a very large source and sink of electrons: the Earth. Illustrated in Figure 38 is the flow of a GIC being drawn out of the ground, through the grounded neutral of a power transformer on the left, down the transmission line, and back into the Earth through the grounded neutral of the transformer on the right.

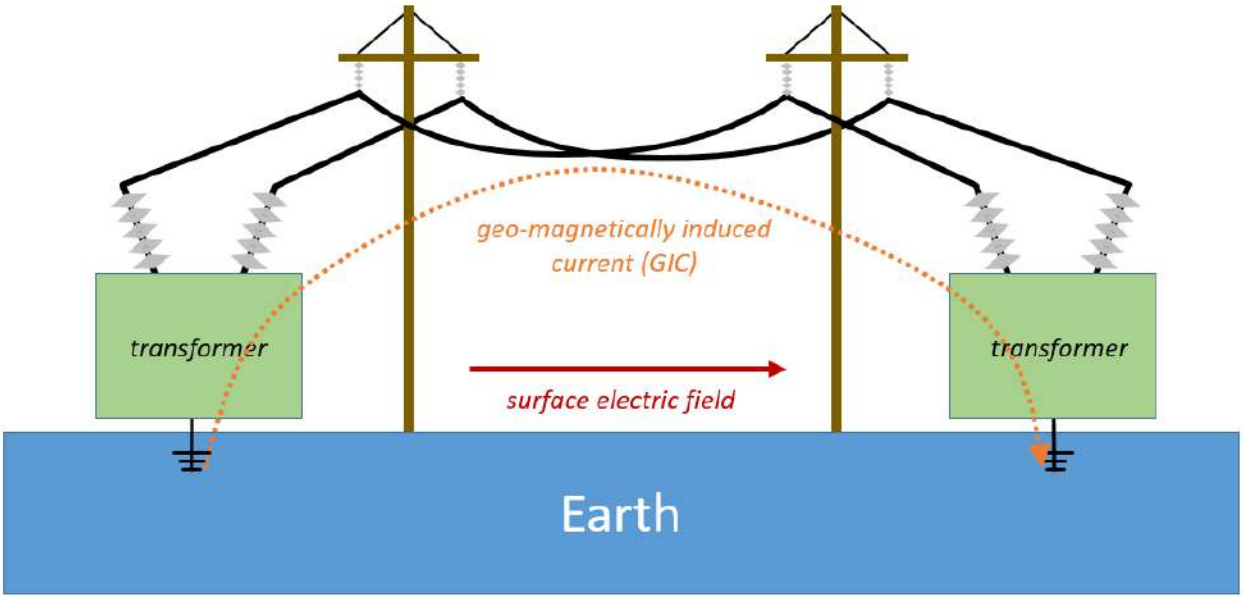

Figure 38: The flow of geo-magnetically induced current (GIC) due to surface electric fields caused by a GMD or late time NEMP.

The total current passing through the transformer divides approximately equally through each of the three phases. This per-phase-current varies slowly in time compared to the normal $60Hz$ frequency in the BES and can be thought of as a quasi-DC current passing through the transformer on top of the

normal AC magnetizing current. The quasi-DC current caused by GICs can grow to be many times larger than the AC magnetizing current within the transformer[21].

When a quasi-DC current adds to an AC current in a transformer, it biases the magnetism in the transformers core. If the quasi-DC offset becomes large enough, the resultant bias in the core can lead to an effect known as half-cycle saturation. All of the negative effects to transformers are ultimately attributable to half-cycle saturation. Among these effects are the following:

1. The transformer draws an increased amount of reactive power that causes the voltage to drop.
2. Magnetic flux, which the now-saturated magnetic core can no longer contain, penetrates and begins to heat the metallic components[22]
3. The transformer begins to generate harmonic voltage fluctuations within the BES.

In the first effect, if it the reactive power load is widespread and becomes large enough, it may leads to voltage collapse and shut down of the BES. The heat of the transformer in the second effect may result in reduced transformer life or potentially catastrophic transformer failure, if the heating is severe. The final effect has important impacts throughout the BES as it distorts the AC voltage waveform, which can lead to relay misoperation, difficulties in switching, overheated capacitor banks and a host of other negative effects that may also lead to shut down of the BES. For more discussion on such effects, the reader can reference (NERC, 2014).

5.3 Standards

In this section we review some of the standards that exist with respect to NEMP and GMD. These standards indicate well known mitigation responses for components that are vulnerable to NEMP and GMD.

5.3.1 International NEMP standards

International standards for exo-atmospheric NEMP were primarily done by the International Electrotechnical Commission based in Geneva, Switzerland, via subcommittee 77C. The more important standards that the IEC produced related to our study are listed in Table 3.

Table 3: International Electrotechnical Commission NEMP standards

Standard number	Title	Summary
IEC-61000-2-9	Description of HEMP Environment – Radiated Disturbance	Provides double exponential waveforms for the three high altitude HEMP stages (E1, E2 and E3)
IEC-61000-2-10	Description of HEMP Environment – Conducted Disturbance	Provides levels of current produced by HEMP on electrical lines.
IEC-61000-2-11	Classification of HEMP Environments	Provides expected levels of radiative and conducted hazard for devices exposed to HEMP. This includes expected levels

[21] The degree to which this occurs depends on the load being born by a transformer at the time the GIC occurs.
[22] This effect is utilized by induction stoves to heat cooking pans.

		within various shielding concepts (e.g. various qualities of control housing in substation yards)
IEC-61000-4-23	Test Method for Protective Devices for HEMP and Other Radiated Disturbances	Describes methods for testing shielding to radiated HEMP hazards.
IEC-61000-4-24	Test Method for Protective Devices for HEMP Conducted Disturbances	Describes methods for testing protective devices to conducted HEMP hazards.
IEC-61000-4-25	HEMP Immunity Test Methods for Equipment and Systems	Describes methods for testing equipment to conducted HEMP hazards.
IEC-61000-4-32	Testing and Measurement Techniques – High-Altitude Electromagnetic Pulse (HEMP) Simulator Compendium	Lists worldwide HEMP simulators and provides characteristics (type, waveform, etc…) or each.

Perhaps the most interesting of these standards, from the point of view of our study, is IEC-61000-2-11. In this standard, the complicated question of control house attenuation is addressed with a simple classification of the control house into a "protection concept". Each protection concept yields expected levels of radiated and conducted hazard within the control house itself. This classification system yields a simple way of characterizing substations, and ultimately the risk to electronics such as relays within the control house. This particular system, or a version of it, will likely form the backbone of the analysis workflows that will be developed in Phase 2 of this this work.

The IEC standards provide a workflow whereby devices and systems can be evaluated for their relative immunity to HEMP. First, the component or subsystems enclosure is classified into a protection concept using IEC-61000-2-11. Alternatively, the efficacy of the protective devices can be classified using IEC-61000-5-3.[23] After establishing these protective concepts, IEC-61000-4-25 can be used to determine appropriate test levels to ensure the system or device is immune to HEMP.

5.3.2 NEMP military standards

[23] We do not listed IEC-61000-5-3 above as it is likely too detailed for the analysis we intend

Table 4 provides a list of some unclassified U.S. military standards related to NEMP. We do not reference or use these standards widely in our proposed study for two reasons. First, to the best knowledge of the authors, these standards are not widely implemented in civilian applications due to the expense. Certainly they are never completely used, although some manufactures may appeal to portions of the standard. Second, there is no gradation of scale in these standards: one either complies with the standard or not. The gradations of scale provided in the IEC standards, as discussed above, will be far more valuable to our study.[24]

[24] This is not to say that the standards are not valuable in general. Indeed, the authors note that MIL-STD-188-125-1 is the preeminent document regarding the complete hardening of a fixed facility to the effects of exo-atmospheric bursts.

Table 4: Unclassified military standards

Standard number	Title	Summary
MIL-STD-2169B (2012)	High-Altitude Electromagnetic Pulse (HEMP) Environment	Sets test procedures required to evaluate the effects of (HEMP) environment on military equipment. Specifies both the pulse generation (e.g., horizontally polarized dipole facility) as well as measurement procedure.
MIL-STD-188-125-1 (2005)	High-Altitude Electromagnetic Pulse (HEMP) Protection for Fixed Ground-Based C4I Facilities Performing Critical, Time-Urgent Missions	Details installation and testing procedure for low-risk fixed military facilities that need to be resilient to EMP environment.
MIL-STD-188-125-2 (1999)	High-Altitude Electromagnetic Pulse (HEMP) protection for Ground Based C41 Facilities…Transportable Systems	Same as 125-2 but for mobile military systems.
MIL-STD-461F (2007)	Requirements for the Control of Electromagnetic Interference Characteristics of Subsystems and Equipment	Sets limits on the susceptibility of electrical components procured by the military to electromagnetic interference (EMI). Specifies appropriate testing for this as well. Also sets limits on the emission of EMI from components.
MIL-STD-464C (2010)	Electromagnetic Environmental Effects Requirements for Systems	A general overview on electromagnetic compatibility requirements for defense system. Has a brief discussion of NEMP that mostly points to 188-125-1 and 2169.
MIL-HDBK-423	High-Altitude Electromagnetic Pulse (HEMP) Protection for Fixed and Transportable Ground-Based Facilities, Volume I: Fixed Facilities	More extensive guidance on implementing the requirements of MIL-STD-188-125-1

6 Anticipated Power System Restoration and Recovery

The recovery and restoration of the BES following any of the events discussed in the Phase 0 report is important in relation to the key bounding assumption of this study—**we limit the study to events that cause $2 billion per day (2016 dollars) impact to gross domestic product from lost BES capacity for at least 3 days.** Nuclear detonation events of any kind are likely to have some impact on the electrical power system, however, not all of these will generate large enough consequences to be of concern. To focus the analysis in the following phases of this study onto events of high consequence and eliminate events that have minor fiscal impact or are of short duration, we discuss the timeline of several major power systems outage and compare them to the bounding assumption above.

In the absence of substantial equipment damage, blackouts that originate in the bulk electric power system are generally restored within 3 days and often much sooner. Below, we summarize some examples of widespread blackouts. In all cases, electric power was restored to at least 90% of the BES within 3 days. These examples of system restoration are particularly relevant to SREMP cases that cause extreme but localized physical damage to the power system and potentially cascade throughout the rest of the system. We expect these cascades to be very similar to the cascading outages and blackouts summarized below as such, they are not expected to result in widespread outages lasting longer than 3 days.

In contrast, HEMP may indeed create widespread physical damage to certain components; e.g., protective relays in the transmission network, distribution network components, and communications; which may result in prolonged restoration timelines. Some of these issues are addressed later in this section.

6.1 Typical Restoration Timeline Following Wide-Spread Blackouts

1989 Hydro Quebec Blackout

On March 13, 1989, Quebec, Canada, experienced a geomagnetic storm that, within 2 minutes, caused a black out of the Quebec electric power grid that affected six million customers and approximately 21,000 MW of load. NERC 1990 provides a concise discussion of the sequence of events, degree of physical damage to transmission components, and the restoration timeline. An intense geomagnetic disturbance, generated high levels of harmonic currents causing the tripping of seven reactive power compensators on the Hydro Quebec transmission grid. The loss of reactive power and voltage support from these components led to the tripping of one major 735 kV transmission line in the La Grande transmission network and two major generation units. The cascading continued with the loss of the three additional 735 kV transmission lines in the La Grande network and subsequent faults in associated equipment. Next, the final 735 kV transmission line tripped and isolated 9,400 MW of generation from the rest of the Hydro Quebec system. The resulting rapid frequency decline could not be compensated by under frequency load shedding. A major portion of the Hydro Quebec system collapsed in an uncontrolled manner in approximately 6 seconds, with subsequent tripping of transmission lines ultimately resulting in collapse of the remainder of the system.

The very rapid cascading event did create some physical damage to transformers, resulting in 1,800 MW of generation being unavailable during restoration. Additional (non-transformer) damage was incurred

at several substations. The collapse resulted in 685 MW of nuclear generation being unavailable for an extended period.

Despite the rapid uncontrolled system collapse and the loss of some major equipment, the bulk electric power system was nearly completely restored within 9 hours. The timeline of the restoration is shown in Figure 39. NERC 1990[25] notes that restoration of transmission was delayed mainly because of the unavailability of strategic equipment, however, the restoration plan and system configuration was modified to compensate for this equipment loss. NERC 1990 notes that Hydro Quebec's communications systems were fully operable during the restoration.

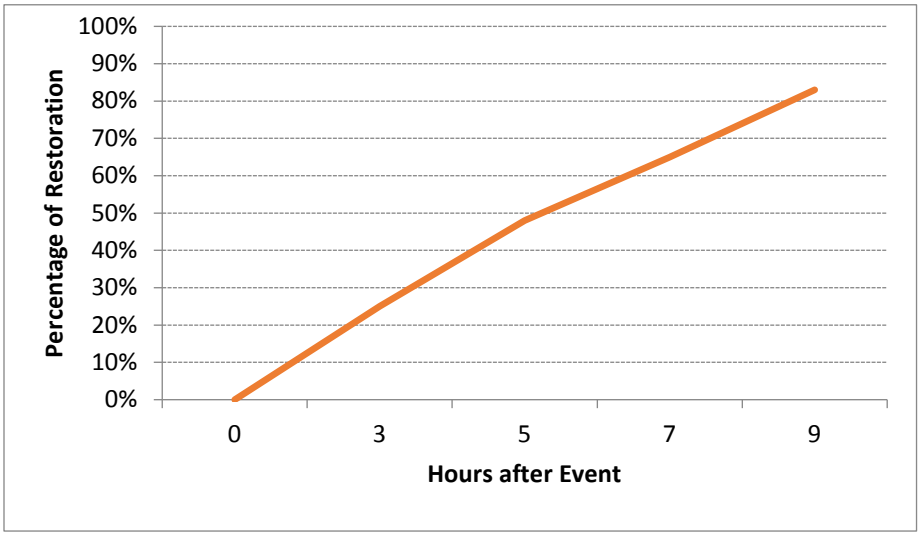

Figure 39: Restoration curve, Hydro-Quebec geomagnetic storm, March 13, 1989

2003 Northeast Blackout

On August 14, 2003, three 345-kV transmission circuits in northeastern Ohio contacted overgrown trees, which started a chain of events that ultimately collapsed the electrical grid across the eastern and northeastern United States and eastern Canada. The sequence of events leading to the blackout is quite complex. An initial high-level summary is available from (FERC 2003)[26] and a more detailed report is available.[27] In contrast to the 1989 Hydro Quebec blackout, the cascade in the 2003 Northeast blackout started slowly, with spatially distributed component tripping occurring over an approximately 4-hour period. When the stress on the system increased sufficiently, the cascade quickly accelerated, completing in roughly 1 to 2 minutes and blacking out major portions of the power system. Although the final incident report[28] indicates damage assessments were completed, no publicly available version was

[25] North American Electric Reliability Corporation, "March 13, 1989, Geomagnetic Disturbance," www.nerc.com/files/1989-Quebec-Disturbance.pdf, accessed August 22, 2016.
[26] Federal Energy Regulatory Commission, "August 14, 2003 Outage Sequence of Events , U.S./Canada Power Outage Task Force," September 3, 2013, www.ferc.gov/industries/electric/indus-act/reliability/blackout/09-12-03-blackout-sum.pdf, accessed August 22, 2016.
[27] U.S.-Canada Power System Outage Task Force, "Final Report on the August 14, 2003 Blackout in the United States and Canada: Causes and Recommendations," April 2014, http://energy.gov/sites/prod/files/oeprod/DocumentsandMedia/BlackoutFinal-Web.pdf, accessed August 22, 2016.
[28] Ibid.

available. There was no indication that grid operators' communications systems were compromised during the event or the following restoration.

ICF Consulting (2003)[29] used NERC press releases about the event to estimate the initial size of the outage (61,800 MW and 50 million customers), the restoration curve over the ensuing three days, and the economic impact. The economic impact estimated by ICF is consistent with the daily values estimated by the Anderson Economic Group (Anderson and Geckil 2003).[30] Despite the uncontrolled collapse of the power system, electrical power was restored to the majority of customers within 72 hours. Figure 40 shows the restoration curve for this event using data reinterpreted from by ICF Consulting (2003).[31]

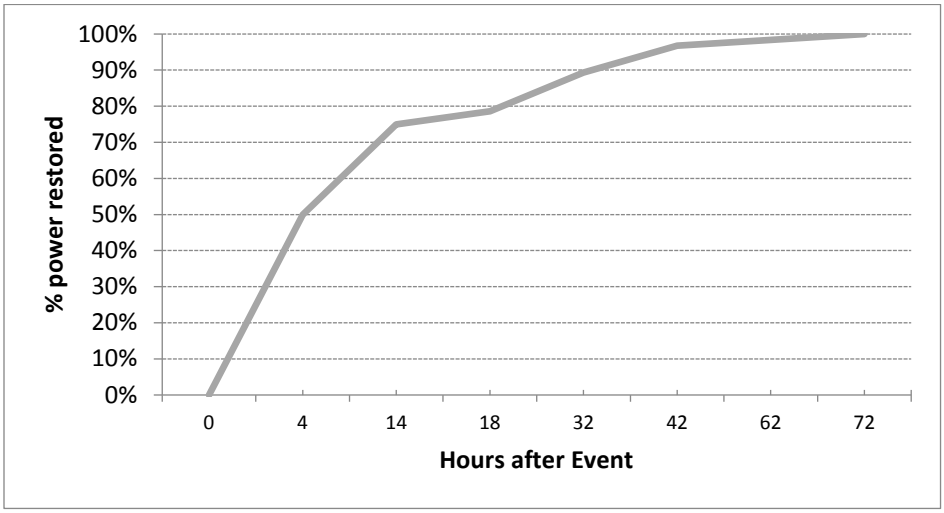

Figure 40: Restoration curve, 2003 Northeast U.S. blackout

2015 Turkey Blackout

On March 31, 2015, a blackout affected the entire electric power grid of Turkey, which has a population of approximately 75 million people. Initiated by tripping of overloaded lines, the subsequent dynamics instabilities led to a rapid collapse of the entire system within approximately 10 seconds. Figure 41 shows the restoration timeline and indicates that to 95% of the system load was restored within 9 hours (TEIAS/ENTSO-E 2015).[32]

[29] ICF Consulting, "The Economic Cost of the Blackout: An issue paper on the Northeastern Blackout, August 14, 2003," www.solarstorms.org/ICFBlackout2003.pdf, accessed August 22, 2016.
[30] Anderson Economic Group, "Northeast Blackout Likely to Reduce US Earnings by $6.4 Billion," August 19, 2003," www.andersoneconomicgroup.com/Portals/0/upload/Doc544.pdf, accessed August 22, 2016
[31] ICF Consulting, "The Economic Cost of the Blackout: An issue paper on the Northeastern Blackout, August 14, 2003," www.solarstorms.org/ICFBlackout2003.pdf, accessed August 22, 2016.
[32] European Network of Transmission System Operators for Electricity, "Report on Blackout in Turkey, 31 March 2015," September 21, 2015, www.entsoe.eu/Documents/SOC%20documents/Regional_Groups_Continental_Europe/20150921_Black_Out_Report_v10_w.pdf, accessed August 22, 2016.

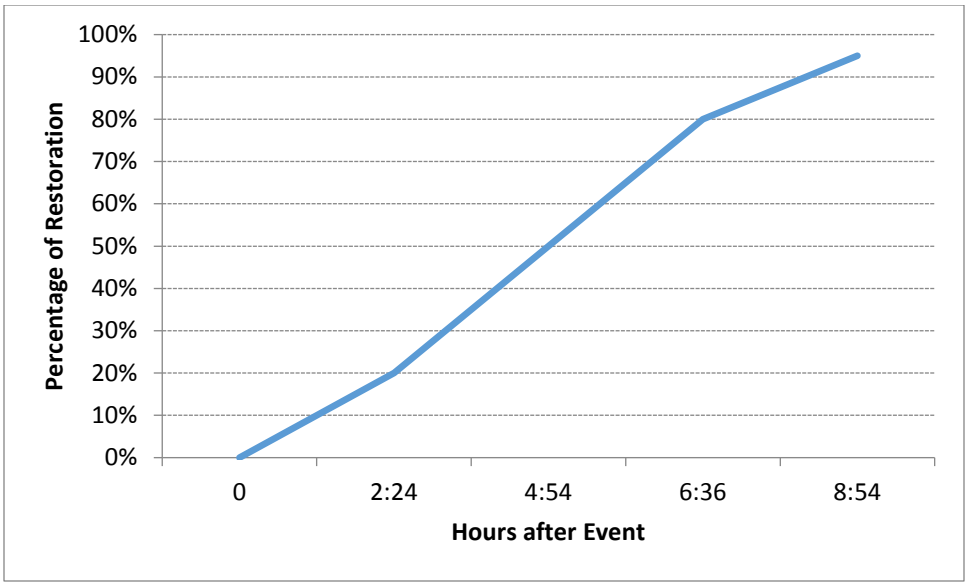

Figure 41: Restoration curve, Turkey blackout event, March 31, 2015

6.2 Potential Differences from Typical Restoration Timelines for NEMP Events

Earlier discussion identified that ground-burst SREMP events are the most likely to cause significant effects on the BES. The bounding assumptions of this study limit the event to single burst. This burst will cause substantial physical and electromagnetic damage to the surrounding BES equipment and devices, however, the propagation of electromagnetic effects to distances far outside the immediate blast zone is not anticipated. The localized damage to the BES components may indeed cascade to other parts to the BES, potentially causing a widespread blackout similar to those discussed above. The lack of widespread direct physical damage from the ground-burst SREMP will likely result in a restoration time line similar to the major blackout events discussed above.

In contrast, a HEMP event may result in widespread physical damage to BES and non-BES components that may significantly extend the restoration time line.

- Widespread damage to relays in the BES will lead to a loss of demonstrable protection on parts of the BES network preventing the ability of the BES operators to re-energize those network components. Restoration will likely be delayed at least until a sufficient number of relays have been replaced to enable demonstrable protection.
- Widespread damage to non-BES power systems and components, e.g. distribution networks and customer load, may significantly affect black start restoration plans. Reduced loading along black start paths may impact the voltage and dynamical stability of these paths potentially forcing real-time adaptation of the plan and associate delays.
- HEMP may also result in the concurrent loss of communications, both SCADA and normal telecom, between BES operators, generator operators, and other utility to personnel. The lack of system visibility and direct control of generators and other devices will lead to conservatism that will likely delay the restoration timeline.

7 Conclusion

Electric power is a national lifeline. Both NEMP and GMD are identified as threats to the system that could potentially create widespread, long-term outages. The potential effects of EMP have been widely discussed but there is yet no agreed-upon metric for defining events of concern. In this initial Phase 0 of a four-phase study, we have identified metrics to use to bound electric power outage events. Many outages, even those that are widespread, are restored within 1 to 2 days, causing inconvenience to customers but not wreaking havoc on society and the economy. Therefore, we are concerned with only truly damaging outages, those longer that 3 days that cause more than $4 billion per day in lost GDP. We have described the qualitative physics of NEMP and GMD and determined methods to parameterize these events to enable the identification of “events of concern”. This parameterization and associated classification will be made more concrete in Phase 1 of the study. We have reviewed the standards documents relevant to NEMP and GMD and their impact on the BES that were identified prior to the execution of Phase 0 and identified additional standards that are potentially required to carry out the work of the subsequent phases. Finally, we have identified several major BES blackouts to validate that, for BES that do not suffer significant physical damage, the BES restoration timeline is shorter than the 3 day timeframe used to define an “event of concern”.

Phase 1-3 Potential Participants and Reviewers

As this study moves beyond Phase 0, additional expertise will be required beyond the participants in Phase 0. These include experts in power systems protection, dynamics, and electromagnetic transients, and other special studies such as Randy Horton and Paul McGlynn at the Electric Power Research Institute, Dmitry Kosterev at Bonneville Power Authority, Anthony Montoya at Western Area Power Authority, and Travis Smith at Oak Ridge National Laboratory. Phases 1-3 may also engage with specific device manufacturers including Schweitzer Engineering Laboratories, Siemens, and ABB.

Many individual reviewers for Phases 1-3 are potentially available via the authors cited in the Phase 0 bibliography. The reviewer pool should also be extended to a range of Federal agencies with expertise in NEMP, GMD, and impacts on power systems including the Department of Energy, Department of Homeland Security, and the Defense Threat Reduction Agency.

Bibliography

EMP Response of Overhead Power Lines; Vol. 1, TLNET Computations (U), RDA TR 000281329001 001. (1990).

Agrawal, A. K., Price, H. J., & Gurbaxani, S. H. (1980). Transient response of multiconductor transmission lines excited by a nonuniform electromagnetic field. *IEEE transactions on electromagnetic compatibility* (2), 119-129.

Air Force Weapons Laboratory, K. A., NM. (1971). *Electromagnetic Pulse Interaction Notes, Volume 4 Notes 48 through 64 (U)", AFWL EMP 3 4*. Retrieved from

Albertson, V., Bozoki, B., Feero, W., Kappenman, J., Larsen, E., Nordell, D.,. . *Power Delivery, 8*(3), 1206-1216.

Albertson, V., Thorson, J., & Miske, S. (1974). The effects of geomagnetic storms on electrical power systems. *IEEE Transactions on Power Apparatus and Systems* (4), 1031-1044.

Anon. (1984). *Electromagnetic coupling of high-altitude, nuclear electromagnetic pulses*. Retrieved from United States:

Arajärvi, E., Pirjola, R., & Viljanen, A. (2011). Effects of neutral point reactors and series capacitors on geomagnetically induced currents in a high-voltage electric power transmission system. *Space Weather, 9*(11).

Babb, D. D., & Martinez, J. P. (1976). *Electromagnetic Pulse Analysis of Small Power Systems*. Retrieved from

Backhaus, S. N., & Rivera, M. K. (2015). *Review of the GMD Benchmark Event in TPL-007-1*. Retrieved from

Bahiana, L. C. (1964). *Electromagnetic induction on an expanding conducting sphere*: Massachusetts Institute of Technology, Research Laboratory of Electronics.

Bainbridge, K. T. (1976). *Trinity*. Retrieved from

Baird, J. K., & Frigo, N. J. (1973). *Effects of Electromagnetic Pulse (EMP) on the Supervisory Control Equipment of a Power System*. Retrieved from

Baker III, G. H. (2012). EMP and geomagnetic storm protection of critical infrastructure.

Barnes, P., McConnell, B., Van Dyke, J., Tesche, F., & Vance, E. (1993). *Electromagnetic pulse research on electric power systems: Program summary and recommendations*. Retrieved from

Barnes, P., Rizy, D., & Tesche, F. (1994). *MHD-EMP and Electric Power Systems*. Retrieved from Oak Ridge, TN:

Barnes, P., Tesche, F. M., & Vance, E. (1992). *Mitigation of Magnetohydrodynamic Electromagnetic Pulse (MHD-EMP) Effects from Commercial Electric Power Systems*.

Barnes, P., Vance, E., & Askins Jr, H. (1984). *Nuclear electromagnetic pulse (EMP) and electric power systems*. Retrieved from

Barnes, P. R., & Hudson, T. L. (1989). Steep-front short-duration voltage surge tests of power line filters and transient voltage suppressors. *IEEE Transactions on Power Delivery, 4*(2), 1029-1036.

Barnes, P. R., Tesche, F. M., McConnell, B. W., & Vance, E. F. (1993). *MHD-EMP analysis and protection*. Retrieved from

Barrett, C. L., Centeno, V., Eubank, S., Evrenosoğlu, C. Y., Marathe, A., Marathe, M. V., Phadke, A. (2014). *Impact of a surface nuclear blast on the transient stability of the power system.* Paper presented at the International Conference on Critical Information Infrastructures Security.

Barrett, C. L., Eubank, S., Evrenosoglu, C. Y., Marathe, A., Marathe, M. V., Phadke, A. Vullikanti, A. (2013). *Effects of hypothetical improvised nuclear detonation on the electrical infrastructure.* Paper presented at the Security in Critical Infrastructures Today, Proceedings of International ETG-Congress 2013; Symposium 1:.

Bassett, K., & Mumford, M. (1996). *Summary Threat to National Security/Emergency Preparedness (NS/EP) Telecommunications (U), DI-2720-1-97*. Retrieved from

Baum, C. E. (1992). From the electromagnetic pulse to high-power electromagnetics. *Proceedings of the IEEE, 80*(6), 789-817.

Baum, C. E. (2007). Reminiscences of high-power electromagnetics. *IEEE transactions on electromagnetic compatibility, 49*(2), 211.

Bedrosian, G. (1979). *E-3A EMP Dipole Test; Vol. 3: Results from Coupling Experiments; Pt. 1: External Coupling Responses and Extrapolation Procedures, AWFL TR 79 90 V3 Pt.1; DC FR 1400 III*. Retrieved from Albuquerque, NM:

Bedrosian, P. A., & Love, J. J. (2015). Mapping geoelectric fields during magnetic storms: Synthetic analysis of empirical United States impedances. *Geophysical Research Letters, 42*(23).

Beers, B., & O'Donnell, H. B. (1984). *Prompt Radiation Effects on Communications Satellites (U)", AC 7873 001*. Retrieved from

Bernstein, G., Cameron, J. A., & Schwartz, J. (1988). *EMP Coupling to Cheyenne Mountain Power Lines (U), MTR 10399*. Retrieved from Bedford, MA:

Bo, D., Ze-Zhong, W., Lian-Guang, L., Li-Ping, L., & Chun-Ming, L. (2015). Proximity Effect on the Induced Geoelectric Field at the Lateral Interface of Different Conductivity Structures During Geomagnetic Storms. *Chinese Journal of Geophysics, 58*(1), 32-40.

Boteler, D. (2006). The super storms of August/September 1859 and their effects on the telegraph system. *Advances in Space Research, 38*(2), 159-172.

Boteler, D., Bui-Van, Q., & Lemay, J. (1994). Directional sensitivity to geomagnetically induced currents of the Hydro-Quebec 735 kV power system. *IEEE Transactions on Power Delivery, 9*(4), 1963-1971.

Boteler, D., Pirjola, R., & Nevanlinna, H. (1998). The effects of geomagnetic disturbances on electrical systems at the Earth's surface. *Advances in Space Research, 22*(1), 17-27.

Bozoki, B., Chano, S., Dvorak, L., Feero, W., Fenner, G., Guro, E., .McLaren, P. (1996). The effects of GIC on protective relaying. *IEEE Transactions on Power Delivery, 11*(2), 725-739.

Broad, W. J. (1981). Nuclear pulse (I): Awakening to the chaos factor. *Science (Washington, DC);(United States), 212*.

Broad, W. J. (1981). Nuclear pulse (II): Ensuring delivery of the doomsday signal. *Science, 212*(4499), 1116-1120.

Burrage, L., Hettwer, P., Howells, E., Veverka, E., Smith, I., Nelson, J., & Dugan, R. (1987). *Assess the impact of the steep-front, short duration impulse on electric power system insulation: Phase 1, Final report*. Retrieved from

Burrage, L., Shaw, J., & McConnell, B. W. (1990). Distribution transformer performance when subjected to steep front impulses. *IEEE Transactions on Power Delivery, 5*(2), 984-990.

Butt, Y. M. (2010). The EMP Threat: Fact, Fiction, and Response. *The Space Review*.

Cannon, P., Angling, M., Barclay, L., Curry, C., Dyer, C., Edwards, R., Jackson, D. (2013). *Extreme space weather: impacts on engineered systems and infrastructure*: Royal Academy of Engineering.

Chandrasena, W., McLaren, P., Annakkage, U., & Jayasinghe, R. (2004). An improved low-frequency transformer model for use in GIC studies. *IEEE Transactions on Power Delivery, 19*(2), 643-651.

Chang, H. T. (1972). *EMP Induced Currents on Power Lines (U), AL 723*. Retrieved from Albuquerque, NM:

Chavin, S., Crevier, W. F., Kilb, R. W., & Longmire, C. L. (1979). *MHDEMP Code Simulation of Starfish*. Retrieved from

Chen, B., Wang, Y., Li, J., & Wang, J. (2007). *Electromagnetic pulse bombs' defense*. Paper presented at the Second International Conference on Spatial Information Technology.

Chen, S., Guo, J., & Kelun, L. *Study of Influence Factors of Transient Enclosure Voltages in GIS*. Retrieved from

Chiariello, A., Maffucci, A., Miano, G., Villone, F., & Zamboni, W. (2008). A transmission-line model for full-wave analysis of mixed-mode propagation. *IEEE Transactions on Advanced Packaging, 31*(2), 275-284.

Chrzanowski, P., & Futterman, J. (1993). *Assessment of Electromagnetic Pulse (EMP) Effects on the U.S. Civilian Infrastructure (U), CD 93 0006*. Retrieved from Livermore, CA:

Cinsavich, A. (1998). Hemp Filters Installed as Part of a Distribution System (U), MRC ABQ R 1123; C3IEP 2 WHC 022 [Press release]

Clayton, R., Grant, I., Hedman, D., & Wilson, D. (1983). Surge arrester protection and very fast surges. *IEEE Transactions on Power Apparatus and Systems*(8), 2400-2412.

Cliver, E. W., & Dietrich, W. F. (2013). The 1859 space weather event revisited: limits of extreme activity. *Journal of Space Weather and Space Climate, 3*, A31.

Commission, I. E. (1996). IEC 61000-2-9: 1996 Electromagnetic compatibility (EMC) - Part 2: Environment - Section 9: Description of HEMP environment - Radiated disturbance. Basic EMC publication.

Commission, I. E. (1996). IEC TS 61000-5-4: 1996 Electromagnetic compatibility (EMC) - Part 5: Installation and mitigation guidelines - Section 4: Immunity to HEMP - Specifications for protective devices against HEMP radiated disturbance. Basic EMC Publication.

Commission, I. E. (1998). IEC 61000-2-10:1998 Electromagnetic compatibility (EMC) - Part 2-10: Environment - Description of HEMP environment - Conducted disturbance.

Commission, I. E. (1999). IEC 61000-2-11:1999 Electromagnetic compatibility (EMC) - Part 2-11: Environment - Classification of HEMP environments International Electrotechnical Commission.

Commission, I. E. (1999). IEC TR 61000-5-3:1999 Electromagnetic compatibility (EMC) - Part 5-3: Installation and mitigation guidelines - HEMP protection concept.

Commission, I. E. (2000). IEC 61000-4-9:1993+AMD1:2000 CSV Electromagnetic compatibility (EMC) - Part 4-9: Testing and measurement techniques - Pulse magnetic field immunity test.

Commission, I. E. (2002). IEC TR 61000-1-3:2002 Electromagnetic compatibility (EMC) - Part 1-3: General - The effects of high-altitude EMP (HEMP) on civil equipment and system.

Commission, I. E. (2002). IEC TR 61000-4-32:2002 Electromagnetic compatibility (EMC) - Part 4-32: Testing and measurement techniques - High-altitude electromagnetic pulse (HEMP) simulator compendium.

Commission, I. E. (2002). IEC TR 61000-5-6:2002 Electromagnetic compatibility (EMC) - Part 5-6: Installation and mitigation guidelines - Mitigation of external EM influences.
Commission, I. E. (2003). IEC 61000-6-6:2003 Electromagnetic compatibility (EMC) - Part 6-6: Generic standards - HEMP immunity for indoor equipment.
Commission, I. E. (2009). IEC TS 61000-5-8:2009 Electromagnetic compatibility (EMC) - Part 5-8: Installation and mitigation guidelines - HEMP protection methods for the distributed infrastructure.
Commission, I. E. (2009). IEC TS 61000-5-9:2009 Electromagnetic compatibility (EMC) - Part 5-9: Installation and mitigation guidelines - System-level susceptibility assessments for HEMP and HPEM.
Commission, I. E. (2012). IEC 61000-4-25:2001+AMD1:2012 CSV Electromagnetic compatibility (EMC) - Part 4-25: Testing and measurement techniques - HEMP immunity test methods for equipment and systems.
Company, B. (1967). *Final Report of CCP 13972, EMP Study of Weapon System Anomalies and Fix Investigations, BOE D2 18149 1*. Retrieved from
Corporation, B. (1966). *HETF Cable Pulse Test, T2 3474 1*. Retrieved from
Crain, C. M. (1982). *Calculation of Radiated Signals from High-Altitude Nuclear Detonations by Use of a Three-Dimensional Distribution of Compton Electrons*. Retrieved from
Crain, C. M., & Booker, H. G. (1963). The effects of nuclear bursts in space on the propagation of high-frequency radio waves between separated Earth terminals. *Journal of Geophysical Research, 68*(8), 2159-2166.
Dinger, D. B., & Haas, W. J. (1964). *Nuclear Electromagnetic Pulse Environment Studies Related to the Nike-X Electrical Power Systems (U), ERDL X 4*. Retrieved from Fort Belvoir, VA:
Division, T. A. G. F. (2002). *North American Electric Power Grid: Innovative Disruption Risks with Serious Impact: 2002-2007 (U), TA-1/FIR 1-03*. Retrieved from
Dolan, P. J. (1972). *Capabilities of Nuclear Weapons*: Defence Nuclear Agency.
Eichler, C. H., Legro, J. R., & Barnes, P. R. (1989). Experimental determination of the effects of steep front-short duration surges on 25 kVA pole mounted distribution transformers. *IEEE Transactions on Power Delivery, 4*(2), 1103-1110.
El-Khamy, S., Shaaban, S., & El-Gendy, A. (1998). *The penetration of nuclear electromagnetic pulses (EMP) through shielded communication cables.* Paper presented at the Radio Science Conference, 1998. NRSC'98. Proceedings of the Fifteenth National.
EMP Commission. (2008). Report of the commission to assess the threat to the United States from electromagnetic pulse (EMP) attack. *Washington DC*.
Eng, C. D. (2011). Development of the time dependence of the nuclear (E1) HEMP electric field. *IEEE transactions on electromagnetic compatibility, 53*(3), 737-748.
Etemadi, A. H., & Rezaei-Zare, A. (2014). Optimal placement of GIC blocking devices for geomagnetic disturbance mitigation. *IEEE Transactions on Power Systems, 29*(6), 2753-2762.
Evans, A., Isley, C. T., & Kincaid, B. E. (1979). *ELECTRONIC WARFARE APPLICATIONS OF FIBER OPTICS (U), AFAL TR 79 1165 ; R 3677 9384*. Retrieved from Belmont, CA:
Fagnan, D. R., Gattens, P., & Johnson, F. (1990). Monitoring solar magnetic disturbances in power systems (a summary). *IEEE Power Engineering Review, 10*(11), 4-6.
Fardoun, A. A., Fuchs, E. F., & Masoum, M. (1994). Experimental analysis of a DC bucking motor blocking geomagnetically induced currents. *IEEE Transactions on Power Delivery, 9*(1), 88-99.
Farrona, A., Gallego, M., Vaquero, J., & Domínguez-Castro, F. (2011). Spanish eyewitness accounts of the great space weather event of 1859. *Acta Geodaetica et Geophysica Hungarica, 46*(3), 370-377.
Faxvog, F., Jensen, W., Fuchs, G., Nordling, G., Jackson, D., Groh, B.. Rooney, M. (2013). *Power grid protection against geomagnetic disturbances (GMD).* Paper presented at the Electrical Power & Energy Conference (EPEC), 2013 IEEE.
Fernberg, P. (2012). One-dimensional earth resistivity models for selected areas of continental United States and Alaska. *EPRI Technical Update, 1026430*, 1-190.
Foster Jr, J. S., Gjelde, E., Graham, W. R., Hermann, R. J., Kluepfel, H. M., Lawson, R. L.,. Woodard, J. B. (2004). *Report of the Commission to Assess the Threat to the United States from Electromagnetic Pulse (EMP) Attack Volume 1: Executive Report*.
Foster, R. A., & Frickey, S. J. (2016). *Strategies, Protections and Mitigations for Electric Grid Affects from Electro-Magnetic Pulse*.
Friedman, A., Cohen, B., Eng, C., Farmer, W., Grote, D., Kruger, H., & Larson, D. (2015). *EMPulse, a new 3-D simulation code for EMP formation and propagation*.

Friedman, A., Cohen, B., Eng, C., Farmer, W., Grote, D., Kruger, H., & Larson, D. (2015). Studies of EMP generation using a Liénard–Wiechert formulation, and progress toward a 3-D EMP code. *submitted. 34*.

Fuchs, E., & Masoum, M. (1992). Suppression of harmonic distortion in power systems due to geomagnetically induced currents (GICs) through enforcing GIC balance in all phases of a system (Invention Disclosure). *University of Colorado*.

Gage, B. P. (1973). *EMP Electronic Design Handbook*. Retrieved from

Gale, G. L. (1976). *FFinal Test Report - Wing 4 Electro-Magnetic Pulse (EMP)/ Lightning Test (M-4) (U), T2 3730 1*. Retrieved from Seattle, WA:

Ghalayini, A., Dawson, F., Slemon, G., Dick, E., Hajagos, L., & Yamada, S. (1995). Mitigating GIC Saturation in Power Transformers. *Journal of the Magnetics Society of Japan, 19*(2), 545-548.

Gilbert, J., Kappenman, J., Radasky, W., & Savage, E. (2010). The Late-Time (E3) High-Altitude Electromagnetic Pulse (HEMP) and Its Impact on the US Power Grid. *FERC, Metatech Corporation*.

Gilbert, J. L. (2005). Modeling the effect of the ocean-land interface on induced electric fields during geomagnetic storms. *Space Weather, 3*(4).

Girgis, R., & Vedante, K. (2012). *Effects of GIC on power transformers and power systems.* Paper presented at the Transmission and Distribution Conference and Exposition (T&D), 2012 IEEE PES.

Glasstone, S. (1964). *The effects of nuclear weapons*. Retrieved from

Granzow, K. D., & Riker, J. F. (1981). *Late-Time EMP Response of Power Lines (U), AFWL TR 81 125*. Retrieved from Albuquerque, NM:

Granzow, K. D., Stephens, M. B., & Bombardt, J. N. (1990). *EMP Response of Overhead Power Lines Vol.2 - Appendix B (U) Technical Report, RDA TR 000281329001 002*. Retrieved from Colorado Springs, CO:

Greetsai, V. N., Kozlovsky, A. H., Kuvshinnikov, V. M., Loborev, V. M., Parfenov, Y. V., Tarasov, O. A., & Zdoukhov, L. N. (1998). Response of long lines to nuclear high-altitude electromagnetic pulse (HEMP). *IEEE transactions on electromagnetic compatibility, 40*(4), 348-354.

Guo, J., Liu, H., Feng, X., Pulkkinen, T. I., Tanskanen, E., Liu, C., . . . Wang, Y. (2014). MLT and seasonal dependence of auroral electrojets: IMAGE magnetometer network observations. *Journal of Geophysical Research: Space Physics, 119*(4), 3179-3188.

Gurevich, V. (2011). Protection of power transformers against geomagnetically induced currents. *Serbian Journal of Electrical Engineering, 8*(2), 333-339.

Gurevich, V. (2015). Protecting power equipment against magnetohydrodynamic effects (MHD) of electromagnetic pulses (EMP). *Serbian Journal of Electrical Engineering, 12*(3), 321-332.

Gurevich, V. (2015). Technologies and Components That Protect Digital Relays from Electromagnetic Pulse. *International Journal of Research Studies in Electrical and Electronics Engineering (IJRSEEE), Volume 1*(Issue 1), 18-28.

Haase, H., Nitsch, J., & Steinmetz, T. (2003). Transmission-line super theory: A new approach to an effective calculation of electromagnetic interactions. *URSI Radio Science Bulletin (Review of Radio Science), 307*, 33-60.

Hutchins, T. R., & Overbye, T. J. (2011). *The effect of geomagnetic disturbances on the electric grid and appropriate mitigation strategies.* Paper presented at the North American Power Symposium (NAPS), 2011.

Ianoz, M., Nicoara, B., & Radasky, W. (1996). Modeling of an EMP conducted environment. *IEEE transactions on electromagnetic compatibility, 38*(3), 400-413.

Jayasinghe, R., McLaren, P., & Gouldsborough, T. (1993). *Effect of GIC on overcurrent protection for filter banks.* Paper presented at the WESCANEX 93.'Communications, Computers and Power in the Modern Environment.'Conference Proceedings., IEEE.

Jie, C., Jie, G., & Ai-ci, Q. *Characteristics Analysis of Metal Oxide Arresters in GIS Excited by Very Fast Impulse* Retrieved from

Kalab, B. (1973). *Analysis of Failure of Electronic Circuits from EMP-Induced Signals: Review and Contribution*. Retrieved from

Kappenman, J. (2010). Geomagnetic storms and their impacts on the US power grid. *FERC, Metatech Corporation*.

Kappenman, J. (2010). Low-frequency protection concepts for the electric power grid: geomagnetically induced current (GIC) and E3 HEMP mitigation. *FERC, Metatech Corporation*.

Kappenman, J., Albertson, V., & Mohan, N. (1981). Current transformer and relay performance in the presence of geomagnetically-induced currents. *IEEE Transactions on Power Apparatus and Systems*(3), 1078-1088.

Kappenman, J., Norr, S., Sweezy, G., Carlson, D., Albertson, V., Harder, J., & Damsky, B. (1991). GIC mitigation: a neutral blocking/bypass device to prevent the flow of GIC in power systems. *IEEE Transactions on Power Delivery, 6*(3), 1271-1281.

Kappenman, J., & Radasky, W. (2005). Too important to fail: the looming threats of large geomagnetic storms and other high-altitude disturbances with modern electric power grids may produce significant damage to critical infrastructure. *Space Weather Journal, 18*.

Kappenman, J. G. (1996). Geomagnetic storms and their impact on power systems. *IEEE Power Engineering Review, 16*(5), 5.

Kappenman, J. G. (2001). An introduction to power grid impacts and vulnerabilities from space weather *Space Storms and Space Weather Hazards* (pp. 335-361): Springer.

Kappenman, J. G. (2004). The evolving vulnerability of electric power grids. *Space Weather, 2*(1).

Kappenman, J. G. (2005). An overview of the impulsive geomagnetic field disturbances and power grid impacts associated with the violent Sun-Earth connection events of 29–31 October 2003 and a comparative evaluation with other contemporary storms. *Space Weather, 3*(8).

Karzas, W., & Latter, R. (1962). Electromagnetic radiation from a nuclear explosion in space. *Physical Review, 126*(6), 1919.

Karzas, W., & Latter, R. (1962). The electromagnetic signal due to the interaction of nuclear explosions with the earth's magnetic field. *Journal of Geophysical Research, 67*(12), 4635-4640.

Kimball, D. S. (1960). A study of the aurora of 1859.

Klein, K. W., Barnes, P. R., & Zaininger, H. W. (1985). Electromagnetic pulse and the electric power network. *IEEE Transactions on Power Apparatus and Systems*(6), 1571-1577.

Koen, J., & Gaunt, C. (2002). Disturbances in the Southern African power network due to geomagnetically induced currents. *Cigré Session paper*(36-206).

Kohlberg, I., Baum, C., & Giri, D. (2011). *Adverse electomagnetic effects on large networks.* Paper presented at the Antennas and Propagation (APSURSI), 2011 IEEE International Symposium on.

Kong, X., Xie, Y.-z., Liu, Q., Wang, S.-F., Sun, X.-m., & Chen, Y.-H. *Transient Electric Field Caused by High-voltage Circuit Breaker's Switching Operation*.

Kramer, D. (2009). US electricity grid still vulnerable to electromagnetic pulses. *Physics today, 62*(9), 24.

Kruse, V., Nickel, D., Bonk, J., & Taylor Jr, E. (1991). *Impacts of a Nominal Nuclear Electromagnetic Pulse on Electric Power Systems. Phase 3. Final Report*.

Kruse, V., Nickel, D., Taylor, E., Bonk, J., & Barnes, P. (1991). Impacts of a nominal nuclear electromagnetic pulse on electric power systems: a probabilistic approach. *IEEE Transactions on Power Delivery, 6*(3), 1251-1263.

Laboratories, H. D. (1986). *Electromagnetic Effects*.

Laboratory, A. F. W. (1972). *EMP Test Plan For MEECN (U)[DRAFT]*.

Lahtinen, M., & Elovaara, J. (2002). GIC occurrences and GIC test for 400 kV system transformer. *IEEE Transactions on Power Delivery, 17*(2), 555-561.

Lee, K. (1986). *EMP interaction: principles, techniques, and reference data: a handbook of technology from the EMP interaction notes*: Taylor & Francis/Hemisphere.

Legro, J., Abi-Samra, N., Crouse, J., Hileman, A., Kruse, V., Taylor Jr, E., & Tesche, F. (1985). *Study to assess the effects of electromagnetic pulse on electric power systems. Phase I. Executive summary*. Retrieved from

Legro, J., Abi-Samra, N., Crouse, J., & Tesche, F. (1986). A methodology to assess the effects of magnetohydrodynamic electromagnetic pulse(MHD-EMP) on power systems. *IEEE Transactions on Power Delivery, 1*(3), 203-210.

Legro, J., & Reed, T. (1985). *Nuclear electromagnetic pulse and the electric power system*. Retrieved from

Lehman, E., & Kline, R. (2005). *2015-2020: The EMP Threat to the United States and Its Forces* Retrieved from

Lemer, E. J. (1981). Military electronics: Electromagnetic pulses: Potential crippler: Three bombs, exploded in space over the US, could black out the nation, wipe out communications, and make computers useless. *IEEE Spectrum, 18*(5), 41-46.

Lerner, E. J. (1981). Military electronics: EMPs and nuclear power: The US Nuclear Regulatory Commission is studying whether electromagnetic pulses from H-bombs could trigger nuclear plant accidents. *IEEE Spectrum, 18*(6), 48-49.

Liu, C.-m., Liu, L.-g., & Niu, X. (2010). *Disastrous space weather risk on large-scale power grid.* Paper presented at the Critical Infrastructure (CRIS), 2010 5th International Conference on.

Loewe, C., & Prölss, G. (1997). Classification and mean behavior of magnetic storms. *Journal of Geophysical Research: Space Physics, 102*(A7), 14209-14213.

Loewe, C., & Prölss, G. (1997). Classification and mean behavior of magnetic storms. *Journal of Geophysical Research: Space Physics, 102*(A7), 14209-14213.
Longley, H., & Longmire, C. (1972). Development of the CHAP EMP Code. *DNA, 3150*, 1972.
Longley, H. J., & Longmire, C. L. (1973). Development of the GLANC EMP Code. *Defence Nuclear Agency, DNA3221T (December 1973)*.
Longmire, C. (1978). On the electromagnetic pulse produced by nuclear explosions. *IEEE Transactions on Antennas and Propagation, 26*(1), 3-13.
Longmire, C. L. (1974). *Direct Interaction Effects in EMP*. Retrieved from
Longmire, C. L. (1978). *Effect of multiple scattering on the Compton recoil current*.
Longmire, C. L. (1986). Justification and Verification of High Altitude EMP Theory.
Longmire, C. L. (1987). Justification and Verification of High-Altitude EMP Theory, Part I. *Lawrence Livermore National Laboratory, Livermore, CA, UCRL-15938*.
Longmire, C. L. (1995). Electromagnetic effects of nuclear explosions. *Hand book of Atmospheric Electrodynamics, 2*, 135-153.
Longmire, C. L. (2004). Fifty Odd years of EMP. *NBC Report*, 47-51.
Longmire, C. L., & Gilbert, J. L. (1980). *Theory of EMP coupling in the source region*. Retrieved from
Longmire, C. L., Hamilton, R. M., & Hahn, J. M. (1987). *A nominal set of high-altitude EMP environments*. Retrieved from
Longmire, C. L., & Longley, H. J. (1973). *Improvements in the treatment of Compton current and air conductivity in EMP problems*. Retrieved from
Love, J. J., Coïsson, P., & Pulkkinen, A. (2016). Global statistical maps of extreme-event magnetic observatory 1 min first differences in horizontal intensity. *Geophysical Research Letters, 43*(9), 4126-4135.
Love, J. J., Rigler, E. J., Pulkkinen, A., & Riley, P. (2015). On the lognormality of historical magnetic storm intensity statistics: Implications for extreme-event probabilities. *Geophysical Research Letters, 42*(16), 6544-6553.
Lu, S., Liu, Y., & De La Ree, J. (1993). Harmonics generated from a DC biased transformer. *IEEE Transactions on Power Delivery, 8*(2), 725-731.
Maize, K. (2013). EMP: The Biggest Unaddressed Threat to the Grid. *Power, 157*(7), 50-52.
Manriquez, R., Gray, R., & Loftus, J. (1982). Theoretical and Scale Model EMP Response Analysis of Interconnected System Cables. *IEEE Transactions on Nuclear Science, 29*(6), 1935-1942.
Manweiler, R. (1975). *Effects of nuclear electromagnetic pulse (EMP) on synchronous stability of the electric power system*. Retrieved from
Marable, J. H., Baird, J. K., & Nelson, D. B. (1972). *Effects of Electromagnetic Pulse (EMP) on a Power System*: Oak Ridge National Laboratory.
Marable, J. H., Barnes, P. R., & Nelson, D. B. (1975). *Power System EMP Protection*: Oak Ridge National Laboratory.
Marti, L., Rezaei-Zare, A., & Narang, A. (2013). Simulation of transformer hotspot heating due to geomagnetically induced currents. *IEEE Transactions on Power Delivery, 28*(1), 320-327.
Martins, V. C. (2009). *Cable Hardened to Nuclear Electro-Magnetic Pulse (NEMP) (U), BDW/W TR72 76 0035*. Retrieved from McLean, VA:
McConnell, B. W., Barnes, P. R., & Tesche, F. M. (1991). *Experimental determination of the MHD-EMP effects on power distribution transformers*. Retrieved from
Meliopoulos, A. P. S., Glytsis, E. N., & Cokkinides, G. J. (1991). *Effects of Geomagnetic Disturbances on Electric Power Transmission Systems*. Retrieved from United States:
Meliopoulos, A. S., Glytsis, E., Cokkinides, G., & Rabinowitz, M. (1994). Comparison of SS-GIC and MHD-EMP-GIC effects on power systems. *IEEE Transactions on Power Delivery, 9*(1), 194-207.
Miller, C. R. (2005). *Electromagnetic pulse threats in 2010*. Retrieved from

Miller, D. B., Lux, A., Grzybowski, S., & Barnes, P. (1990). The effects of steep-front, short-duration impulses on power distribution components. *IEEE Transactions on Power Delivery, 5*(2), 708-715.
MIL-STD-B. (1993). *High Altitude Electromagnetic Pulse Environment*. Retrieved from
Myllys, M., Viljanen, A., Rui, Ø. A., & Ohnstad, T. M. (2014). Geomagnetically induced currents in Norway: the northernmost high-voltage power grid in the world. *Journal of Space Weather and Space Climate, 4*, A10.
Nayak, R., Sasmal, R., Sen, S., Pelly, B., & Riedel, P. (2006). *Experience with blocking devices during monopolar operation of 6500 kV; 2000 MW Talcher–Kolar HVDC system in India*. Paper presented at the Paris, France: Paper presented at the CIGRE Session.
Neal, R., Radasky, W., & Kappenman, J. G. (2011). *Developing an actionable EMP/GMD hardening program for an electric utility.* Paper presented at the 2011 IEEE Power and Energy Society General Meeting.
Nelson, D. (1972). *PROGRAM TO COUNTER THE EFFECTS OF NUCLEAR ELECTROMAGNETIC PULSE IN COMMERCIAL POWER SYSTEMS*. Retrieved from
NERC. (2014). Transmission System Planned Performance During Geomagnetic Disturbances. *NERC TPL-007-1*.
Nevanlinna, H. (2004). Historical space climate data from Finland: compilation and analysis. *Solar Physics, 224*(1-2), 395-405.
Nevanlinna, H. (2004). *Results of the Helsinki magnetic observatory 1844-1912.* Paper presented at the Annales Geophysicae.
Ngwira, C. M., Pulkkinen, A., Kuznetsova, M. M., & Glocer, A. (2014). Modeling extreme "Carrington-type" space weather events using three-dimensional global MHD simulations. *Journal of Geophysical Research: Space Physics, 119*(6), 4456-4474.
Ngwira, C. M., Pulkkinen, A., Wilder, F. D., & Crowley, G. (2013). Extended study of extreme geoelectric field event scenarios for geomagnetically induced current applications. *Space Weather, 11*(3), 121-131.
Nucci, C., Rachidi, F., Ianoz, M., & Mazzetti, C. (1995). Comparison of two coupling models for lightning-induced overvoltage calculations. *IEEE Transactions on Power Delivery, 10*(1), 330-339.
Odenwald, S. (2007). Newspaper reporting of space weather: End of a golden age. *Space Weather, 5*(11).
Odenwald, S. F., & Green, J. L. (2007). Forecasting the impact of an 1859-caliber superstorm on geosynchronous Earth-orbiting satellites: Transponder resources. *Space Weather, 5*(6).
O'Donnell, H. B., & Tasca, D. M. (1978). *Development of High Level Electrical Stress Failure Threshold and Prediction Model for Small Scale Junction Integrated Circuits*. Retrieved from
Office, U. S. G. A. (2011). DOD Critical Infrastructure Preparedness for EMP and Cyber Attack: Preliminary Observations (U), GAO-11-690C.
Office, U. S. G. A. (2012). Report to the Committee on Armed Services, House of Representatives: Electromagnetic Pulse and Cyber Threats, Actions Needed to Improve Protection and Integrate Risk into Installation Preparedness, GAO-12-170C.
Oreskovic, R. (2011). *Electromagnetic Pulse-A Catastrophic Threat to the Homeland*. Retrieved from
Oyedokun, D., Gaunt, C., Tenbohlen, S., Heindl, M., Beltle, M., Reuter, M., & Schneider, D. (2011). Laboratory test for GIC effects on power transformers. *Currents, 1*, 2.
Parkinson, W., & Jones, F. (1979). The geomagnetic coast effect. *Reviews of Geophysics, 17*(8), 1999-2015.
Pirjola, R. (1985). On currents induced in power transmission systems during geomagnetic variations. *IEEE Transactions on Power Apparatus and Systems* (10), 2825-2831.
Pirjola, R. (2000). Geomagnetically induced currents during magnetic storms. *IEEE Transactions on Plasma Science, 28*(6), 1867-1873.
Pirjola, R. (2007). Space weather effects on power grids *Space Weather-Physics and Effects* (pp. 269-288): Springer.
Pirjola, R. (2008). Study of effects of changes of earthing resistances on geomagnetically induced currents in an electric power transmission system. *Radio Science, 43*(1).
Pirjola, R. J., & Boteler, D. H. (2006). *Geomagnetically induced currents in European high-voltage power systems.* Paper presented at the 2006 Canadian Conference on Electrical and Computer Engineering.
Portante, E. C., Malone, L. T., Kavicky, J. A., Tanzman, E. A., Folga, S. F., & Wulfkuhle, G. R. (2013). *Simulating the potential impacts of a 10-kiloton nuclear explosion on an electric power system serving a major city.* Paper presented at the 2013 Winter Simulations Conference (WSC).
Price, P. R. (2002). Geomagnetically induced current effects on transformers. *IEEE Transactions on Power Delivery, 17*(4), 1002-1008.

Pulkkinen, A., Lindahl, S., Viljanen, A., & Pirjola, R. (2005). Geomagnetic storm of 29–31 October 2003: Geomagnetically induced currents and their relation to problems in the Swedish high-voltage power transmission system. *Space Weather, 3*(8).

Pulkkinen, A., Pirjola, R., & Viljanen, A. (2008). Statistics of extreme geomagnetically induced current events. *Space Weather, 6*(7).

Rabinlowitz, M. (1987). Effect of the fast nuclear electromagnetic pulse on the electric power grid nationwide: A different view. *IEEE Transactions on Power Delivery, 2*(4), 1199-1222.

Rachidi, F. (1993). Formulation of the field-to-transmission line coupling equations in terms of magnetic excitation field. *IEEE transactions on electromagnetic compatibility, 35*(3), 404-407.

Radasky, D. W. A. (2002). High Altitude EMP (HEMP) Environments and Effects. *NBC Report (Spring/Summer 2002)*, 24-29.

Radasky, W. (2009). Protection of Commercial Installations from the. *Triple Threat" of HEMP, IEMI, and Severe Geomagnetic Storms," Interference Technology EMC Directory and Design Guide*.

Radasky, W. (2010). *Protection of commercial installations from the high-frequency electromagnetic threats of HEMP and IEMI using IEC standards*. Paper presented at the 2010 Asia-Pacific International Symposium on Electromagnetic Compatibility.

Radasky, W. (2011). *Overview of the impact of intense geomagnetic storms on the US high voltage power grid*. Paper presented at the Electromagnetic Compatibility (EMC), 2011 IEEE International Symposium on.

Radasky, W., & Kappenman, J. (2010). *Impacts of geomagnetic storms on EHV and UHV power grids*. Paper presented at the 2010 Asia-Pacific International Symposium on Electromagnetic Compatibility.

Radasky, W., & Knight, R. (1971). *HAPS-A Two-Dimensional High Altitude EMP Environment Code*. Retrieved from

Radasky, W., & Savage, E. (2010). High-Frequency Protection Concepts for the Electric Power Grid. *FERC, Metatech Corporation*.

Radasky, W. A. (2012). The potential impacts of three high power electromagnetic (HPEM) threats on smart grids. *IEEE Electromagnetic Compatibility Magazine, 1*(2), 107-110.

Radasky, W. A. (2013). Impacts of Variations of Geomagnetic Storm Disturbances on High Voltage Power Systems. *IEEJ Transactions on Power and Energy, 133*(12), 931-934.

Radasky, W. A., Kappenman, J., & Pfeffer, R. (2001). Nuclear and Space Weather Effects on the Electric Power Infrastructure. *NBC Report*, 37-42.

Rajapakse, A., Perera, N., Faxvog, F., Jensen, W., Nordling, G., Fuchs, G.,. Groh, B. (2012). *Power grid stability protection against GIC using a capacitive grounding circuit*. Paper presented at the Transmission and Distribution Conference and Exposition (T&D), 2012 IEEE PES.

Ringlee, R. J., & Stewart, J. R. (1989). Geomagnetic effects on power systems. *IEEE Power Engineering Review, 9*(7), 6-9.

Rooney, M. (2011). *High-Altitude Electromagnetic Pulse*. Retrieved from

Roussel-Dupré, R. A. (2005). Prompt nuclear EMP and synchrotron radiation: A resolution of two approaches. *IEEE transactions on electromagnetic compatibility, 47*(3), 552-558.

Savage, E., Gilbert, J., & Radasky, W. (2010). The early-time (E1) high-altitude electromagnetic pulse (HEMP) and its impact on the US power grid. *FERC, Metatech Corporation*.

Schnurr, A. (2013). Vulnerability of National Power Grids to Electromagnetic Threats: Domestic and International Perspectives. *Energy LJ, 34*, 1.

Schrijver, C. J., & Mitchell, S. D. (2013). Disturbances in the US electric grid associated with geomagnetic activity. *Journal of Space Weather and Space Climate, 3*, A19.

Schulz, M. (1997). Direct influence of ring current on auroral oval diameter. *Journal of Geophysical Research: Space Physics, 102*(A7), 14149-14154.

Seiler Jr, L. W. (1975). *A calculational model for high altitude EMP*.

Serafin, D. (1986). *Electromagnetic pulse effect on civilian facilities*.

Shea, M., & Smart, D. (2006). Compendium of the eight articles on the "Carrington Event" attributed to or written by Elias Loomis in the American Journal of Science, 1859–1861. *Advances in Space Research, 38*(2), 313-385.

Silverman, S., & Cliver, E. (2001). Low-latitude auroras: the magnetic storm of 14–15 May 1921. *Journal of Atmospheric and Solar-Terrestrial Physics, 63*(5), 523-535.

Simpson, S. (2004). Protecting the Power Grid From Electromagnetic Pulses. *Space Weather, 2*(10).

Smith, I., Riepe, K., Champney, P., Corcoran, P., & Tesche, F. (1985). *Study to simulate high altitude EMP surges induced in overhead power lines. Final report*.

Stanek, E. (1978). *Feasibility of Isolating Vulnerable Equipment of the Electric Power System from Sources of EMP*.

Starkov, G., & Feldstein, Y. I. (1967). Variation of auroral oval zone boundaries. *Geomagn. Aeron, 7*(1), 62-71.
Tay, H.-c., & Swift, G. W. (1984). A novel method of detecting asymmetrical transformer core saturation due to GIC. *IEEE Transactions on Power Apparatus and Systems* (1), 183-189.
Taylor, C., Satterwhite, R., & Harrison, C. (1965). The response of a terminated two-wire transmission line excited by a nonuniform electromagnetic field. *IEEE Transactions on Antennas and Propagation, 13*(6), 987-989.
Teller, E. (1982). Electromagnetic pulses from nuclear explosions. *IEEE Spectrum, 19*(10), 65-65.
Tesche, F., & Barnes, P. (1988). Development of a new high altitude electromagnetic pulse (HEMP) environment and resulting overhead line responses. *Electromagnetics, 8*(2-4), 213-239.
Tesche, F., & Barnes, P. (1989). A multiconductor model for determining the response of power transmission and distribution lines to a high altitude electromagnetic pulse (HEMP). *IEEE Power Engineering Review, 9*(7), 82-82.
Tesche, F. M. (1992). Comparison of the transmission line and scattering models for computing the HEMP response of overhead cables. *IEEE transactions on electromagnetic compatibility, 34*(2), 93-99.
Tesche, F. M., Barnes, P., & Meliopoulos, A. S. (1992). *Magnetohydrodynamic electromagnetic pulse (MHD-EMP) interaction with power transmission and distribution systems*. Retrieved from
Tesche, F. M., & Barnes, P. R. (1989). The HEMP response of an overhead power distribution line. *IEEE Transactions on Power Delivery, 4*(3), 1937-1944.
Tesche, F. M., & Barnes, P. R. (1990). Transient response of a distribution circuit recloser and control unit to a high-altitude electromagnetic pulse (HEMP) and lightning. *IEEE transactions on electromagnetic compatibility, 32*(2), 113-124.
Thomson, A. W., Dawson, E. B., & Reay, S. J. (2011). Quantifying extreme behavior in geomagnetic activity. *Space Weather, 9*(10).
Tomita, S., Nosé, M., Iyemori, T., Toh, H., Takeda, M., Matzka, J., Troshichev, O. (2010). *Magnetic local time dependence of geomagnetic disturbances contributing to the AU and AL indices.* Paper presented at the Annales Geophysicae.
Trichtchenko, L., & Boteler, D. (2007). *Effects of recent geomagnetic storms on power systems.* Paper presented at the Electromagnetic Compatibility and Electromagnetic Ecology, 2007 7th International Symposium on.
Trichtchenko, L., & Boteler, D. H. (2006). *Response of power systems to the temporal characteristics of geomagnetic storms.* Paper presented at the 2006 Canadian Conference on Electrical and Computer Engineering.
Tsubouchi, K., & Omura, Y. (2007). Long-term occurrence probabilities of intense geomagnetic storm events. *Space Weather, 5*(12).
Tsurutani, B., Gonzalez, W., Lakhina, G., & Alex, S. (2003). The extreme magnetic storm of 1–2 September 1859. *Journal of Geophysical Research: Space Physics, 108*(A7).
Tyagi, S. K. (1997). *Development of line filter for EMP applications.* Paper presented at the Electromagnetic Interference and Compatibility'97. Proceedings of the International Conference on.
Tyasto, M., Ptitsyna, N., Veselovsky, I., & Yakovchouk, O. (2009). Extremely strong geomagnetic storm of September 2–3, 1859, according to the archived data of observations at the Russian network. *Geomagnetism and Aeronomy, 49*(2), 153-162.
U.S. Department of Energy: National Nuclear Security Administration Nevada Field Office. (2015). United States Nuclear Tests July 1945 through September 1992. *DOE/NV--209-REV 16.*
Unknown. (1984). *Catalogue of Penetration Treatments for EMP Protection*.
USSTRATCOM/DJ3. (2012). INTEGRATED NUCLEAR SURVIVABILITY and ENDURABILITY REPORT.
V.C., M., & C, K. (1971). Cable Hardened To Nuclear Electro-Magnetic Pulse (NEMP); Semi-Annual Report (U)", BDM/W TR71 67 0035 ; ECOM 0035 1.
Vance, E. F. (1975). *Electromagnetic-pulse handbook for electric power systems*.
Vestine, E. H., & Chapman, S. (1938). The electric current-system of geomagnetic disturbance. *Terrestrial Magnetism and Atmospheric Electricity, 43*(4), 351-382.
Viljanen, A., Nevanlinna, H., Pajunpää, K., & Pulkkinen, A. (2001). *Time derivative of the horizontal geomagnetic field as an activity indicator.* Paper presented at the Annales Geophysicae.
Viljanen, A., Pirjola, R., Prácser, E., Ahmadzai, S., & Singh, V. (2013). Geomagnetically induced currents in Europe: characteristics based on a local power grid model. *Space Weather, 11*(10), 575-584.
Viljanen, A., Thomson, A., Wik, M., Wintoft, P., Wesztergom, V., Sakharov, Y., & Ngwira, C. (2014). The European risk from geomagnetically induced currents (EURISGIC).
Vittitoe, C. N. (1989). Did high-altitude EMP cause the Hawaiian streetlight incident? *Sandia National Laboratories, 2.*

Volzka, D. (1984). Electromagnetic pulse effects on a typical electric utility system. *IEEE Transactions on Power Apparatus and Systems, 8*(PAS-103), 2215-2221.

Wagner, C. L., & Feero, W. (1992). *Recommended engineering practice to enhance the EMI/EMP immunity of electric power systems*.

Wait, J. R. (1953). Propagation of radio waves over a stratified ground. *Geophysics, 18*(2), 416-422.

Walling, R., & Khan, A. (1991). Characteristics of transformer exciting-current during geomagnetic disturbances. *IEEE Transactions on Power Delivery, 6*(4), 1707-1714.

Wang, Q., Zhou, X., Li, X., & Jia, R. (2013). *The modeling and experimental investigation on coupling of transmission line network with electromagnetic pulse (EMP).* Paper presented at the Smart Energy Grid Engineering (SEGE), 2013 IEEE International Conference.

Woodroffe, J. R., S. K. Morley, M. G. Henderson, V. K. Jordanova, M. M. Cowee, and J. G. Gjerloev (2016). The latitudinal variation of geoelectromagnetic disturbances during large geomagnetic storms. *Space Weather, submitted*.

Wunsch, D., & Bell, R. (1968). Determination of threshold failure levels of semiconductor diodes and transistors due to pulse voltages. *IEEE Transactions on Nuclear Science, 15*(6), 244-259.

Xie, H., Du, T., Zhang, M., Li, Y., Qiao, H., Yang, J., Wang, J. (2015). Theoretical and experimental study of effective coupling length for transmission lines illuminated by HEMP. *IEEE transactions on electromagnetic compatibility, 57*(6), 1529-1538.

Xie, H., Li, Y., Qiao, H., & Wang, J. (2016). Empirical Formula of Effective Coupling Length for Transmission Lines Illuminated by E1 HEMP. *IEEE transactions on electromagnetic compatibility, 58*(2), 581-587.

Yang, B., Egbert, G. D., Kelbert, A., & Meqbel, N. M. (2015). Three-dimensional electrical resistivity of the north-central USA from EarthScope long period magnetotelluric data. *Earth and Planetary Science Letters, 422*, 87-93.

Yeo, S.-M., & Kim, C.-H. (2012). Analysis of Transient Overvoltages within a 345kV Korean Thermal Plant. *Journal of Electrical Engineering and Technology, 7*(3), 297-303.

Zaininger, H. (1984). *Electromagnetic pulse (EMP) interaction with electric power systems. Power Systems Technology Program. Final report*. Retrieved from

Zanetti, L. J. (2013). Review of North American Electric Reliability Corporation (NERC) Interim Report: Effects of Geomagnetic Disturbances on the Bulk Power System—February 2012. *Space Weather, 11*(6), 335-336.

Zhang, L. Y., & Wang, Z. Z. (2014). *Study and Calculation of Geomagnetic Induced Current in Power Grid.* Paper presented at the Applied Mechanics and Materials.

Zheng, K., Liu, L.-g., Boteler, D., & Pirjola, R. (2013). *Calculation analysis of geomagnetically induced currents with different network topologies.* Paper presented at the 2013 IEEE Power & Energy Society General Meeting.

Zheng, T., Chen, P., Lu, T., Jin, Y., & Liu, L. (2013). *Effects of Geomagnetically Induced Currents on current transformer and differential protection.* Paper presented at the 2013 IEEE Power & Energy Society General Meeting.